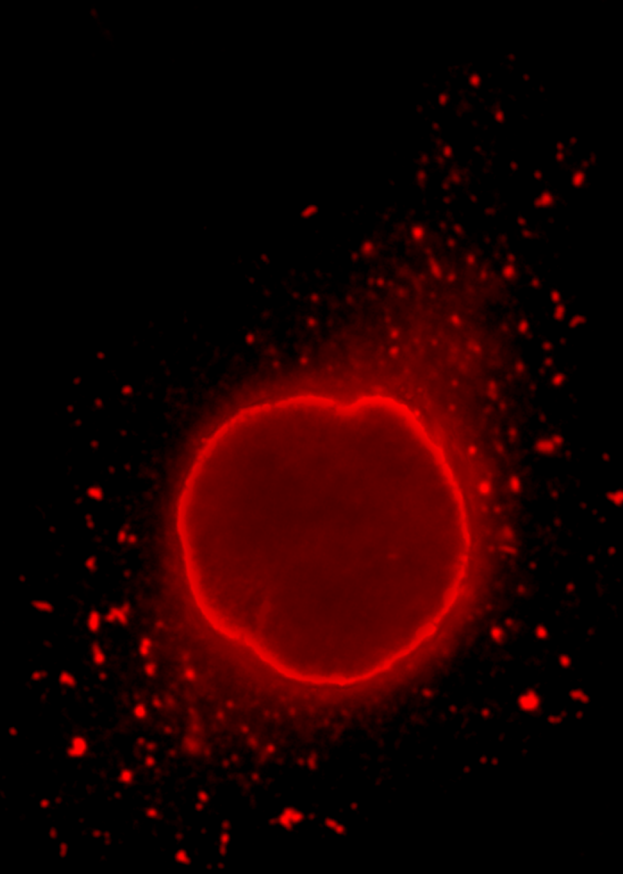# Bicaudal-D: Switching motors, cargo and direction

Daniël Splinter

Bicaudal-D: Switching motors, cargo and direction

G.D. Splinter

Cover: Daniël Splinter
The cover shows a nocodazole treated HeLa cell which is fixed with methanol and stained for RanBP2. RanBP2 is a part of the nuclear pore complex, which acts as an anchor for Bicaudal-D and microtubule motors at the nuclear envelope

Bicaudal-D: Switching motors, cargo and direction

Bicaudal-D: Verandering van motoren, lading en richting

ERASMUS UNIVERSITEIT ROTTERDAM

Promotiecommissie

Promotor: Prof.dr. F.G. Grosveld

Overige leden: Dr.ir N.J. Galjart
                       Dr. C.C. Hoogenraad
                       Dr. G. Jansen

Copromotor: Dr. A. Akhmanova

Voor Boren, Amber en mijn ouders

Index

Scope of this thesis

Transport of vesicles and organelles is an essential cellular process. Proteins like Rab GTPases, specialized adaptor proteins and motor proteins are involved in targeting and movement of cargos to their destination. This thesis describes the function of the mammalian adaptor protein Bicaudal-D in intracellular transport and its potential role in bidirectional movement of several cargos.

Chapter 1 gives an overall introduction of the components involved in transport mechanisms. It starts with a description of the three major types of cytoskeletal filaments, actin, intermediate filaments and microtubules. Subsequently, microtubule associated proteins and motor proteins are discussed in more detail. Chapter 1 concludes with a description of Bicaudal-D, its role in Drosophila development and the function of Bicaudal-D in cargo transport along the microtubules in mammalian cells.

Chapter 2 describes the behaviour of vesicles associated with the small GTPase Rab6. It shows that Rab6 is a marker of exocytotic vesicles that are mainly driven by the microtubule plus-end directed motor kinesin-1.

Chapter 3 reports a novel interaction partner of mammalian Bicaudal-D, RanBP2. Bicaudal-D binds RanBP2 in the late G2/early prophase and through this interaction targets the microtubule minus end-directed dynein/dynactin motor complex to the nuclear envelope. This interaction contributes to the positioning of the nucleus in close proximity of the microtubule organising centre prior to mitosis.

Chapter 4 shows that the N-terminal part of Bicaudal-D acts as a linker between cytoplasmic dynein and its accessory complex dynactin. It explores this finding in the context of dynein motility in vitro.

Chapter 5 reviews the role of Rab GTPases in the movement of membrane organelles and discusses several well-studied examples of intracellular transport, such as aggregation and dispersion of melanosomes in pigment cells. The described transport systems are compared with the model of Bicaudal-D function that emerged from the experimental work described in this thesis.

Transport, an essential process

1

Chapter 1. Transport, an essential cellular process

1.1 The cytoskeleton

Every eukaryote contains a cytoskeleton – a network of fibres that provides the cells with structural support to maintain their shape and to adjust to their environment. The cytoskeleton is involved in processes such as organelle anchorage, cell motility, chromosome segregation and intracellular transport. Cytoskeletal networks are composed of three main types of fibres: microfilaments or actin filaments, intermediate filaments and microtubules (Fig.1). The three types of filaments differ in subunit composition, mechanisms of assembly and functions.
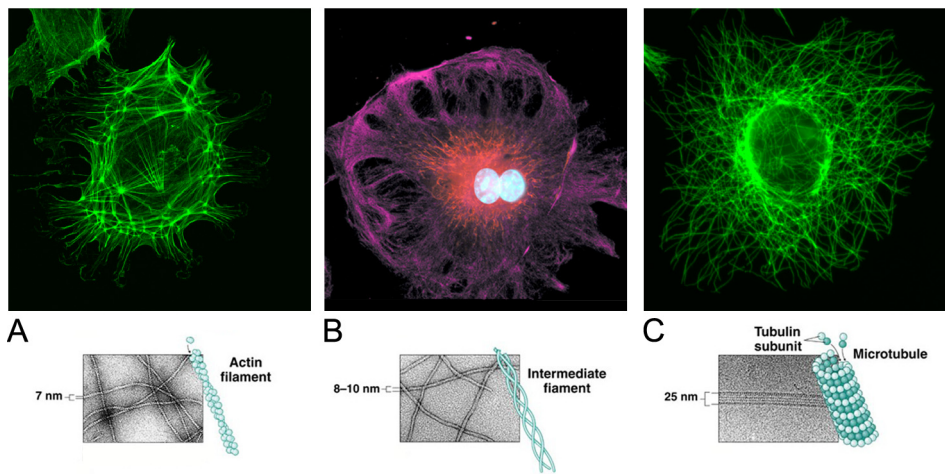
Figure 1. The cytoskeleton

Immunofluorescent staining images, electron micrographs and schematic representations of the three major cytoskeletal components. (A) Actin filaments, (B) intermediate filaments (desmin) and (C) microtubules. (Actin image reproduced from: http://www.bms.ed.ac.uk; electron micrographs reproduced from http://migration.files. wordpress.com; intermediate filament image reproduced from http://probes.invitrogen.com; tubulin image, courtesy of J. van Haren).

1.1.1 Actin filaments

Actin filaments form one of the three main fibrous cellular networks. They are composed of actin subunits, which are highly conserved in evolution. Higher eukaryotes generally express several isoforms of actin encoded by a family of related genes. Mammals have at least six actin isoforms, which are divided into three classes: α, β and γ actin according to their isoelectric point (Vandekerckhove and Weber, 1978; Furukawa and Fechheimer, 1997). In muscle tissue, α actin is the main component, whereas the β and γ isoforms are prominent in non-muscle cells.

Non muscular eukaryotic cells contain a large pool of globular actin monomers bound to ATP (G-actin). The pool of G-actin is essential for fast remodelling of actin structures. The actin filaments, also called F-actin, are formed by two helical polymers of G-actin with a diameter of 7 nm. Because all actin subunits in the polymer face the same direction, the filament is polarised. Actin filament

polarity can be determined by myosin decoration (Wegner 1976); based on this property, the two ends of actin filaments are called the barbed end (the fast growing end in vitro) and the pointed end (Fig.2). The barbed and the pointed ends have different binding partners that regulate assembly and architecture of the actin network (Carlier 1998).
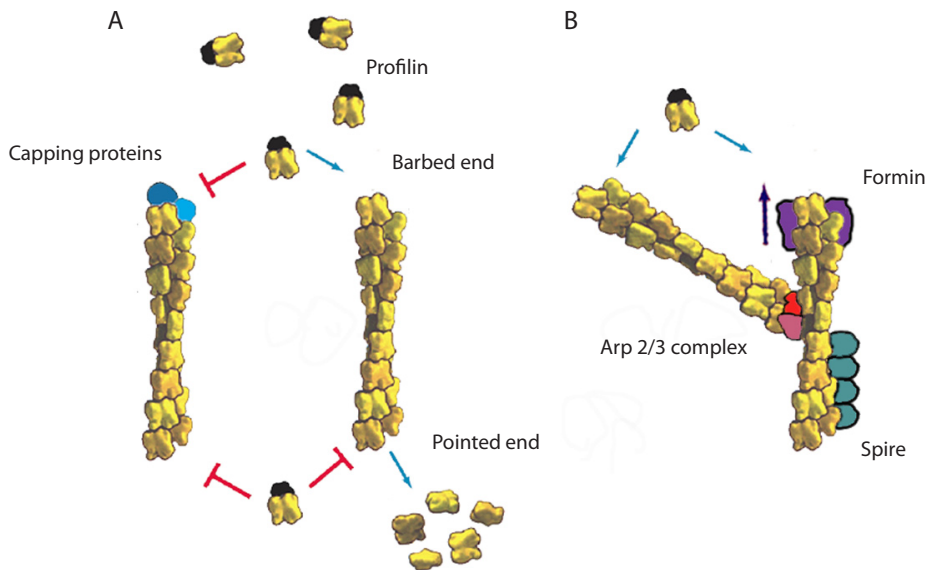
Figure 2. Actin dynamics
(A) Actin filaments polymerise from the barbed end and lose monomers from the pointed end. Profilin inhibits growth from the pointed end, and capping proteins stabilise actin filaments and inhibit their growth. (B) Nucleation of actin filaments by the Arp2/3 complex, formins and Spire (modified from original artwork by Graham Johnson in "Cell Biology" by T.D. Pollard and W.C. Earnshaw, W.B. Saunders, 2002).

Actin polymerisation starts with the formation of new nucleation sites. In vivo, self-assembly by formation of actin dimers and trimers is highly unfavourable; therefore nucleation factors are required (Pollard et al., 2000). At present, three classes of nucleation factors are known: the Arp2/3 complex, formin proteins and the protein Spire (Kerkhoff, 2006; Pollard, 2007) (Fig.2). The Arp2/3 complex can nucleate new filaments from the side of an existing filament, causing filament branching. Formins nucleate new filaments and move processively with the barbed end as it elongates, while Spire nucleates a new filament by stabilizing an actin tetramer. After nucleation, polymerisation occurs very rapidly as ATP-bound actin monomers are added to the barbed end of the actin filament. In certain conditions, the addition of new monomers to the barbed end can be balanced by the loss of monomers from the pointed end of the actin filament. This leads to treadmilling of the actin subunits from the barbed end to the pointed end (Wang, 1985).

Various proteins control the dynamics of the actin network. Capping proteins, for example, prevent filament growth from the barbed end. Profilin, another actin-controlling factor, binds to actin monomers to promote subunit association at the barbed end and to inhibit growth from the pointed end (Amann and Pollard, 2000).

In vivo, actin fibres form a highly dynamic network of polarised filaments that play a role in maintaining cell shape, intracellular trafficking, cell motility and cell division. A well-known example is the function of actin in the muscle, where actin is the major component of the thin filaments. The motor protein myosin II (see chapter 1.2.1) forms the thick filaments in the muscle fibre. Together, thin and thick filaments are arranged into actomyosin myofibrils (Selby and Bear, 1956). With the hydrolysis of ATP, myosin heads undergo a cycle during which they attach to the thin filaments, exert tension, and then, depending on the load, perform a power stroke, which causes shortening of the muscle by making thin filaments slide against each other.

1.1.2 Intermediate filaments

Intermediate filaments are formed by a large group of proteins, which are encoded in the human genome by approximately 65 genes (Hesse et al., 2001). Intermediate filaments are composed of rod-shaped proteins that can self-assemble in vitro into 10-12-nm non-polarised structures in the absence of both ATP and GTP (Strelkov et al., 2003). Five different intermediate filament classes are recognised, of which four are located in the cytoplasm. Only the lamins (class V intermediate filaments) are located in the nucleus. Expression patterns of different intermediate filaments are cell type- and tissue-specific (Parry et al., 2007; Goldman et al., 2008).

Polymerisation of intermediate filaments starts with the parallel dimerisation of two chains. There is some variation in the formation of dimers. Vimentin (a type III intermediate filament), for example, forms homodimers, while type I and II intermediate filaments such as keratins assemble into heterodimers (Parry et al., 2007). In vitro studies suggest that dimers assemble into anti-parallel, half-staggered tetramers that bind laterally to form unit-length filaments (Kirmse et al., 2007) (Fig. 3). In vivo, polymerisation of intermediate filaments is organised in a comparable way, but controlled by cellular factors (Helfand et al., 2003).

Intermediate filaments are highly resistant against mechanical stress and form strong but flexible polymers. The higher the mechanical stress on such fibres, the more resistant they become against further deformation, a phenomenon called strain stiffening (Janmey et al., 1991). It has been shown that intermediate filaments are highly dynamic. Overexpression of GFP-vimentin showed that vimentin fibrils continuously assemble, disassemble and change their shape; in addition, vimentin filaments can move in both anterograde and retrograde directions, as shown by photobleaching studies (Yoon et al., 1998; Martys et al., 1999; Yoon et al., 2001).

The functions of intermediate filaments are very diverse: they can interact with both actin and microtubule networks via a variety of linker proteins, such as plectin and fliaggrin (Capetanaki et al., 2007). Intermediate filaments are capable of binding to the outer nuclear membrane, thereby coupling it to the cytoplasmic cytoskeleton and they are involved in the positioning of organelles, such as mitochondria and the Golgi apparatus (Tzur et al., 2006; Toivola et al., 2005). Another group of

well described intermediate filaments are the keratins, which lay the basis for hairs, nails, scales and other epidermis-derived structures, which provide protection and elasticity of our skin (Coulombe and Omary , 2002).
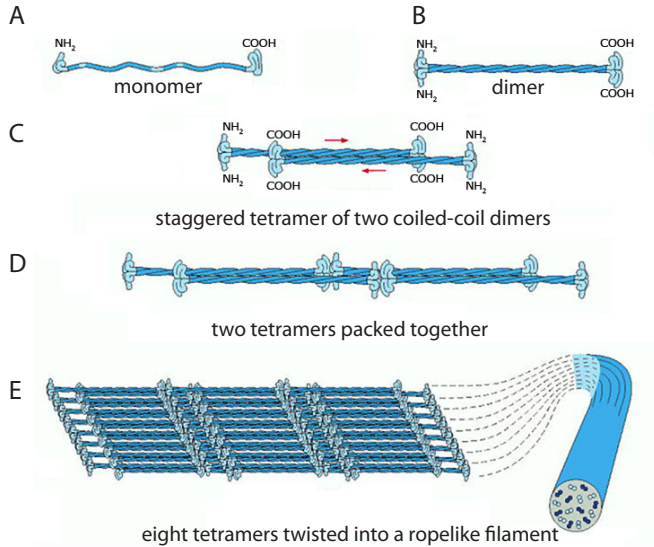
Figure 3. Intermediate filament assembly.
The monomer shown in (A) pairs with an identical monomer to form a dimer (B), in which the conserved central rod domains are aligned in parallel and wind together into a coiled-coil. (C) Two dimers then line up side by side to form an antiparallel tetramer of four polypeptide chains. The tetramer is the soluble subunit of intermediate filaments. (D) Within each tetramer, the two dimers are shifted with respect to one another, thereby allowing it to associate with another tetramer. (E) In the final 10-nm rope-like filament, tetramers are packed together in a helical array, which has 16 dimers in cross-section. Half of these dimers are pointing in opposite directions (Molecular Biology Of The Cell, B. Alberts et al., 4th edition).

1.1.3 Microtubules

Microtubules are hollow tubes with a diameter of approximately 25 nanometres that are composed of α and β tubulin subunits. Other tubulin family members are γ, δ and ε tubulin. γ tubulin is mainly located at the centrosomes and the spindle pole bodies. Both δ and ε tubulin localise at the centrioles and are believed to be involved in the formation of the mitotic spindle (Chang and Stearns, 2000). Further diversity of tubulin isoforms is caused by post-translational modifications. Acetylation, for example, occurs on the α tubulin subunit and might play a role in cell motility (Hubbert et al., 2002). Polyglycylation on β tubulin is important for the formation of cilia (Xia et al., 2000; Thazhath et al., 2002; Thazhath et al., 2004). Other tubulin modifications are detyrosination, phosphorylation, and palmitoylation (Verhey and Gaertig, 2007).

Microtubules provide a network for anchoring and positioning of cellular structures like the Golgi, endoplasmic reticulum and mitochondria. They contribute to the cell shape and provide tracks for the transport of cargo. During mitosis, microtubules are vital for the segregation of chromosomes. The dynamic behaviour of microtubules is essential for most of these functions.

1.1.3.1 Microtubule dynamics

Similar to actin filaments, microtubules are polarised: they have a plus-end (the fast-growing end in vitro) and a minus-end. In vivo, microtubule growth primarily initiates at structures called Microtubule Organising Centres (MTOC) (Osborn and Weber, 1976). The mammalian MTOC consists of a pair of centrioles surrounded by pericentriolar material. Microtubules nucleate from the γ tubulin ring structures and most of them are anchored with their minus-ends at the MTOC while their plus-ends grow towards the cell periphery.

Microtubules consist of α/β-tubulin dimers that form a tube of 13 protofilaments. In vivo, microtubule polymerisation occurs at the plus-end. Free α/β-tubulin dimers, bound to GTP, are incorporated into the tubule (Tian et al., 1997). After subunit addition to the protofilament, GTP on the β-tubulin is hydrolysed to GDP. This induces a bent conformation and the protofilament tries to curve outwards (Desai and Mitchison, 1997). However, this outward curving is constrained by the lattice and a cap of GTP-associated tubulin at the growing end of the microtubule (Fig. 4). When the GTP cap is lost due to, for example, a decrease in the polymerisation rate, the microtubule rapidly depolymerises (Fig. 4). Such a transition from the growing to the shrinking phase is called catastrophe. A rescue (a switch from shrinkage to growth) occurs when a microtubule starts growing again and regains a cap of GTP tubulin. During its lifetime, a microtubule may undergo multiple episodes of shrinkage and growth, a behaviour called dynamic instability (Heald and Nogales, 2002; Burbank and Mitchison, 2006).
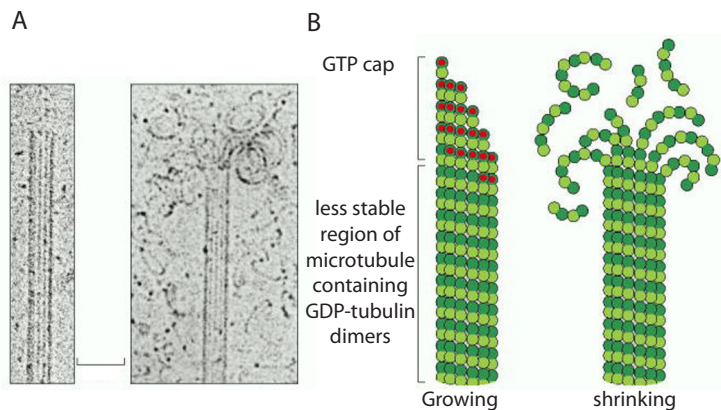
Figure 4. Microtubule dynamics
(A) Electron micrograph and (B) schematic representation of a growing and a shrinking microtubule. The growing microtubule is composed of GDP-containing subunits and a stable GTP-tubulin-containing cap. Loss of the GTP cap, however, allows the GDP-containing protofilaments to adopt a curved conformation. This leads to catastrophe, the transition from growing to shrinking. (Molecular Biology Of The Cell, B. Alberts & others, 4th edition).

Other features of microtubule dynamics are pausing, during which microtubule length does not change, and treadmilling, a loss of subunits from the minus-end compensated by subunit addition to the plus-end, a behaviour that has already been described for actin. Dynamic instability allows a cell to react quickly to environmental cues; it enables the cells to rearrange its microtubule network during mitosis or migration. Different phases of dynamic instability such as growth, shrinkage and pausing are influenced and controlled by multiple cellular factors like microtubule-associated proteins.

During mitosis or meiosis, the microtubule network undergoes a dramatic reorganisation – it is rearranged into the mitotic spindle, a structure in which three types of microtubules can be distinguished. A set of microtubules called kinetochore fibres connects the spindle poles to the kinetochores of chromosomes, to which they attach with their plus-ends. Interpolar microtubules stabilise the spindle and enable spindle pole separation. Astral microtubules radiate from the poles to the cell periphery and help to position the spindle (McIntosh and McDonald, 1989; Kline-Smith and Walczak, 2004).

1.1.3.2 Microtubule-associated proteins

Microtubule associated proteins or MAPs are known to influence the dynamic behaviour of microtubules. Some MAPs, like MAP2 and Tau in neurons, decorate microtubules, stabilise them and protect them against microtubule-severing proteins such as katanin (Steward et al., 1984).

An interesting group of MAPs are the microtubule plus-end tracking proteins (+TIPs) (Akhmanova and Steinmetz, 2008). These are structurally different factors which all share specific association with the microtubule plus-ends. One of the first proteins for which plus end tracking behaviour was described, was Cytoplasmic Linker Protein of 170 kDa (CLIP170) (Perez et al., 1999). CLIPs act as microtubule rescue factors in mammalian cells (Komarova et al., 2002). CLIP-170 was also shown to interact with several other +TIPs like CLASPs and p150[glued], a part of the dynactin complex, which will be discussed in more detail in chapter 1.2.3. (Lansbergen et al., 2004) CLIP-170 and its partners stabilise microtubules and may assist in capturing them at the cell cortex (Lansbergen et al., 2004; Lansbergen and Akhmanova, 2006).

Another important +TIP family is the End Binding (EB) protein family. The EBs bind to most other known +TIPs, like CLIPs and CLASPs, and help to recruit them, directly or indirectly, to microtubule plus-ends. The EB proteins seem to function as a hub where other plus-end binding proteins can bind and influence microtubule dynamics (Lansbergen and Akhmanova, 2006).

1.2 Motor proteins

Active transport in cells depends on motor proteins that move along the cytoskeletal filaments. Both actin and microtubule networks (but not the intermediate filaments) are used as tracks by motor proteins. There are three major classes of molecular motors: myosins, kinesins and dyneins. Myosins use actin filaments for their motility, while both kinesins and dyneins bind to and move along microtubules.
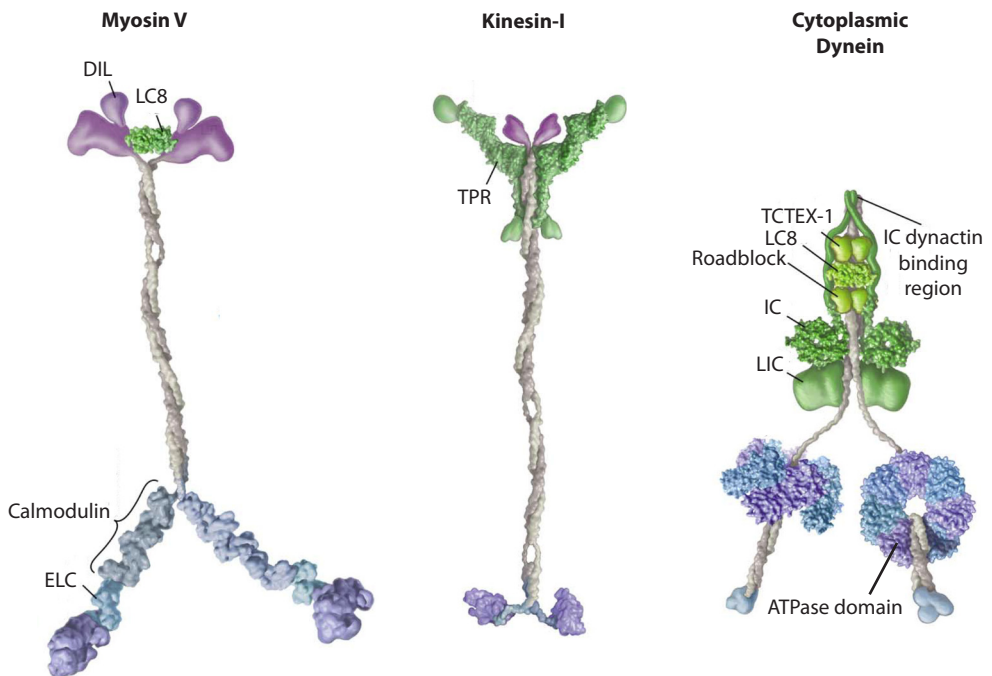
Figure 5. Molecular motors

Depicted are three members of the three motor families. Common protein structures and functional domains share the same colors. Catalytic domains are shown in dark blue, the mechanical amplifiers are light blue and the coiled-coil regions are shown in white. MyosinV is a dimeric motor with two catalytic domains and large calmodulin domains on each side of the molecule. The light chain of Myosin V is in green (LC8) and the cargo-binding domain "dilute" (DIL) in purple. Kinesin- I is also a dimeric motor with a similar architecture as MyosinV with in purple the cargo binding domains. Cytoplasmic dynein has 6 ATpase domains which are shown in mixed purple, blue shadings to illustrate the distinct domains that compromise the motor head. The intermediate (IC), light intermediate chains (LIC) and light chains (TCTEX-1, LC8 and Roadblock) are shown in green. (Adapted from Vale R.D. 2003, Cell, Vol. 112, 467–480).

1.2.1 Myosins

Myosins diversified very early in evolution and most eukaryotic cells contain several representatives of this family. Based on the phylogenetic analysis of the motor domain the myosin superfamily can be divided into ~25 classes. Mammals have approximately forty genes encoding myosin motors. Not all classes are represented in mammals, some myosins are plant-specific (Thompson and Langford, 2002; Richards and Cavalier-Smith, 2005).

To illustrate the diversity of the myosin motors, two myosin classes, myosin II and V, will be described. Myosin II, also called conventional myosin, is well known for its function in the muscle. The myosin II family contains at least 15 members in vertebrates, including non-muscle myosin II (Conti and Adelstein, 2008). A myosin II motor is composed of a pair of heavy chains that contain an N-terminal motor domain, a neck domain, which functions as a lever arm, and a long coiled-coil region that ends with a short tail. Myosin light chains bind the neck domain to control the ATPase activity of the motor (Conti and Adelstein, 2008). The N-terminal motor domains generate force on the actin filaments and are responsible for movement. The coiled-coil domains have a rod-like structure and bind another myosin dimer in an anti-parallel fashion. Muscle myosin forms bundles, which are called thick filaments, while the non-muscle myosin II forms tetramers. The motor domains at the each end of the tetrameric complex associate with actin filaments (Cai et al., 2006). In muscle cells myosin II is responsible for producing the contractile force. The long coiled-coil tails of the individual molecules of the muscle myosin join together, forming the thick filaments of the sarcomere. The force-producing head domains stick out from the side of the thick filament and move along actin-based thin filaments (Kovats, 1949; Viniegra-Gonzalez and Morales, 1972). Non-muscle myosin II functions as an actin crosslinker and plays a role in cell migration, polarisation and adhesion (Even-Ram et al., 2007).

Another important myosin family member is myosin V (Fig. 5). The human genome contains three genes that code for myosin V motors, namely myosin Va, Vb, and Vc. The distribution of these three isoforms differs among tissues: myosin Va is highly expressed in neurons, myosin Vb has a broader distribution but seems to be enriched in kidney and myosin Vc is particularly abundant in epithelial cells (Rodriguez and Cheney, 2002). Myosin V is structurally similar to myosin II; the main structural difference between the two motors is that myosin V is dimeric. The long C-terminal coiled-coil region of the myosin V tail plays a role in binding to cargo and can regulate motor activity (Liu et al., 2006). Myosin V is involved in the short-range transport of synaptic vesicles, endosomes and pigment granules (melanosomes) in the actin-rich peripheral cell regions.

Binding of myosin V to its cargo is best understood in pigment-producing cells, melanocytes. In these cells, Rab27, a small GTPase of the Rab family, forms a complex with the linker protein melanophilin and recruits Myosin Va to melanosomes (Kuroda and Fukuda 2005). Rab11a, another member of the Rab family, is thought to recruit myosin Vb to endosomes (Lapierre et al., 2001),

while myosin Vc binds to Rab8-positive vesicles (Rodriguez and Cheney, 2002). It should be noted that members of the Rab family participate in transport not only in complex with myosins, but also with the microtubule-based motors, kinesin and dynein. The mechanistic behaviour of Myosin V is very similar to, for example, the behaviour of some kinesin family members, which will be discussed in the next chapter.

1.2.2. Kinesins

Kinesins are a family of microtubule-dependent motors that move mainly towards the microtubule plus-end. Similar to myosins, kinesins form a large family of motor proteins. The latest classification identifies 14 different classes of kinesins (Miki et al., 2005). Most kinesins possess an N-terminal motor domain, which has ATPase activity and is responsible for the movement of the motor. The C-terminal part contains a stalk and a tail essential for the binding to cargo (Hirokawa et al., 1989; Kanai et al., 2004). The motor head and the stalk/tail domain are connected by the neck domain, a short region with family-specific features that seems to regulate the activity of the kinesin motor (Endow and Waligora, 1998).

The best-studied example of an N-terminal motor is kinesin-1, also called conventional kinesin. Kinesin-1 forms dimers that transport various cargos to the plus-end of the microtubule. It has been reported that kinesin-1 transports mitochondria (Stowers et al., 2002). This phenomenon has been thoroughly investigated in *Drosophila* and Milton has been identified as an adaptor molecule linking kinesin-1 to the mitochondria and it facilitates their transport into the axon (Rice and Gelfand, 2006). The interaction between Milton, kinesin-1 and mitochondrial membrane is controlled by Miro, a small Rho-like GTPase. In mammalian cells, GRIF-1, a possible orthologue of the *Drosophila* Milton, is a candidate for facilitating the binding between mitochondria and kinesin-1 (Brickley et al., 2005). Other potential kinesin-1 cargos include early endosomes, exocytotic carriers, neuronal mRNA granules and synaptic vesicles (Ong et al., 2000; Setou et al., 2002; Miller et al., 2005; Gindhart, 2006)

The kinesin motor domain is not always positioned at the N-terminus of the molecule. Members of the kinesin-13 family, such as MCAK, have their motor domain located in the middle. Mitotic centromere associated kinesin (MCAK) binds the plus-ends of the microtubules and functions as a microtubule depolymerase aned is particularly important during mitosis (Hunter et al., 2003; Ogawa et al., 2004). Yet other kinesins, like KIFC2, possess a C-terminal motor domain and interestingly, these kinesins are minus-end directed (Hanlon et al., 1997; Saito et al., 1997; Yang et al., 2001). The variety of kinesin motors is large: they appear mostly as dimers, but also monomeric, dimeric and tetrameric motors are known. They functions in transport routes for vesicles and organelles or have specific mitotic functions such as involvement in spindle formation and chromosome segregation.

1.2.2.1 Kinesin movement

How do kinesins move? The kinesin motor head contains an ATPase domain; conversion of ATP into ADP results in conformational changes and movement. Similar to kinesin-1, most kinesins are dimers – two-headed motors that can literary step along the microtubule (Howard et al., 1989). In vitro, kinesin-1 is capable of making up to a hundred steps along the microtubule before dissociation. In vivo, cargos can be transported over very long distances without losing their track, most likely because several motors are simultaneously attached to a cargo.

The movement of a kinesin molecule can be dissected into a number of stages. When there are no microtubules, the detached motor heads prefer ADP molecules. Once a motor head binds to the microtubule, it releases its ADP and binds ATP. The bound motor head hydrolyses its ATP and possibly pushes the other motor head forward. After this second motor head finds a suitable spot on the microtubule to bind, it becomes the leading motor head. Firmly bound, it will release ADP and might pull the trailing motor head loose. It will then bind ATP, convert it into ADP and push the trailing motor head forward, closing the movement cycle (Cross et al., 2000; Carter and Cross, 2005; Carter and Cross, 2006)

Three hypotheses have been proposed to explain the coordination of motor domains which result in a processive kinesin motor (Auerbach and Johnson, 2005; Yildiz and Selvin, 2005) (Fig. 6). The inchworm model proposes a stepping behaviour in which there is only one leading motor head. Initially, the leading head is attached to the microtubule; the trailing head steps towards the leading one and attaches; next, the leading head makes a new step forward. This stepping behaviour results in 8nm steps and does not cause the rotation of the motor.

According to the symmetric hand-over-hand model, the heads exchange their position every step. In this model, the moving head passes the attached head on the same side of the microtubule, which means that the motor undergoes a 360 degrees rotation around its axis each two steps. However it is hard to imagine a similar 360 degrees rotation of the cargo, unless the interaction between cargo and motor is very flexible. The head displacements in this model are 16nm steps.

The asymmetric hand-over-hand model is similar to the symmetric one; the only difference is that the moving head passes the attached head on the other side of the microtubule. With every step the motor rotates 180 degrees and the rotation reverses with each subsequent step; therefore, the netto rotation after two steps is zero (Hua et al., 2002; Asbury et al., 2003). Single molecule and optical trap assays have shown that in vitro kinesin-1 seems to prefer asymmetric hand-over-hand behaviour. Whether kinesin-1 and other kinesins walk via a similar mechanism in vivo still has to be elucidated.
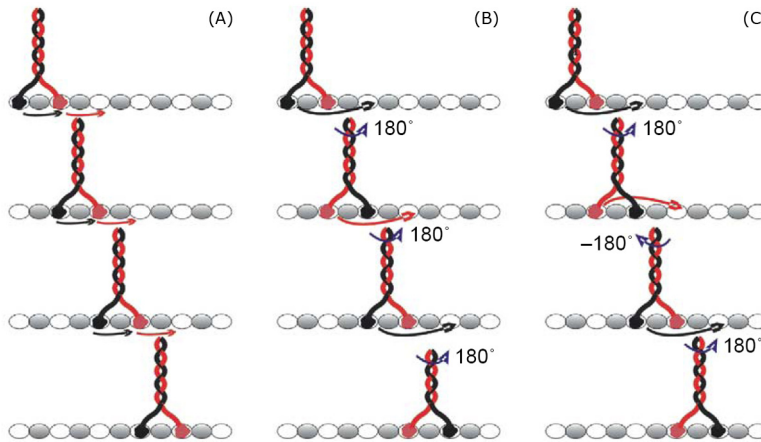
Figure 6. Conventional kinesin "stepping" models
(a) The inchworm model states that both heads move 8 nm with each ATP hydrolysed. The motor reverts to the same conformation without rotation of the stalk. (b) In the symmetric hand-over-hand model, the rear head moves forward while the front head stays bound to the microtubule. To revert to same physical state, kinesin rotates its stalk 180° every step. (c) During asymmetric hand-over-hand motion the trailing head passes the leading head and the stalk rotates 180° the next step it rotates back -180º (adapted and modified from Yildiz A, 2005, Trends in Cell Biol., Vol. 5 no. 2, 112–120)

1.2.3 Dynein

Dyneins are very large motor complexes that consist of one, two or three heavy chains, each more than 500 kDa, as well as a variable number of intermediate, light intermediate and light chains (Fig. 5 and 7)(Wickstead and Gull, 2007). The N-terminus of the heavy chain binds to the light and intermediate chains. The C-terminus contains a stalk, a microtubule binding domain and six ATPase domains that form a ring-like structure (King, 2000). The first ATPase domain of the dynein heavy chain provides the ATPase activity required for the movement. Intermediate and light chains of the dynein complex are thought to provide cargo binding and specificity. The total size of this large complex is up to two megadaltons.

Dynein steps along the microtubule by converting ATP with its ATPase domains in the heavy chains. The affinity for microtubules is regulated by a microtubule-binding site between the 4th and 5th ATPase domain and depends on the binding of ATP at the P1 site in the first ATPase domain. When the heavy chains are in an ATP-bound state, the affinity for microtubules is very low. When ATP is hydrolysed at the P1 site, a conformational change occurs resulting in a forward power stroke. The step size of a dimeric heavy chain dynein molecule is 8 nm (Kon et al., 2005; Numata et al., 2008). In vitro, dynein alone is capable of moving along the microtubule lattice over long distances. However, in vivo a second large complex, dynactin, is thought to be needed to keep cytoplasmic dynein on the microtubule track (Fig. 7).
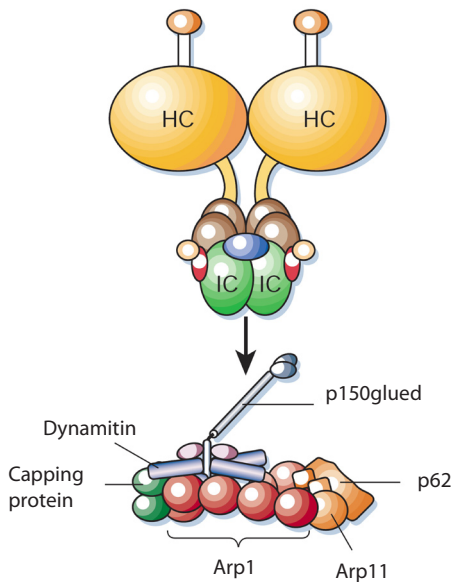
Figure 7. Schematic overview of the dynein and dynactin complexes
The dynein complex consists of Heavy Chains (Orange), Light Intermediate Chains (brown), Intermediate Chains (green) and the light chains Roadblock (yellow), LC8 (blue) and Tctex-1 (red). The dynactin complex is build from an actin-like filament Arp1 (red), capping proteins (green), Arp11 and p62 (orange). The Arp1 filament including capping proteins is linked to two p150^{glued} molecules (blue) by dynamitin (purple). (Image reproduced from Schliwa M., 2003, Nature 422, 759-765)

Two different types of dyneins have been identified, axonemal and cytoplasmic dynein. Axonemal dynein is an immobile motor located in cilia and flagella. Both cilia and flagella contain an axoneme. This is a specialised structure that consists of a central pair of microtubules (Fig. 8) surrounded by nine fused pairs of microtubule doublets (Summers and Gibbons, 1971). All axonemal dyneins are stably attached to the outer microtubule of the paired microtubules. Two forms of axonemal dyneins can be recognised: the outer-arm dyneins, which are located on the outside of the microtubule and the inner-arm dyneins that are located on the inside of the microtubule. In protozoa, the outer-arm dynein contains three heavy chains, while in metazoans only two heavy chains are present. The inner-arm dynein can be monomeric or dimeric and also contains light and intermediate chains (Fig. 7). Some light intermediate and light chains are shared by both axonemal and cytoplasmic dynein; other intermediate chains are isoform-specific. Movement of both inner and outer-arm dyneins results in sliding of the microtubules in the flagella. The sliding causes the beating of flagella, which propels forward certain algae or spermatozoa or causes the waving of cilia in the bronchia to move extracellular fluids.

Two forms of cytoplasmic dynein can be distinguished: cytoplasmic dynein 1 and cytoplasmic dynein 2 (Fig. 8). Dynein 2 is involved in the retrograde transport in cilia and flagella where it uses the microtubule doublets for cargo transport. Cytologically it is mainly found at the base of cilia and flagella and is required for axoneme maintenance (Porter et al., 1999; Mikami et al., 2002). Cytoplasmic dynein 1 is much more abundant and is the major motor responsible for minus-end directed cellular transport (Gibbons, 1996; Hirokawa, 1998).
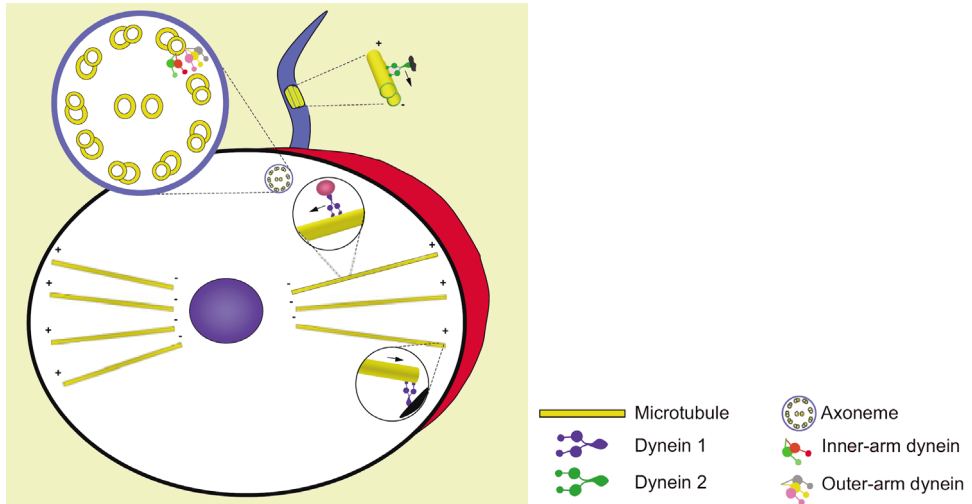
Figure 8. Axonemal and cytoplasmic dynein.
(Adopted from Hook P. 2003, Journal of Cell Science 119, 4369-4371)

Function and processivity of cytoplasmic dynein depends on another megadalton-sized complex, dynactin (Gill et al., 1991; King and Schroer, 2000). Dynactin contains a dimeric large subunit (called p150glued) that binds to the dynein intermediate chains (Vaughan and Vallee, 1995; Karki and Holzbaur, 1999). p150glued also binds microtubules and specifically recognises microtubule plus-ends via its CAP-Gly domain, a motif shared by other +TIPs like CLIP170 (Vaughan and Vallee, 1995; Lansbergen et al., 2004). The plus-end localisation of dynactin might serve as a cargo-docking site for minus-end directed transport where multimeric protein complexes such as plus-end directed motors or vesicles are loaded and transported back into the cell body.

Other components of dynactin include p50 (also known as dynamitin) and an actin-like filament, which contains Arp1 and capping proteins as its major subunits. The Arp1 filament of dynactin is believed to help dynein bind to its cargo (Holleran et al., 2001).

Several adaptor proteins have been described that form bridges between vesicle components and dynein/dynactin complexes. Lysosomes use the small GTPase Rab7 to recruit the dynein/dynactin motor complex via p150glued through the interaction with Rab7-interacting lysosomal protein (RILP) (Jordens et al., 2001; Johansson, et al., 2007). Another example of an adaptor protein is Bicaudal-D (BICD), which recruits dynein/dynactin to vesicles coated with the small GTPase Rab6. Whether BICD binds to dynein, dynactin or both complexes is not clear yet (Hoogenraad et al., 2001; Matanis et al., 2002; Hoogenraad et al., 2003). The functional properties of BICD are the main topic of this thesis and will be discussed in detail below.

1.2.3.1 Dynein/dynactin in mitosis

Dynein and dynactin play important roles in mitosis. Mutation of dynein and dynactin subunit-encoding genes that result in a non-functional dynein/dynactin motor complex are reported to be lethal in both mouse and in flies (Gepner et al., 1996; Harada et al., 1998). There are several functions for dynein/dynactin during cell division. First, the dynein/dynactin complex captures the astral microtubules at the cell periphery and helps to position the spindle, a process best studied in worms and budding yeast (Pearson and Bloom, 2004). Second, the dynein/dynactin complex interacts with microtubules at the kinetochore. It is known that dynein/dynactin is a part of the corona at the outer plate of the kinetochore (King et al., 2000), where it interacts with the Rod, Zw10 and Zwilch (RZZ) complex. During interphase, the components of this complex are localised in the cytoplasm (Basto et al., 2004). After Nuclear Envelope (NE) breakdown in prophase, they enter the nuclear region and attach to the kinetochores. ZW10 has been shown to bind to p50, an interaction likely to be responsible for targeting dynein/dynactin to the kinetochore (Williams et al., 2003). The concentrations of dynein are high on non-attached kinetochores. After the capture of the kinetochore fibres, dynein levels decrease and dynein appears to be responsible for removing outer domain and checkpoint proteins from the kinetochore (Howell et al., 2001). With the removal of these proteins from the kinetochores the cell will proceed into anaphase. Inhibition of dynein results in high concentrations of the spindle checkpoint factors at the kinetochore and an anaphase delay (Wojcik et al., 2001). Furthermore, dynein participates in poleward movement of chromosomes during chromosome alignment and in anaphase (Sharp et al., 2000)

1.3 Bicaudal-D - a conserved adaptor protein

Bicaudal-D (BicD) was first described as an essential factor required for *Drosophila* oogenesis and embryogenesis. Much later BicD was linked to the dynein/dynactin motor complex and was shown to be involved in the transport of vital components in the developing fruit fly embryo. BicD is conserved in higher eukaryotic organisms. To understand the function of BicD and its homologues I will first describe the development of the *Drosophila* oocyte and the contribution of BicD to this process.

1.3.1 The role of Bicaudal-D in *Drosophila*

Normal oocyte development in *Drosophila melanogaster* starts with an asymmetric division of a germline stem cell in the germarium which gives rise to a new stem cell and a cystoblast (Spradling et al., 1997) (Fig. 9). The cystoblast undergoes four rounds of mitosis with incomplete cytokinesis. This results in a cyst of 16 cells that remain interconnected via so-called ring canals (Kinderman, 1973) The ring canals are actin-rich structures that form cytoplasmic bridges.

The determination of the oocyte will occur in the first of the four mitotic events. One of the cells inherits the spectrosome, a germline specific organelle. During the other three mitotic divisions the spectrosome grows into the other cells forming a structure called the fusome, a large cytoplasmic organelle that connects all the cystocytes of the cyst through the ring canals. The spectrosome and fusome seem to lay the base for a new microtubule network that connects the 16 cells (Mahowald,

1972; Mahowald and Hardy, 1985). The MTOC of this microtubule network is established in the oocyte and the other 15 cells will become polyploid nurse cells, which grow in size by accumulating yolk material. The highly specialised nurse cells will provide the oocyte with mRNAs and other cellular components that drive the development of the oocyte.

BicD and Egalitarian, another factor involved in transport, are among the first components that
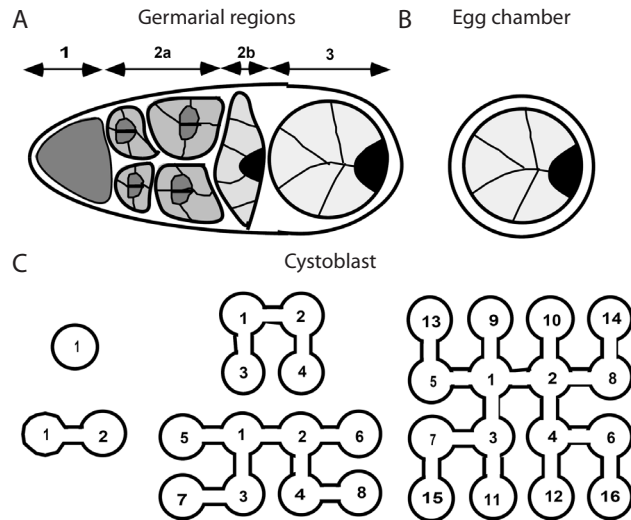
Figure 9. Diagram of the development of the *Drosophila* oocyte.
A) Germarial regions of *Drosophila melanogaster.* Region 1 contain germ line stem cells and mitotic cystoblasts. Region 2 contains early cystoblasts with 16 cells. In the 2b region oocyte determination has occurred and the microtubule network has been set up. Region 3 contains the egg chambers (B) with the oocyte positioned on the posterior pole of the egg chamber (Black). C) Schematic diagram of the 4 incomplete mitotic events, which result in a cyst with 16 cells interconnected via ring canals. (Adopted from Theurkauf W.E., 1993, Dev., 118. 1169-1180).

will accumulate in the oocyte. Together with the dynein/dynactin complex, BicD and Egalitarian facilitate the transport of mRNAs and other components into the oocyte. When the nurse cells have released their cellular content, they are broken down. Oocytes are absent in fruit flies homozygous or hemizygous for the loss-of-function alleles of BicD: all 16 cells in the cyst will adopt a nurse cell fate (Mohler and Wieschaus, 1986; Schupbach and Wieschaus, 1991). This indicates that BicD plays a role in the determination oocyte and the development and maintenance of the MTOC and microtubule network (Theurkauf et al., 1993). Mutations in dynein heavy chain and other dynein-influencing factors like Lis-1 also result in 16 nurse cell phenotypes, suggesting that dynein is likely to participate in this process (Gepner et al., 1996).

Dominant gain-of-function mutations of BicD give rise to the bicaudal phenotype (Mohler and

Wieschaus, 1986; Suter et al., 1989), which occurs much later in the development of the *Drosophila* embryo. Embryos with these mutations do not develop the head, thorax, and anterior-most three to five abdominal segments. Instead, these structures are replaced by a mirror image of the posterior abdominal segments and terminalia (Mohler and Wieschaus, 1986; Suter et al., 1989) (Fig. 10). In this stage of oocyte development, a microtubule-dependent gradient of mRNAs and proteins is being set up to determine the formation of the embryonic axes. Specific factors that coordinate the axes development are *Oskar* (osk) and *Gurken* (Grk), k10, *bicoid* and *orb* mRNAs (Swan and Suter, 1996; Clark et al., 2007). The specific localisation of, for example, bicoid, grk and osk mRNAs to the anterior and posterior poles of the oocyte defines the anterior/posterior and ventral/dorsal axes of the embryo (Riechmann and Ephrussi, 2001). The localisation, anchoring and transport of these mRNAs relies on the cooperation between kinesins, dynein/dynactin and their adaptor proteins. Mislocalisation of osk mRNAs to the anterior pole of the oocyte results in the bicaudal phenotype and is caused by gain of function mutations in BicD (Ephrussi et al., 1991; Kim-Ha et al., 1991). Other functions of BicD in flies include the positioning of the oocyte nucleus and involvement in the nuclear migration in the developing eye (Swan et al., 1999; Houalla et al., 2005).
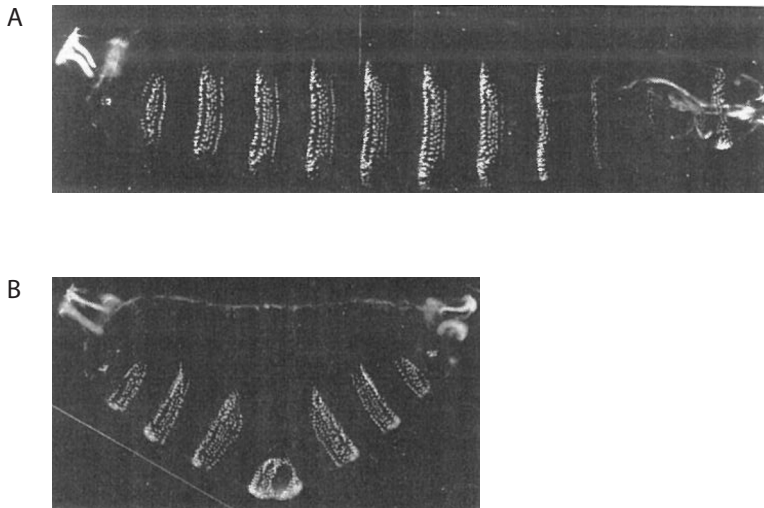
Figure 10. The Bicaudal phenotype
(A) Wild type *Drosophila* embryo with an anterior (left) and a posterior (right) part. (B) A bicaudal embryo. Note that the anterior part is missing and is replaced by a mirror image of the posterior part (images reproduced from Wharton R.P., 1989, Cell, vol. 59, 881-892)

1.3.2 The function of Bicaudal-D in mammalian cells

Two homologues of Bicaudal-D are present in the human genome: BICD1 and BICD2. Both proteins are highly conserved and show a remarkable homology to their *Drosophila* counterpart. Both BICD1 and BICD2 are rod-like proteins that consist of 5 coiled-coil regions (Baens and Marynen, 1997). The N-terminus of BICD2 has been shown to bind to the dynein/dynactin complex (Hoogenraad et al., 2001; Hoogenraad et al., 2003), although the exact binding site is not yet clear. Nocodazole-treated cells show a clear colocalisation between dynein/dynactin components and endogenous BICD1 and 2. Overexpression of the N-terminus of BICD2 induces Golgi and endosome dispersion, indicating that it inhibits dynein/dynactin function. The C-terminus of BICD2 is the cargo binding-domain, which interacts with the small GTPase Rab6 (Matanis et al., 2002). Overexpression of BICD2 C-terminus inhibits the minus-end directed movement of Rab6-positive vesicles. Therefore, BICD2 seems to function as an adaptor molecule, which couples dynein/dynactin motor complex to a cargo. This view is fully consistent with the function of BicD in flies.

1.3.3 Potential role of Bicaudal-D in motor coordination

Observation of microtubule-based transport of different cargos indicates that they do not move unidirectionally, but instead switch continuously between anterograde and retrograde movement. For example, BICD-positive Rab6 vesicles preferentially move to the cell periphery, towards microtubule plus ends but can stop and undergo short episodes of minus-end-directed motion (Matanis et al., 2002; Grigoriev et al., 2007). This transport is primarily dependent on a plus-end directed kinesin, while the major binding partner of BICD is the dynein/dynactin complex, which is responsible for movement in the opposite direction. Another example is mRNA transport during patterning of the *Drosophila* oocyte, which is also based on both dynein/dynactin and kinesin motors. How this bidirectional transport is regulated is a major question. Multiple studies have shown that although both kinesin and dynein are bound to the same vesicle, they do not engage in a tug of war. Instead, it is believed that a motor coordination machinery exists, the nature of which is not yet known, that steers the cargo to its destination by shutting down one motor while the opposing one is active (Welte, 2004). BICD as a linker protein might be part of such a coordination complex by binding both kinesin and dynein/dynactin. But if BICD is a part of the coordination machinery, what are the cellular regulators that control BICD and bidirectionality of vesicle movement? Which cargos, in addition to Rab6 vesicles, and which motors, in addition to dynein/dynactin, does BICD bind? What is the architecture of the motor complexes in which BICD participates? The aim of this thesis is to address these questions and in this way to uncover general principles underlying microtubule-based transport.

1.4 References

Akhmanova, A. and M. O. Steinmetz (2008). "Tracking the ends: a dynamic protein network controls the fate of microtubule tips." Nat Rev Mol Cell Biol 9(4): 309-22.

Amann, K. J. and T. D. Pollard (2000). "Cellular regulation of actin network assembly." Curr Biol 10(20): R728-30.

Asbury, C. L., A. N. Fehr, et al. (2003). "Kinesin moves by an asymmetric hand-over-hand mechanism." Science 302(5653): 2130-4.

Auerbach, S. D. and K. A. Johnson (2005). "Kinetic effects of kinesin switch I and switch II mutations." J Biol Chem 280(44): 37061-8.

Baens, M. and P. Marynen (1997). "A human homologue (BICD1) of the Drosophila bicaudal-D gene." Genomics 45(3): 601-6.

Basto, R., F. Scaerou, et al. (2004). "In vivo dynamics of the rough deal checkpoint protein during Drosophila mitosis." Curr Biol 14(1): 56-61.

Brickley, K., M. J. Smith, et al. (2005). "GRIF-1 and OIP106, members of a novel gene family of coiled-coil domain proteins: association in vivo and in vitro with kinesin." J Biol Chem 280(15): 14723-32.

Burbank, K. S. and T. J. Mitchison (2006). "Microtubule dynamic instability." Curr Biol 16(14): R516-7.

Cai, Y., N. Biais, et al. (2006). "Nonmuscle myosin IIA-dependent force inhibits cell spreading and drives F-actin flow." Biophys J 91(10): 3907-20.

Capetanaki, Y., R. J. Bloch, et al. (2007). "Muscle intermediate filaments and their links to membranes and membranous organelles." Exp Cell Res 313(10): 2063-76.

Carlier, M. F. (1998). "Control of actin dynamics." Curr Opin Cell Biol 10(1): 45-51.

Carter, N. J. and R. A. Cross (2005). "Mechanics of the kinesin step." Nature 435(7040): 308-12.

Carter, N. J. and R. A. Cross (2006). "Kinesin's moonwalk." Curr Opin Cell Biol 18(1): 61-7.

Chang, P. and T. Stearns (2000). "Delta-tubulin and epsilon-tubulin: two new human centrosomal tubulins reveal new aspects of centrosome structure and function." Nat Cell Biol 2(1): 30-5.

Clark, A., C. Meignin, et al. (2007). "A Dynein-dependent shortcut rapidly delivers axis determination transcripts into the Drosophila oocyte." Development 134(10): 1955-65.

Conti, M. A. and R. S. Adelstein (2008). "Nonmuscle myosin II moves in new directions." J Cell Sci 121(Pt 1): 11-8.

Coulombe, P. A. and M. B. Omary (2002). "'Hard' and 'soft' principles defining the structure, function and regulation of keratin intermediate filaments." Curr Opin Cell Biol 14(1): 110-22.

Cross, R. A., I. Crevel, et al. (2000). "The conformational cycle of kinesin." Philos Trans R Soc Lond B Biol Sci 355(1396): 459-64.

Desai, A. and T. J. Mitchison (1997). "Microtubule polymerization dynamics." Annu Rev Cell Dev Biol 13: 83-117.

Endow, S. A. and K. W. Waligora (1998). "Determinants of kinesin motor polarity." Science 281(5380): 1200-2.

Ephrussi, A., L. K. Dickinson, et al. (1991). "Oskar organizes the germ plasm and directs localization of the posterior determinant nanos." Cell 66(1): 37-50.

Even-Ram, S., A. D. Doyle, et al. (2007). "Myosin IIA regulates cell motility and actomyosin-microtubule crosstalk." Nat Cell Biol 9(3): 299-309.

Furukawa, R. and M. Fechheimer (1997). "The structure, function, and assembly of actin filament bundles." Int Rev Cytol 175: 29-90.

Gepner, J., M. Li, et al. (1996). "Cytoplasmic dynein function is essential in Drosophila melanogaster." Genetics 142(3): 865-78.

Gibbons, I. R. (1996). "The role of dynein in microtubule-based motility." Cell Struct Funct 21(5): 331-42.

Gill, S. R., T. A. Schroer, et al. (1991). "Dynactin, a conserved, ubiquitously expressed component of an activator of vesicle motility mediated by cytoplasmic dynein." J Cell Biol 115(6): 1639-50.

Gindhart, J. G. (2006). "Towards an understanding of kinesin-1 dependent transport pathways through the study of protein-protein interactions." Brief Funct Genomic Proteomic 5(1): 74-86.

Goldman, R. D., B. Grin, et al. (2008). "Intermediate filaments: versatile building blocks of cell structure." Curr Opin Cell Biol 20(1): 28-34.

Grigoriev, I., D. Splinter, et al. (2007). "Rab6 regulates transport and targeting of exocytotic carriers." Dev Cell 13(2): 305-14.

Hanlon, D. W., Z. Yang, et al. (1997). "Characterization of KIFC2, a neuronal kinesin superfamily member in mouse." Neuron 18(3): 439-51.

Harada, A., Y. Takei, et al. (1998). "Golgi vesiculation and lysosome dispersion in cells lacking cytoplasmic dynein." J Cell Biol 141(1): 51-9.

Heald, R. and E. Nogales (2002). "Microtubule dynamics." J Cell Sci 115(Pt 1): 3-4.

Helfand, B. T., L. Chang, et al. (2003). "The dynamic and motile properties of intermediate filaments." Annu Rev Cell Dev Biol 19: 445-67.

Hesse, M., T. M. Magin, et al. (2001). "Genes for intermediate filament proteins and the draft sequence of the human genome: novel keratin genes and a surprisingly high number of pseudogenes related to keratin genes 8 and 18." J Cell Sci 114(Pt 14): 2569-75.

Hirokawa, N. (1998). "Kinesin and dynein superfamily proteins and the mechanism of organelle transport." Science 279(5350): 519-26.

Hirokawa, N., K. K. Pfister, et al. (1989). "Submolecular domains of bovine brain kinesin identified by electron microscopy and monoclonal antibody decoration." Cell 56(5): 867-78.

Holleran, E. A., L. A. Ligon, et al. (2001). "beta III spectrin binds to the Arp1 subunit of dynactin." J Biol Chem 276(39): 36598-605.

Hoogenraad, C. C., A. Akhmanova, et al. (2001). "Mammalian Golgi-associated Bicaudal-D2 functions in the dynein-dynactin pathway by interacting with these complexes." Embo J 20(15): 4041-54.

Hoogenraad, C. C., P. Wulf, et al. (2003). "Bicaudal D induces selective dynein-mediated microtubule minus end-directed transport." Embo J 22(22): 6004-15.

Houalla, T., D. Hien Vuong, et al. (2005). "The Ste20-like kinase misshapen functions together with Bicaudal-D and dynein in driving nuclear migration in the developing drosophila eye." Mech Dev 122(1): 97-108.

Howard, J., A. J. Hudspeth, et al. (1989). "Movement of microtubules by single kinesin molecules." Nature 342(6246): 154-8.

Howell, B. J., B. F. McEwen, et al. (2001). "Cytoplasmic dynein/dynactin drives kinetochore protein transport to the spindle poles and has a role in mitotic spindle checkpoint inactivation." J Cell Biol 155(7): 1159-72.

Hua, W., J. Chung, et al. (2002). "Distinguishing inchworm and hand-over-hand processive kinesin movement by neck rotation measurements." Science 295(5556): 844-8.

Hubbert, C., A. Guardiola, et al. (2002). "HDAC6 is a microtubule-associated deacetylase." Nature 417(6887): 455-8.

Hunter, A. W., M. Caplow, et al. (2003). "The kinesin-related protein MCAK is a microtubule depolymerase that forms an ATP-hydrolyzing complex at microtubule ends." Mol Cell 11(2): 445-57.

Janmey, P. A., U. Euteneuer, et al. (1991). "Viscoelastic properties of vimentin compared with other filamentous biopolymer networks." J Cell Biol 113(1): 155-60.

Johansson, M., N. Rocha, et al. (2007). "Activation of endosomal dynein motors by stepwise assembly of Rab7-RILP-p150Glued, ORP1L, and the receptor betalll spectrin." J Cell Biol 176(4): 459-71.

Jordens, I., M. Fernandez-Borja, et al. (2001). "The Rab7 effector protein RILP controls lysosomal transport by inducing the recruitment of dynein-dynactin motors." Curr Biol 11(21): 1680-5.

Kanai, Y., N. Dohmae, et al. (2004). "Kinesin transports RNA: isolation and characterization of an RNA-transporting granule." Neuron 43(4): 513-25.

Karki, S. and E. L. Holzbaur (1999). "Cytoplasmic dynein and dynactin in cell division and intracellular transport." Curr Opin Cell Biol 11(1): 45-53.

Kerkhoff, E. (2006). "Cellular functions of the Spir actin-nucleation factors." Trends Cell Biol 16(9): 477-83.

Kim-Ha, J., J. L. Smith, et al. (1991). "oskar mRNA is localized to the posterior pole of the Drosophila oocyte." Cell 66(1): 23-35.

Kinderman, N. B. (1973). "Oogenesis in Drosophila virilis. Interactions between the ring canal rims and the nucleus of the oocyte " Bio bulletin 144.

King, J. M., T. S. Hays, et al. (2000). "Dynein is a transient kinetochore component whose binding is regulated by microtubule attachment, not tension." J Cell Biol 151(4): 739-48.

King, S. J. and T. A. Schroer (2000). "Dynactin increases the processivity of the cytoplasmic dynein motor." Nat Cell Biol 2(1): 20-4.

King, S. M. (2000). "The dynein microtubule motor." Biochim Biophys Acta 1496(1): 60-75.

Kirmse, R., S. Portet, et al. (2007). "A quantitative kinetic model for the in vitro assembly of intermediate filaments from tetrameric vimentin." J Biol Chem 282(25): 18563-72.

Kline-Smith, S. L. and C. E. Walczak (2004). "Mitotic spindle assembly and chromosome segregation: refocusing on microtubule dynamics." Mol Cell 15(3): 317-27.

Komarova, Y. A., A. S. Akhmanova, et al. (2002). "Cytoplasmic linker proteins promote microtubule rescue in vivo." J Cell Biol 159(4): 589-99.

Kon, T., T. Mogami, et al. (2005). "ATP hydrolysis cycle-dependent tail motions in cytoplasmic dynein." Nat Struct Mol Biol 12(6): 513-9.

Kovats, J. (1949). "Myosin and actomyosin content of the heart-muscle." Nature 163(4146): 606.

Kuroda, T. S. and M. Fukuda (2005). "Identification and biochemical analysis of Slac2-c/MyRIP as a Rab27A-, myosin Va/VIIa-, and actin-binding protein." Methods Enzymol 403: 431-44.

Lansbergen, G. and A. Akhmanova (2006). "Microtubule plus end: a hub of cellular activities." Traffic 7(5): 499-507.

Lansbergen, G., Y. Komarova, et al. (2004). "Conformational changes in CLIP-170 regulate its binding to microtubules and dynactin localization." J Cell Biol 166(7): 1003-14.

Lapierre, L. A., R. Kumar, et al. (2001). "Myosin vb is associated with plasma membrane recycling systems." Mol Biol Cell 12(6): 1843-57.

Liu, J., D. W. Taylor, et al. (2006). "Three-dimensional structure of the myosin V inhibited state by cryoelectron tomography." Nature 442(7099): 208-11.

Mahowald, A. P. (1972). "Ultrastructural observations on oogenesis in Drosophila." J Morphol 137(1): 29-48.

Mahowald, A. P. and P. A. Hardy (1985). "Genetics of Drosophila embryogenesis." Annu Rev Genet 19: 149-77.

Martys, J. L., C. L. Ho, et al. (1999). "Intermediate filaments in motion: observations of intermediate filaments in cells using green fluorescent protein-vimentin." Mol Biol Cell 10(5): 1289-95.

Matanis, T., A. Akhmanova, et al. (2002). "Bicaudal-D regulates COPI-independent Golgi-ER transport by recruiting the dynein-dynactin motor complex." Nat Cell Biol 4(12): 986-92.

McIntosh, J. R. and K. L. McDonald (1989). "The mitotic spindle." Sci Am 261(4): 48-56.

Mikami, A., S. H. Tynan, et al. (2002). "Molecular structure of cytoplasmic dynein 2 and its distribution in neuronal and ciliated cells." J Cell Sci 115(Pt 24): 4801-8.

Miki, H., Y. Okada, et al. (2005). "Analysis of the kinesin superfamily: insights into structure and function." Trends Cell Biol 15(9): 467-76.

Miller, K. E., J. DeProto, et al. (2005). "Direct observation demonstrates that Liprin-alpha is required for trafficking of synaptic vesicles." Curr Biol 15(7): 684-9.

Mohler, J. and E. F. Wieschaus (1986). "Dominant maternal-effect mutations of Drosophila melanogaster causing the production of double-abdomen embryos." Genetics 112(4): 803-22.

Numata, N., T. Kon, et al. (2008). "Molecular mechanism of force generation by dynein, a molecular motor belonging to the AAA+ family." Biochem Soc Trans 36(Pt 1): 131-5.

Ogawa, T., R. Nitta, et al. (2004). "A common mechanism for microtubule destabilizers-M type kinesins stabilize curling of the protofilament using the class-specific neck and loops." Cell 116(4): 591-602.

Ong, L. L., A. P. Lim, et al. (2000). "Kinectin-kinesin binding domains and their effects on organelle motility." J Biol Chem 275(42): 32854-60.

Osborn, M. and K. Weber (1976). "Cytoplasmic microtubules in tissue culture cells appear to grow from an organizing structure towards the plasma membrane." Proc Natl Acad Sci U S A 73(3): 867-71.

Parry, D. A., S. V. Strelkov, et al. (2007). "Towards a molecular description of intermediate filament structure and assembly." Exp Cell Res 313(10): 2204-16.

Pearson, C. G. and K. Bloom (2004). "Dynamic microtubules lead the way for spindle positioning." Nat Rev Mol Cell Biol 5(6): 481-92.

Perez, F., G. S. Diamantopoulos, et al. (1999). "CLIP-170 highlights growing microtubule ends in vivo." Cell 96(4): 517-27.

Pollard, T. D. (2007). "Regulation of actin filament assembly by Arp2/3 complex and formins." Annu Rev Biophys Biomol Struct 36: 451-77.

Pollard, T. D., L. Blanchoin, et al. (2000). "Molecular mechanisms controlling actin filament dynamics in nonmuscle cells." Annu Rev Biophys Biomol Struct 29: 545-76.

Porter, M. E., R. Bower, et al. (1999). "Cytoplasmic dynein heavy chain 1b is required for flagellar assembly in Chlamydomonas." Mol Biol Cell 10(3): 693-712.

Rice, S. E. and V. I. Gelfand (2006). "Paradigm lost: milton connects kinesin heavy chain to miro on mitochondria." J Cell Biol 173(4): 459-61.

Richards, T. A. and T. Cavalier-Smith (2005). "Myosin domain evolution and the primary divergence of eukaryotes." Nature 436(7054): 1113-8.

Riechmann, V. and A. Ephrussi (2001). "Axis formation during Drosophila oogenesis." Curr Opin Genet Dev 11(4): 374-83.

Rodriguez, O. C. and R. E. Cheney (2002). "Human myosin-Vc is a novel class V myosin expressed in epithelial cells." J Cell Sci 115(Pt 5): 991-1004.

Saito, N., Y. Okada, et al. (1997). "KIFC2 is a novel neuron-specific C-terminal type kinesin superfamily motor for dendritic transport of multivesicular body-like organelles." Neuron 18(3): 425-38.

Schupbach, T. and E. Wieschaus (1991). "Female sterile mutations on the second chromosome of Drosophila melanogaster. II. Mutations blocking oogenesis or altering egg morphology." Genetics 129(4): 1119-36.

Selby, C. C. and R. S. Bear (1956). "The structure of actin-rich filaments of muscles according to x-ray diffraction." J Biophys Biochem Cytol 2(1): 71-85.

Setou, M., D. H. Seog, et al. (2002). "Glutamate-receptor-interacting protein GRIP1 directly steers kinesin to dendrites." Nature 417(6884): 83-7.

Sharp, D. J., G. C. Rogers, et al. (2000). "Cytoplasmic dynein is required for poleward chromosome movement during mitosis in Drosophila embryos." Nat Cell Biol 2(12): 922-30.

Spradling, A. C., M. de Cuevas, et al. (1997). "The Drosophila germarium: stem cells, germ line cysts, and oocytes." Cold Spring Harb Symp Quant Biol 62: 25-34.

Steward, R., F. J. McNally, et al. (1984). "Isolation of the dorsal locus of Drosophila." Nature 311(5983): 262-5.

Stowers, R. S., L. J. Megeath, et al. (2002). "Axonal transport of mitochondria to synapses depends on milton, a novel Drosophila protein." Neuron 36(6): 1063-77.

Strelkov, S. V., H. Herrmann, et al. (2003). "Molecular architecture of intermediate filaments." Bioessays 25(3): 243-51.

Summers, K. E. and I. R. Gibbons (1971). "Adenosine triphosphate-induced sliding of tubules in trypsin-treated flagella of sea-urchin sperm." Proc Natl Acad Sci U S A 68(12): 3092-6.

Suter, B., L. M. Romberg, et al. (1989). "Bicaudal-D, a Drosophila gene involved in developmental asymmetry: localized transcript accumulation in ovaries and sequence similarity to myosin heavy chain tail domains." Genes Dev 3(12A): 1957-68.

Swan, A., T. Nguyen, et al. (1999). "Drosophila Lissencephaly-1 functions with Bic-D and dynein in oocyte determination and nuclear positioning." Nat Cell Biol 1(7): 444-9.

Swan, A. and B. Suter (1996). "Role of Bicaudal-D in patterning the Drosophila egg chamber in mid-oogenesis." Development 122(11): 3577-86.

Thazhath, R., M. Jerka-Dziadosz, et al. (2004). "Cell context-specific effects of the beta-tubulin glycylation domain on assembly and size of microtubular organelles." Mol Biol Cell 15(9): 4136-47.

Thazhath, R., C. Liu, et al. (2002). "Polyglycylation domain of beta-tubulin maintains axonemal architecture and affects cytokinesis in Tetrahymena." Nat Cell Biol 4(3): 256-9.

Theurkauf, W. E., B. M. Alberts, et al. (1993). "A central role for microtubules in the differentiation of Drosophila oocytes." Development 118(4): 1169-80.

Thompson, R. F. and G. M. Langford (2002). "Myosin superfamily evolutionary history." Anat Rec 268(3): 276-89.

Tian, G., S. A. Lewis, et al. (1997). "Tubulin subunits exist in an activated conformational state generated and maintained by protein cofactors." J Cell Biol 138(4): 821-32.

Toivola, D. M., G. Z. Tao, et al. (2005). "Cellular integrity plus: organelle-related and protein-targeting functions of intermediate filaments." Trends Cell Biol 15(11): 608-17.

Tzur, Y. B., K. L. Wilson, et al. (2006). "SUN-domain proteins: 'Velcro' that links the nucleoskeleton to the cytoskeleton." Nat Rev Mol Cell Biol 7(10): 782-8.

Vandekerckhove J. and Weber K. (1978). "At least six different actins are expressed in a higher mammal: an analysis based on the amino acid sequence of the amino-terminal tryptic peptide." J Mol Biol 126:783–802

Vaughan, K. T. and R. B. Vallee (1995). "Cytoplasmic dynein binds dynactin through a direct interaction between the intermediate chains and p150Glued." J Cell Biol 131(6 Pt 1): 1507-16.

Verhey, K. J. and J. Gaertig (2007). "The tubulin code." Cell Cycle 6(17): 2152-60.

Viniegra-Gonzalez, G. and M. F. Morales (1972). "Toward a theory of muscle contraction." J Bioenerg 3(1): 55-64.

Wang, Y. L. (1985). "Exchange of actin subunits at the leading edge of living fibroblasts: possible role of treadmilling." J Cell Biol 101(2): 597-602.

Wegner, A. (1976). "Head to tail polymerization of actin." J Mol Biol 108(1): 139-50.

Welte, M. A. (2004). "Bidirectional transport along microtubules." Curr Biol 14(13): R525-37.

Wickstead, B. and K. Gull (2007). "Dyneins across eukaryotes: a comparative genomic analysis." Traffic 8(12): 1708-21.

Williams, B. C., Z. Li, et al. (2003). "Zwilch, a new component of the ZW10/ROD complex required for kinetochore functions." Mol Biol Cell 14(4): 1379-91.

Wojcik, E., R. Basto, et al. (2001). "Kinetochore dynein: its dynamics and role in the transport of the Rough deal checkpoint protein." Nat Cell Biol 3(11): 1001-7.

Xia, L., B. Hai, et al. (2000). "Polyglycylation of tubulin is essential and affects cell motility and division in Tetrahymena thermophila." J Cell Biol 149(5): 1097-106.

Yang, Z., E. A. Roberts, et al. (2001). "Functional analysis of mouse C-terminal kinesin motor KifC2." Mol Cell Biol 21(7): 2463-6.

Yildiz, A. and P. R. Selvin (2005). "Kinesin: walking, crawling or sliding along?" Trends Cell Biol 15(2): 112-20.

Yoon, K. H., M. Yoon, et al. (2001). "Insights into the dynamic properties of keratin intermediate filaments in living epithelial cells." J Cell Biol 153(3): 503-16.

Yoon, M., R. D. Moir, et al. (1998). "Motile properties of vimentin intermediate filament networks in living cells." J Cell Biol 143(1): 147-57.

Rab6 regulates transport and targeting of exocytotic carriers

2

Rab6 Regulates Transport and Targeting of Exocytotic Carriers

Ilya Grigoriev,[1] Daniël Splinter,[1] Nanda Keijzer,[2] Phebe S. Wulf,[2] Jeroen Demmers,[3] Toshihisa Ohtsuka,[5] Mauro Modesti,[4] Ivan V. Maly,[6] Frank Grosveld,[1] Casper C. Hoogenraad,[2] and Anna Akhmanova[1,*]

[1] Department of Cell Biology
[2] Department of Neuroscience
[3] Department of Biochemistry
[4] Department of Genetics
Erasmus Medical Center, 3000 CA Rotterdam, The Netherlands
[5] Department of Clinical and Molecular Pathology, University of Toyama, Sugitani 2630, Toyama 930-0194, Japan
[6] Department of Computational Biology, University of Pittsburgh School of Medicine, Pittsburgh, PA 15261, USA
*Correspondence: anna.akhmanova@chello.nl
DOI 10.1016/j.devcel.2007.06.010

SUMMARY

Constitutive exocytosis delivers newly synthesized proteins, lipids, and other molecules from the Golgi apparatus to the cell surface. This process is mediated by vesicles, which bud off the trans-Golgi network, move along cytoskeletal filaments, and fuse with the plasma membrane. Here, we show that the small GTPase Rab6 marks exocytotic vesicles and, together with the microtubule plus-end-directed motor kinesin-1, stimulates their processive microtubule-based transport to the cell periphery. Furthermore, Rab6 directs targeting of secretory vesicles to plasma-membrane sites enriched in the cortical protein ELKS, a known Rab6 binding partner. Our data demonstrate that although Rab6 is not essential for secretion, it controls the organization of exocytosis within the cellular space.

INTRODUCTION

Constitutive exocytosis transports newly synthesized lipids and membrane proteins as well as components of the extracellular matrix to the plasma membrane in all eukaryotic cells. It is generally accepted that this process is mediated by Golgi-derived vesicles, which move along microtubules (MTs) or actin filaments and fuse with the plasma membrane. In spite of the ubiquitous nature of constitutive secretion and its essential role in the cellular flow of membranes and proteins, relatively little is known about the mechanisms that control the motility, docking, and fusion of its carriers.

Rab GTPases are important regulatory factors of vesicular traffic in the secretory and endocytic pathways (Grosshans et al., 2006; Jordens et al., 2005). Members of the Rab6 family, Rab6A, Rab6A', and Rab6B, decorate the Golgi apparatus and cytoplasmic vesicles and regulate protein transport between the Golgi, endoplasmic reticulum (ER), plasma membrane, and endosomes (Del Nery et al., 2006; Girod et al., 1999; Jasmin et al., 1992; Martinez et al., 1997; Martinez et al., 1994; Opdam et al., 2000; Utskarpen et al., 2006; White et al., 1999; Young et al., 2005). Rab6B is predominantly expressed in the brain tissue (Opdam et al., 2000) and is absent from HeLa cells that were the subject of this study. Rab6A and Rab6A' differ by only a few amino acids, and their differential functions are not yet entirely clear (Del Nery et al., 2006; Utskarpen et al., 2006; Young et al., 2005). They are both expressed in HeLa cells; in this manuscript, we will collectively call them Rab6 when referring to the endogenous protein. Although a number of studies demonstrated an important role for Rab6 in retrograde transport from endosomes to the Golgi and in COPI-independent recycling of the Golgi enzymes to the ER (Del Nery et al., 2006; Girod et al., 1999; White et al., 1999; Young et al., 2005), the role of Rab6-decorated vesicles in these processes remained unclear. In HeLa cells, the majority of GFP-Rab6A and GFP-Rab6A'-positive vesicles exit from the Golgi and move along MTs to the plus ends at the cell periphery where they disappear by presumably fusing with their target (Del Nery et al., 2006; White et al., 1999). It has been suggested that this target is a specialized peripheral compartment of the ER and that Rab6 vesicles represent carriers responsible for Golgi-ER recycling (Sannerud et al., 2003; White et al., 1999). However, a subsequent study demonstrated the importance of minus-end-directed MT motors for the Rab6-dependent Golgi-ER recycling and proposed that this process occurs in close proximity to the Golgi apparatus (Young et al., 2005). Here, we investigated the function of Rab6-positive vesicles moving to MT plus ends and found that they represent carriers of constitutive secretion and that Rab6 is important for regulating their movement and fusion.

RESULTS AND DISCUSSION

Rab6 Vesicles Contain Exocytotic Markers

To analyze in detail the function and behavior of Rab6 vesicles, we have generated a HeLa cell line stably

Figure 1. Rab6 Colocalizes with Markers of Exocytosis in HeLa Cells

(A) Representative frame of a simultaneous two-color movie of a HeLa cell expressing VSVG-YFP and mStrawberry-Rab6A. Cells were incubated overnight at 39.5°C, 2 hr at 19°C, and 10 min at 37°C prior to imaging.

(B) Representative frame of a simultaneous two-color movie of a HeLa cell expressing GFP-Rab6A and NPY-mRFP. Cells were maintained at 37°C during the whole experiment.

(C) Representative frame of a simultaneous two-color movie of a HeLa cell expressing GFP-Rab6A, incubated with Cy3-STB at 4°C for 30 min, and, after unbound STB was washed away, incubated for 1 hr at 37°C prior to imaging. In (A)–(C), cell edges are shown by a stippled line.

(D) Staining for endogenous Rab6 in HeLa cells expressing the indicated exocytosis markers. VSVG-YFP and NPY-Venus-expressing cells were treated as described in (A) and (B), respectively; BDNF-GFP-expressing cells were incubated for 2 hr at 19°C and for 10 min at 37°C prior to fixation.

(E) Quantification of vesicle colocalization in cells prepared as described in (D). Red and green bars in each plot correspond to all counted vesicles (Rab6 and cargo, respectively), whereas yellow parts of each bar correspond to double-labeled vesicles. Numbers of counted vesicles are as follows: Rab6A/VSVG-YFP: 2303 vesicles in 30 cells; Rab6A/BDNF-GFP: 2583 vesicles in 25 cells; Rab6A/NPY-Venus: 2717 vesicles in 35 cells. Error bars indicate SD.

expressing GFP-Rab6A (Figure S1A in the Supplemental Data available with this article online). In agreement with the published data (Del Nery et al., 2006; White et al., 1999), the majority of GFP-Rab6A-positive vesicles emerged from the Golgi and moved to the cell periphery where they disappeared (Movie S1; Figure S1). This long-range movement strongly depended on intact MTs and was not significantly affected by the actin-depolymerizing drug latrunculin B (Figure S1B). We noticed that in contrast to saltatory motion of many other organelles in HeLa cells, both GFP-Rab6A vesicles and

exocytotic carriers labeled with the temperature-sensitive vesicular stomatitis virus glycoprotein (VSVG)-YFP (a membrane protein) or neuropeptide Y (NPY)-Venus (a secreted protein) displayed persistent flow from the Golgi complex to the cell periphery (for VSVG, this type of movement was already described [Hirschberg et al., 1998]). A similarity in motility patterns prompted us to investigate the colocalization of these markers. Indeed, Golgi-derived motile vesicles containing VSVG-YFP or NPY-mRFP showed a significant overlap with fluorescently tagged Rab6A (Figures 1A and 1B; Movies S2 and S3).

Not only GFP-Rab6A but also endogenous Rab6 displayed extensive colocalization with the two above-mentioned markers of exocytosis as well as with another secreted protein, BDNF-GFP (Figure 1D). In HeLa cells, ~60%–70% of Rab6-positive vesicles contained exocytotic markers, and 35%–70% of the latter colocalized with Rab6 vesicles (Figure 1E). Localization of endogenous Rab6 to the vesicles bearing exocytotic markers was also observed in other cell lines (Figure S2). Although the optimal colocalization of VSVG-YFP and BDNF-GFP with Rab6 required a preceding incubation at 19°C, and this incubation could be used to synchronize their transport from the Golgi (Saraste and Kuismanen, 1984), such treatment was not necessary for observing ~70% overlap between Rab6 and NPY-Venus vesicles (Figures 1D and 1E), indicating that in steady-state conditions, a major proportion of NPY-Venus exits from the Golgi in Rab6-positive carriers.

Previous studies suggesting that Rab6-positive vesicles fuse with the ER were based on observing the trafficking of Shiga toxin B (STB) subunit, which travels from the plasma membrane to the Golgi through endosomes and subsequently moves from the Golgi to the ER (White et al., 1999). We could readily reproduce this pattern of STB trafficking (Figure S3A). At the stage when STB moves from the Golgi to ER, we observed occasional colocalization of Cy3-labeled STB with GFP-Rab6A in vesicle-like structures (Figures S3B and S3C; Movies S4 and S5). However, most of the colocalizing structures were immotile, and the majority of GFP-Rab6A vesicles moving from the Golgi to the cell margin were devoid of Cy3-STB (Figure 1C; Movie S4). Because of the high background labeling by Cy3-STB, it was difficult to estimate the exact degree of colocalization between STB and Rab6 in fixed cells. Therefore, we used live cells in which we photobleached Cy3-STB signals in the lamella outside the Golgi area. Because there was very little redistribution of the Cy3-STB background labeling on the time scale of minutes, we could reliably monitor the presence of even very weak Cy3-STB signals in GFP-Rab6A-positive vesicles exiting from the Golgi (Figure S3C). On the basis of these experiments, ~8% of Golgi-derived GFP-Rab6A vesicles contained Cy3-STB (Figure S3D). Existence of such double-positive vesicles is in line with previous studies (White et al., 1999) and explains why we previously observed Golgi-to-ER recycling cargo in Rab6-vesicle accumulations induced by overexpression of Bicaudal D2 (BICD2) C terminus (Matanis et al., 2002). We cannot exclude that STB-positive Rab6 vesicles fuse with a different compartment than the Rab6-vesicles bearing exocytotic markers. Alternatively, the presence of STB in a small proportion of Rab6 vesicles may reflect its missorting into the secretory route.

Rab6 Vesicles Fuse with the Plasma Membrane

HeLa cells stably expressing NPY-Venus secrete a considerable amount of this protein into culture medium (Figure 2E), although no detectable ER labeling by NPY-Venus can be discerned (Figures 1B and 1D; Figure S2).

These observations indicate that NPY/Rab6 double-positive vesicles fuse with the plasma membrane and not with the ER.

Exocytotic events at the ventral plasma membrane can be visualized by total internal reflection fluorescence microscopy (TIRFM): Because of the fact that the evanescent wave displays an exponential decay, vesicles approaching the coverslip and fusing with the membrane display a sharp increase in their fluorescence intensity (Schmoranzer et al. [2000] and Toomre et al. [2000] and references therein). By using TIRFM, we could readily visualize "bursts" of fluorescence preceding the disappearance of vesicles labeled with all three exocytotic markers and with GFP-Rab6A (Figures 2A–2C). Interestingly, signal fading occurred more rapidly for secreted proteins NPY-Venus and BDNF-GFP than for membrane-bound VSVG-YFP or for GFP-Rab6A. In agreement with this observation, simultaneous two-color TIRF imaging of NPY-mRFP and GFP-Rab6A-positive vesicles showed that during fusion, the disappearance of the NPY-mRFP signal preceded the loss of the GFP-Rab6A marker (Figures 2D and 2F). After the NPY-mRFP signal vanished, the GFP-Rab6A signal persisted and then gradually spread out, possibly because of diffusion in the plasma membrane (Figure 2F).

Next, we used fluorescence recovery after photobleaching (FRAP) experiments to show that mStrawberry-Rab6A did not recover on individual NPY-Venus-positive vesicles; this finding indicates that once the vesicle exits the Golgi, no exchange of Rab6 takes place until its fusion with the target site (Figures 2G and 2H). We conclude that a significant proportion of exocytotic carriers bear Rab6 GTPase when they exit the Golgi and that they lose this marker only after fusing with the plasma membrane.

Rab6 Is Required for Processive Movement of Exocytotic Vesicles

To address the role of Rab6 in exocytotic vesicle transport, we used previously published siRNAs to deplete both Rab6A and Rab6A' (Young et al., 2005). Three days after siRNA transfection, we observed at least 90% depletion of both Rab6 isoforms (Figure S4A). In agreement with previously published data, such depletion did not block exocytosis of NPY-Venus (Del Nery et al. [2006] Martinez et al. [1994], and White et al. [1999]; data not shown). The secretion of VSVG was delayed but not abolished after Rab6 knockdown (Figure 3A). This effect could reflect some abnormalities in ER-Golgi or intra-Golgi transport because we did observe defects in Golgi morphology similar to those described by others (Del Nery et al. [2006] and Young et al. [2005]; data not shown).

After Rab6 depletion, NPY-Venus-containing vesicles still exited the Golgi and fused with the plasma membrane, but the pattern of their motion was altered (Figure 3B; Movie S6). Although the total number of NPY-positive vesicles did not change significantly (Figure 3D), vesicle motility was reduced: The number of displacements per vesicle was diminished by a factor 2.5 (number of
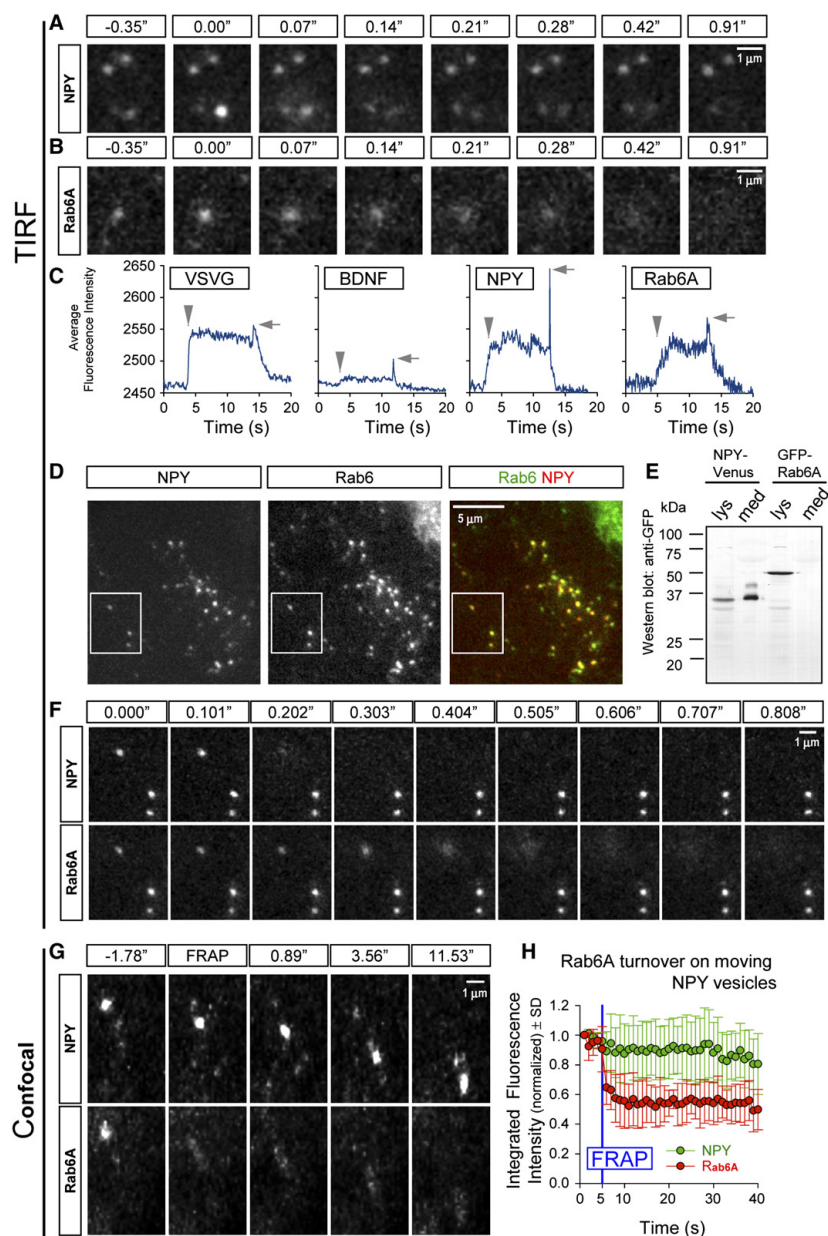
Figure 2. The Behavior of Rab6 on Individual Exocytotic Vesicles

(A and B) Frames from TIRFM movies showing the behavior of single NPY-Venus and GFP-Rab6A vesicles immediately before and during fusion. Time is indicated; 0″ corresponds to the sharp increase of fluorescent signal.

(C) Average fluorescent intensity of a single VSVG-YFP, BDNF-GFP, NPY-Venus, and GFP-Rab6A vesicle (a circle with a radius 0.78 µm) plotted versus time. Vesicle appearance in the focal plane is indicated by arrowheads. Arrows point to the peaks of fluorescence intensity, corresponding to vesicle fusion with the plasma membrane.

displacements longer than 1 μm with a velocity exceeding 0.3 μm/s per 100 μm^2 per 1 min per 10 vesicles was 17.24 ± 8.3 [mean ± SD] in control cells and 6.84 ± 3.22 in Rab6-depleted cells). The processivity of NPY-vesicle movement to the cell periphery was reduced in Rab6-depleted cells because of frequent interruptions by pauses and short reversals (Figure 3C). The length of individual tracks was significantly diminished, although the velocity of vesicle movement was slightly increased (Figure 3D). These data suggest that Rab6 regulates recruitment or activity of MT-based motors on exocytotic vesicles. Still, exocytotic vesicles exhibit bidirectional motility also in the absence of Rab6, indicating that alternative mechanisms for motor association with such vesicles must exist.

Kinesin-1 and Cytoplasmic Dynein Participate in Transport of Rab6 Vesicles

Because most of Rab6-vesicle movements are directed to MT plus ends, they should be powered by a kinesin; the exact nature of the motor involved is a subject of dispute (Echard et al., 1998; Hill et al., 2000). Previous studies identified Bicaudal D1/D2 (BICD1/2) proteins as linkers between Rab6-bound membranes and cytoplasmic dynein (Matanis et al., 2002; Short et al., 2002; Young et al., 2005). We performed a mass-spectrometry-based screen for BICD2 partners and identified the heavy chain of kinesin-1 (KIF5B) as a potential interacting protein (Table S1). The binding between kinesin-1 and BICD2 was much weaker than the previously identified association of BICD2 with dynein-dynactin; this was reflected in our inability to find significant coprecipitation of BICD1/2 and kinesin-1 (Hoogenraad et al. [2003]; data not shown). However, by using yeast two-hybrid system, we were able to confirm the interaction between the middle part of BICD2 and the tail of kinesin-1 (Figure S5A). This interaction was further supported by reciprocal immunoprecipitation of the middle part of BICD2 and the full-length kinesin-1 isoforms KIF5A and KIF5B from overexpressing HEK293 cells (Figure S5B). This interaction was strongly suppressed in the full-length BICD2, in agreement with our previous data that BICD2 may selfinactivate by intramolecular interaction of its N- and C-termini (Hoogenraad et al., 2001; Hoogenraad et al., 2003) (Figure S5B).

We used two different siRNAs to deplete kinesin-1 (KIF5B) by at least ∼90% (Figures S4A and S4B) and found that such a treatment significantly affected the processive motility of GFP-Rab6A or NPY-Venus-positive vesicles because of frequent reversals in the direction of movement (Figures 3B, 3C, and 3E; Movie S7; and data

not shown). However, MT plus-end-directed transport of these vesicles was not abolished, and its velocity was slightly increased (Figure 3E). The effects of Rab6 and kinesin-1 knockdown on vesicle transport were not due to defects in MT organization, which appeared normal (Figure S4E). Taken together, our findings show that Rab6 and kinesin-1 ensure processive MT plus-end-directed motion of exocytotic carriers. The residual plus-end-directed movement of Rab6 vesicles is most likely to be powered by another kinesin because it was abolished by nocodazole but was not significantly affected by latrunculin B (Figures S6A and S6B).

Because previous studies provided strong indications for association among Rab6, BICD1/2, and cytoplasmic dynein (Matanis et al., 2002; Short et al., 2002; Young et al., 2005), we also investigated dynein involvement in Rab6-vesicle movement. Two different siRNAs caused a ∼70% and ∼80% depletion of the cytoplasmic dynein heavy chain (DHC) and a concomitant depletion of the dynein intermediate chain (Figure S4C). In agreement with previously published data, dynein depletion caused Golgi dispersion (Harada et al., 1998) (Figure S4D). Still, Rab6 vesicles were motile, and their velocity was slightly increased (Figure S6E); it was difficult to compare their motion patterns to those in control cells because the MT network in dynein-depleted cells was substantially disorganized (Figure S4E).

A striking feature of dynein knockdown cells was a significant increase in the number of immotile Rab6 vesicles: ∼80% depletion of DHC caused an almost 4-fold reduction in the number of displacements per vesicle (Figures S6C and S6D). This suggests that cytoplasmic dynein constitutes an important part of the Rab6-bound motor complex, necessary for bidirectional vesicle movement. The association of BICD1/2 with Rab6, kinesin-1, and dynein-dynactin is likely to contribute to motor recruitment and regulation. Interestingly, in *Drosophila*, BicD acts in mRNA transport processes that also involve both cytoplasmic dynein and kinesin-1 (Riechmann and Ephrussi, 2001).

Cortical Protein ELKS Is Involved in the Docking/ Fusion of Rab6 Vesicles

Next, we investigated whether Rab6 participates in the selection of vesicle-fusion sites. Previous studies have identified ELKS (also known as CAST2, Rab6IP2, or ERC1 [Deguchi-Tawarada et al., 2004; Monier et al., 2002; Nakata et al., 1999; Wang et al., 2002]) as a direct binding partner of Rab6 and showed that it is present at the cortical sites of regulated secretion in neurons and

---

(D and F) Simultaneous two-color TIRFM imaging of a cell expressing NPY-mRFP and GFP-Rab6A. (F) shows time-lapse images of the enlarged area of the cell boxed in (D). Time is indicated.

(E) Western blots with GFP antibodies of cell lysates ("lys") and culture media ("med") of HeLa cells stably expressing NPY-Venus and GFP-Rab6A.

(G) Frames from a two-color confocal movie of a single vesicle double labeled for NPY-Venus and mStrawberry-Rab6A. In the second shown frame, the mStrawberry signal was bleached in a small part of the cell by five iterations of 561 nm diode laser (100% of power).

(H) Quantification of the FRAP data obtained as in (G). Mean integrated fluorescence intensity (normalized for the first value) of NPY-Venus and mStrawberry-Rab6A on single vesicles. Measurements were performed in a circle with a radius 0.7 μm; five vesicles in five cells were measured. Error bars indicate SD.
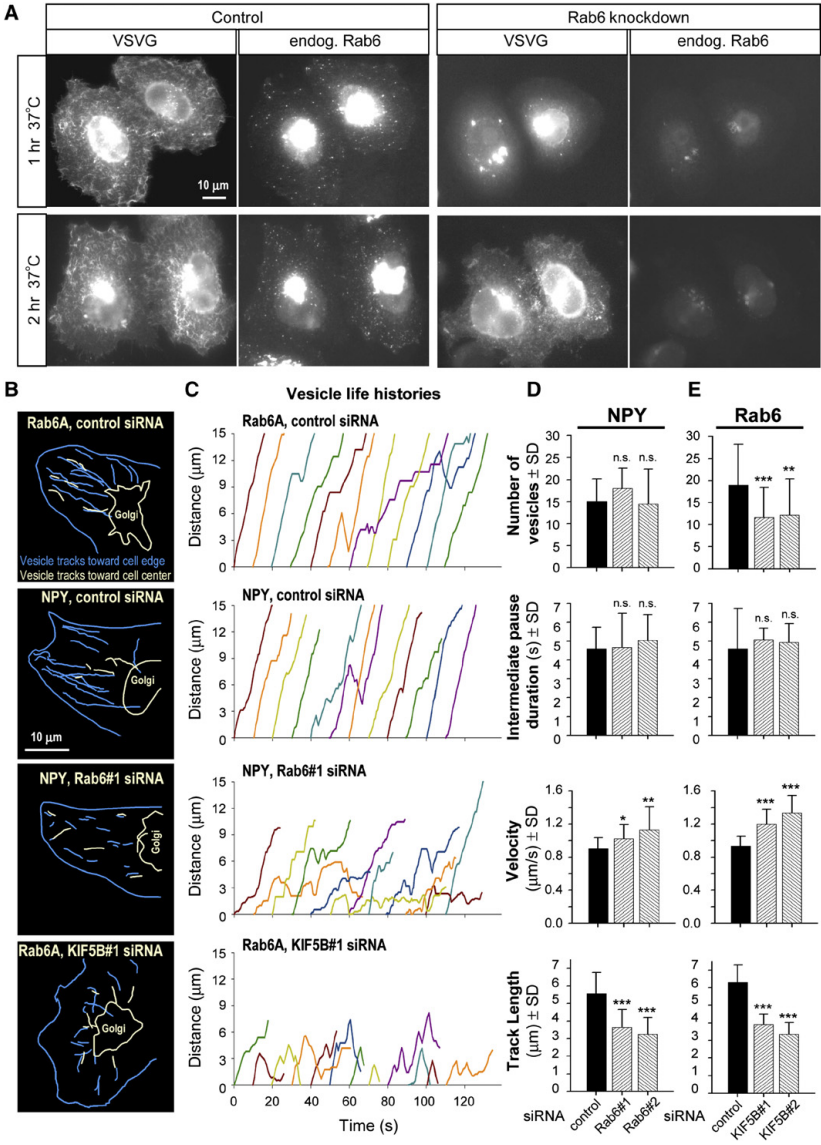
Figure 3. Effects of Rab6 and Kinesin-1 Depletion on Exocytosis and Vesicle Trafficking

(A) VSVG-YFP trafficking assays in cells transfected with the control or Rab6#1 siRNAs. Cells were incubated overnight at 39.5°C, 2 hr at 19°C, and 1 or 2 hr at 37°C prior to fixation.

(B) Vesicle tracks in HeLa cells stably expressing GFP-Rab6A or NPY-Venus transfected with the indicated siRNAs. Tracks were defined as unidirectional movement episodes not interrupted by pauses (periods longer than two frames [1.14 s] when the vesicle moved with a velocity less than ~0.3 μm/s).

(C) Life-history plots of the vesicles traced from the Golgi in HeLa cells stably expressing GFP-Rab6A or NPY-Venus, transfected with the indicated siR-NAs. Each plot shows representative histories of vesicles from at least three different cells. Position (0) corresponds to the initial position of the vesicle near the Golgi.

(D and E) NPY-Venus- and Rab6-vesicle number (per 100 μm² in fixed cells) and characterization of cell-edge-directed vesicle movements in cells stably expressing NPY-Venus or GFP-Rab6A, transfected with the indicated siRNAs. Velocity was computed as displacement between frames divided by the

pancreatic β-cells and is important for efficient exocytosis (Inoue et al., 2006; Ohara-Imaizumi et al., 2005). Depletion of ELKS by a previously characterized siRNA (Lansbergen et al., 2006) caused a dramatic accumulation of Rab6 vesicles at the cell periphery (Figures 4A and 4B; Movie S8). Most of these vesicles contained NPY-Venus, indicating that they were exocytotic carriers (Figure 4C). Vesicle accumulation could be rescued by a GFP-fused ELKSα or ELKSε expression constructs bearing silent mutations that made them resistant to the used siRNA (Figure 4D and data not shown). ELKS deletion mutants lacking either the C-terminal part of the Rab6-binding domain (the last 171 amino acids of ELKSε, [Monier et al., 2002]) or the N-terminal 121 amino acids were unable to rescue Rab6-vesicle accumulation in ELKS-depleted cells (Figure 4D and data not shown), indicating that the full-length ELKS molecule is needed to control Rab6-vesicle number.

Depletion of ELKS had no effect on the frequency of vesicle appearance at the Golgi or on any parameters of MT-based movement (Figures 4E–4H). However, the duration of the pause between vesicle arrival to the cell margin and the actual fusion was increased in ELKS knockdown cells by a factor of three (Figure 4I). These data indicate that ELKS knockdown impairs either docking and (or) fusion of Rab6 vesicles. In ELKS-depleted cells, the GFP-Rab6A vesicles remained more motile in the vicinity of the cell margin (the diffusion coefficient D was significantly greater than that in control cells: D was 0.025 ± 0.008 $\mu m^2/s$ (mean ± SD) in ELKS knockdown cells and 0.015 ± 0.004 $\mu m^2/s$ in control cells), suggesting that ELKS may participate in vesicle docking.

The prolonged delay in vesicle docking/fusion induced by ELKS depletion was not sufficient to block secretion in HeLa cells (data not shown). However, the fact that ELKS normally accelerates Rab6-vesicle docking/fusion may cause preferential exocytosis at the ELKS-positive sites. In HeLa cells, ELKS is present in peripheral cortical clusters, where it colocalizes almost completely with its binding partner LL5β (Lansbergen et al., 2006). We found that the disappearance of individual GFP-Rab6A vesicles indeed often correlated with their interaction with the ELKS-LL5β patches visualized by mRFP-LL5β (Figure 4J; Movie S9). Similarly to GFP-Rab6A, NPY-Venus-labeled vesicles also displayed delayed fusion after ELKS knockdown (Figure 4I), and the majority (~80%) of exocytosis events at the ventral plasma membrane observed by TIRFM occurred at the cell periphery directly at or adjacent to ELKS-LL5β patches (Figure 4K). Interestingly, although the depletion of Rab6 made the trafficking of NPY-Venus vesicles more chaotic (Figures 3B and 3C), it actually reduced the duration of the last pause preceding fusion (Figure 4I). Moreover, in cells depleted for both Rab6 and ELKS, NPY-Venus-containing vesicles did not show peripheral accumulation, in contrast to depletion of ELKS alone, and the duration of the pause

before fusion was again shorter than that in control cells (Figure 4I and data not shown). Exocytosis events in Rab6-depleted cells were distributed randomly throughout the cell and displayed much less colocalization with ELKS-LL5β patches (Figure 4K). It appears therefore that one of the functions of Rab6 on exocytotic vesicles is to prevent their premature fusion so that they can be targeted to ELKS-positive cortical sites.

Conclusions

Taken together, our data show that Rab6 is abundantly present on exocytotic vesicles and is needed to regulate their behavior. Our data do not preclude the involvement of Rab6 GTPase in recycling from Golgi to ER; they do indicate, however, that in contrast to previously published studies, including our own (Matanis et al., 2002; Sannerud et al., 2003; White et al., 1999), the major target for Rab6-vesicle fusion is the plasma membrane and not the ER. Our findings help to explain the recently discovered exocytosis defects in Rab6 mutants during *Drosophila* oogenesis (Coutelis and Ephrussi, 2007) as well as the observations on the role of Rab6 in the trafficking of membrane proteins such as rhodopsin (Deretic, 1998). In addition to its role at the Golgi, Rab6 regulates exocytosis by enhancing processive kinesin-dependent motion of secretory vesicles from the Golgi to MT plus ends. Furthermore, Rab6 is required for targeting these vesicles to the cortical ELKS-containing patches where MT plus ends are attached (Lansbergen et al., 2006). Therefore, although Rab6 is not essential for anterograde transport, it plays an important role in the spatial organization of constitutive exocytosis.

EXPERIMENTAL PROCEDURES

Cell Culture and Transfection of Plasmids and siRNAs

HeLa, COS-7, CHO, MDCK, MRC5, HEK293, and NRK cells were grown as described previously (Lansbergen et al., 2006). PolyFect (QIAGEN), Lipofectamine 2000 (Invitrogen), or FuGENE 6 (Roche) were used for plasmid transfection. The stable HeLa clones were selected with fluorescence activated cell sorting (FACS) and cultured in the presence of 0.4 mg/ml G418 (Roche).

siRNAs were synthesized by Ambion; their target sequences can be found in the Supplemental Data. Cells were transfected with 5 nM siRNAs with HiPerFect (QIAGEN) and analyzed 3 days after transfection. For rescue experiments, cells were transfected with siRNAs, transfected with the rescue plasmids 2 days later, and imaged after an additional day in culture.

Expression Constructs

We used the following previously described expression vectors: GFP-Rab6A (Matanis et al., 2002), VSVG3-SP-YFP (Toomre et al., 2000) (a gift of Dr. K.Simons, MPI Molecular Cell Biology and Genetics, Dresden, Germany), NPY-Venus (Nagai et al., 2002) (a gift of Dr. A. Miyawaki, RIKEN, Wako City, Japan), GFP-ELKSα (Deguchi-Tawarada et al., 2004), GFP-ELKSε, mRFP-LL5β, and BirA (Lansbergen et al., 2006). BDNF-GFP was constructed from a BDNF-encoding rat cDNA in pEGFP-N1 by a PCR-based strategy. For generating

interval between frames. Tracks and pauses were defined as in (B). Pauses were divided into intermediate (preceded and followed by movement episodes) and terminal (followed by vesicle disappearance) (see also Figure S1). Error bars indicate SD. Values significantly different from control are indicated by asterisks (***$p < 0.001$, **$p < 0.01$, *$p < 0.05$, n.s., $p > 0.05$, Mann-Whitney U test; see Supplemental Data for details).
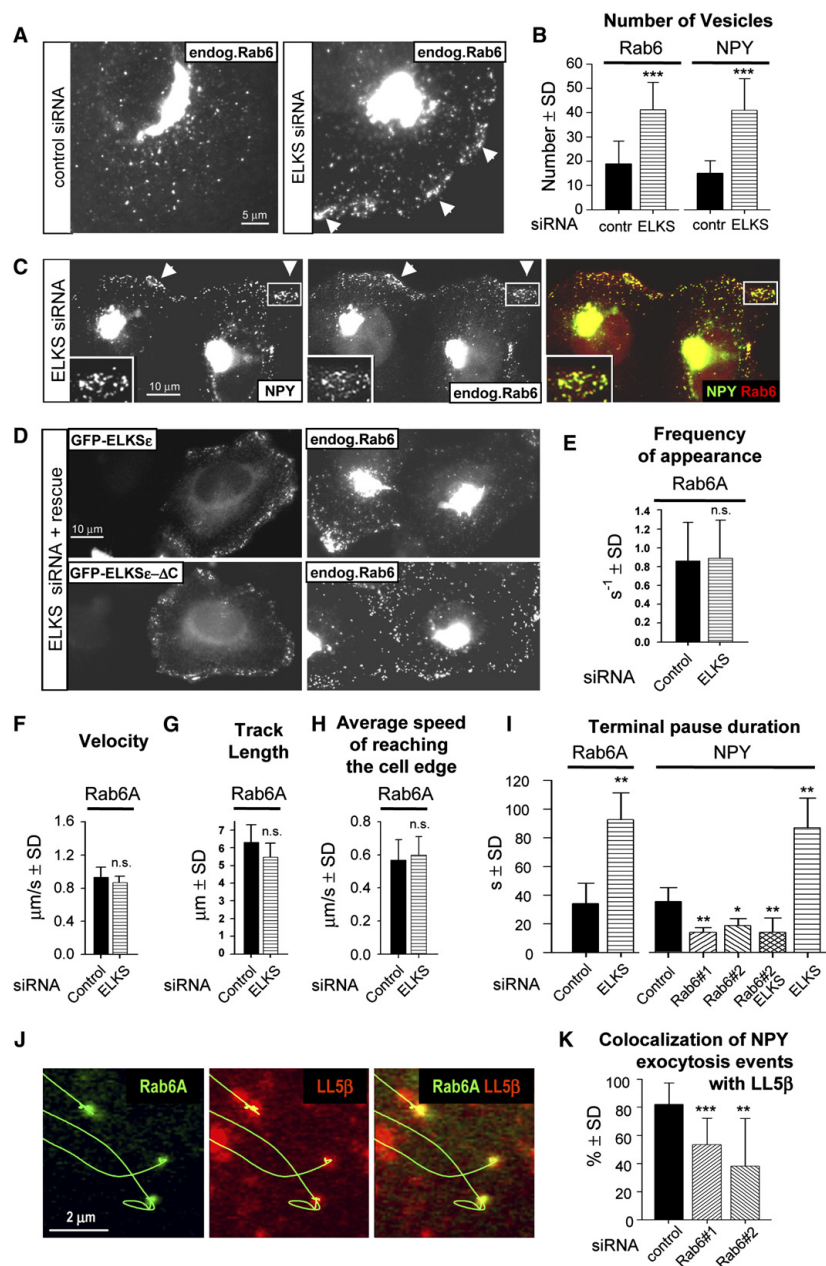
Figure 4. Effects of ELKS Depletion on the Behavior of Rab6 Vesicles

(A and C) The original HeLa cell line (A) or HeLa cells stably expressing NPY-Venus (C) were transfected with the control or ELKS siRNAs and stained for Rab6. Peripheral accumulations of Rab6 vesicles are indicated by arrowheads.

(B) Number of endogenous Rab6 vesicles and NPY-Venus vesicles (per 100 μm^2 in fixed cells) after transfection with the control or ELKS siRNAs.

mStrawberry-Rab6A and PA-GFP-Rab6A, GFP in GFP-Rab6A was substituted for mStrawberry (Shaner et al., 2004) (a gift of Dr. R.Tsien, UCSD, La Jolla, USA) or PA-GFP (Patterson and Lippincott-Schwartz, 2002) (a gift from J. Lippincott-Schwartz, NIH, Bethesda, USA). NPY-mRFP was constructed by substituting Venus for mRFP (a gift of Dr. R.Tsien). We generated biotinylation and GFP-tagged BICD2 N-terminus (Bio-GFP-BICD2-NT, BICD2 amino acids 1–575) from GFP-BICD2-NT by cloning in front of the GFP a linker encoding the amino acid sequence MASGLNDIFEAQKIEWHEGGG. KIF5A and KIF5B with an N-terminal Myc tag were generated in the GW1 vector by a PCR-based strategy with IMAGE clones 1630386/6195468 (KIF5A) and 4422906/6165834 (KIF5B). GFP-ELKSα and ε rescue constructs were generated by conversion of the siRNA target region 5′-AGTGGG AAAACCCTTTCAATG-3′ to 5′-TCAGGAAAGACCTTAAGCATG-3′ with a PCR-based strategy. The GFP-ELKSε-ΔC was generated from the full-length rescue construct by XbaI-NotI digestion and religation. GFP-ELKSα construct that was missing the N-terminal 121 amino acids was described previously (Inoue et al., 2006).

Antibodies, Immunofluorescent Staining, Immunoprecipitation, Western Blotting, Fluorescence Microscopy, and Image Analysis

We used rabbit polyclonal antibodies against GFP (Abcam), ELKS (Deguchi-Tawarada et al., 2004), DHC, KIF5B (Santa Cruz), Myc tag (Cell Signaling) and used mouse monoclonal antibodies against Rab6 (which recognizes Rab6A and Rab6A', a gift of A. Barnekow, University of Muenster, Germany), β-tubulin (Sigma), dynein intermediate chain (Chemicon), Myc tag (Santa Cruz), and GFP (Roche). For secondary antibodies, Alexa-350-, Alexa-488-, and Alexa-594-conjugated goat antibodies against rabbit, rat, and mouse IgG were purchased from Molecular Probes. Fresh medium was added to cells ∼1–2 hr before fixation. For vesicle visualization, cells were fixed with 4% paraformaldehyde in PBS for 15 min at room temperature. For visualizing MTs, a 15 min –20°C methanol fixation was used. Staining procedures were described previously (Matanis et al., 2002). Mitochondria were visualized with MitoTracker Red CMXRos (Molecular Probes). Immunoprecipitation and western blotting was performed as described previously (Lansbergen et al., 2006).

Images of fixed and live cells were acquired with fluorescent wide-field and confocal microscopes. Details of the microscope setups used and image processing are described in the Supplemental Data.

Identification of BICD2 Binding Partners by Mass Spectrometry and Yeast Two-Hybrid Assay

Streptavidin pulldown assays were performed with lysates of HeLa cells coexpressing bio-GFP-BICD2-NT together with BirA and BirA alone as described previously (Lansbergen et al., 2006). Proteins bound to streptavidin beads were separated on a 3%–8% NuPAGE Tris-Acetate Gel (Invitrogen). Experimental details of mass spectrometry and yeast two-hybrid analysis can be found in the Supplemental Data.

REFERENCES

Coutelis, J.B., and Ephrussi, A. (2007). Rab6 mediates membrane organization and determinant localization during Drosophila oogenesis. Development *134*, 1419–1430.

Deguchi-Tawarada, M., Inoue, E., Takao-Rikitsu, E., Inoue, M., Ohtsuka, T., and Takai, Y. (2004). CAST2: Identification and characterization of a protein structurally related to the presynaptic cytomatrix protein CAST. Genes Cells *9*, 15–23.

Del Nery, E., Miserey-Lenkei, S., Falguieres, T., Nizak, C., Johannes, L., Perez, F., and Goud, B. (2006). Rab6A and Rab6A' GTPases play non-overlapping roles in membrane trafficking. Traffic *7*, 394–407.

Deretic, D. (1998). Post-Golgi trafficking of rhodopsin in retinal photoreceptors. Eye *12*(Pt 3b), 526–530.

Echard, A., Jollivet, F., Martinez, O., Lacapere, J.J., Rousselet, A., Janoueix-Lerosey, I., and Goud, B. (1998). Interaction of a Golgi-associated kinesin-like protein with Rab6. Science *279*, 580–585.

Girod, A., Storrie, B., Simpson, J.C., Johannes, L., Goud, B., Roberts, L.M., Lord, J.M., Nilsson, T., and Pepperkok, R. (1999). Evidence for a COP-I-independent transport route from the Golgi complex to the endoplasmic reticulum. Nat. Cell Biol. *1*, 423–430.

Grosshans, B.L., Ortiz, D., and Novick, P. (2006). Rabs and their effectors: Achieving specificity in membrane traffic. Proc. Natl. Acad. Sci. USA *103*, 11821–11827.

Harada, A., Takei, Y., Kanai, Y., Tanaka, Y., Nonaka, S., and Hirokawa, N. (1998). Golgi vesiculation and lysosome dispersion in cells lacking cytoplasmic dynein. J. Cell Biol. *141*, 51–59.

Hill, E., Clarke, M., and Barr, F.A. (2000). The Rab6-binding kinesin, Rab6-KIFL, is required for cytokinesis. EMBO J. *19*, 5711–5719.

(D) ELKS-depleted HeLa cells were transfected with the indicated GFP-fused rescue constructs, fixed, and stained for Rab6.

(E–H) Characterization of cell-edge-directed vesicle movements in GFP-Rab6A-expressing cells transfected with the control or ELKS siRNAs. (E) shows the frequency of vesicle appearance at the Golgi. (F) and (G) show the velocity of vesicle movement and track length calculated as in Figure 3D. (H) shows the distance separating the sites of vesicle appearance at the Golgi and disappearance at the cell periphery divided by the total duration of vesicle movement between these sites (including intermediate pauses).

(I) Terminal pause duration in HeLa cells stably expressing GFP-Rab6A or NPY-Venus after transfection with the indicated siRNAs.

(J) Single frames from a two-color confocal movie of cells coexpressing PA-GFP-Rab6A and mRFP-LL5β. PA-GFP-Rab6A was photoactivated at the Golgi to allow unambiguous identification of Golgi-derived vesicles. Trajectories of the vesicles prior to their immobilization at the LL5β patches are indicated by green lines.

(K) Colocalization of NPY-Venus exocytosis events, registered as an increase of NPY vesicle fluorescence by TIRFM, with mRFP-LL5β patches. Exocytosis event was regarded as colocalizing with LL5β if it overlapped or was directly adjacent to mRFP-LL5β signal. Statistical analysis was performed as shown in Figure 3. Error bars indicate SD.

Hirschberg, K., Miller, C.M., Ellenberg, J., Presley, J.F., Siggia, E.D., Phair, R.D., and Lippincott-Schwartz, J. (1998). Kinetic analysis of secretory protein traffic and characterization of golgi to plasma membrane transport intermediates in living cells. J. Cell Biol. *143*, 1485–1503.

Hoogenraad, C.C., Akhmanova, A., Howell, S.A., Dortland, B.R., De Zeeuw, C.I., Willemsen, R., Visser, P., Grosveld, F., and Galjart, N. (2001). Mammalian Golgi-associated Bicaudal-D2 functions in the dynein-dynactin pathway by interacting with these complexes. EMBO J. *20*, 4041–4054.

Hoogenraad, C.C., Wulf, P., Schiefermeier, N., Stepanova, T., Galjart, N., Small, J.V., Grosveld, F., de Zeeuw, C.I., and Akhmanova, A. (2003). Bicaudal D induces selective dynein-mediated microtubule minus end-directed transport. EMBO J. *22*, 6004–6015.

Inoue, E., Deguchi-Tawarada, M., Takao-Rikitsu, E., Inoue, M., Kitajima, I., Ohtsuka, T., and Takai, Y. (2006). ELKS, a protein structurally related to the active zone protein CAST, is involved in Ca2+-dependent exocytosis from PC12 cells. Genes Cells *11*, 659–672.

Jasmin, B.J., Goud, B., Camus, G., and Cartaud, J. (1992). The low molecular weight guanosine triphosphate-binding protein Rab6p associates with distinct post-Golgi vesicles in Torpedo marmorata electrocytes. Neuroscience *49*, 849–855.

Jordens, I., Marsman, M., Kuijl, C., and Neefjes, J. (2005). Rab proteins, connecting transport and vesicle fusion. Traffic *6*, 1070–1077.

Lansbergen, G., Grigoriev, I., Mimori-Kiyosue, Y., Ohtsuka, T., Higa, S., Kitajima, I., Demmers, J., Galjart, N., Houtsmuller, A.B., Grosveld, F., and Akhmanova, A. (2006). CLASPs attach microtubule plus ends to the cell cortex through a complex with LL5beta. Dev. Cell *11*, 21–32.

Martinez, O., Antony, C., Pehau-Arnaudet, G., Berger, E.G., Salamero, J., and Goud, B. (1997). GTP-bound forms of rab6 induce the redistribution of Golgi proteins into the endoplasmic reticulum. Proc. Natl. Acad. Sci. USA *94*, 1828–1833.

Martinez, O., Schmidt, A., Salamero, J., Hoflack, B., Roa, M., and Goud, B. (1994). The small GTP-binding protein rab6 functions in intra-Golgi transport. J. Cell Biol. *127*, 1575–1588.

Matanis, T., Akhmanova, A., Wulf, P., Del Nery, E., Weide, T., Stepanova, T., Galjart, N., Grosveld, F., Goud, B., De Zeeuw, C.I., et al. (2002). Bicaudal-D regulates COPI-independent Golgi-ER transport by recruiting the dynein-dynactin motor complex. Nat. Cell Biol. *4*, 986–992.

Monier, S., Jollivet, F., Janoueix-Lerosey, I., Johannes, L., and Goud, B. (2002). Characterization of novel Rab6-interacting proteins involved in endosome-to-TGN transport. Traffic *3*, 289–297.

Nagai, T., Ibata, K., Park, E.S., Kubota, M., Mikoshiba, K., and Miyawaki, A. (2002). A variant of yellow fluorescent protein with fast and efficient maturation for cell-biological applications. Nat. Biotechnol. *20*, 87–90.

Nakata, T., Kitamura, Y., Shimizu, K., Tanaka, S., Fujimori, M., Yokoyama, S., Ito, K., and Emi, M. (1999). Fusion of a novel gene, ELKS, to RET due to translocation t(10;12)(q11;p13) in a papillary thyroid carcinoma. Genes Chromosomes Cancer *25*, 97–103.

Ohara-Imaizumi, M., Ohtsuka, T., Matsushima, S., Akimoto, Y., Nishiwaki, C., Nakamichi, Y., Kikuta, T., Nagai, S., Kawakami, H., Watanabe, T., and Nagamatsu, S. (2005). ELKS, a protein structurally related to the active zone-associated protein CAST, is expressed in pancreatic beta cells and functions in insulin exocytosis: Interaction of ELKS with exocytotic machinery analyzed by total internal reflection fluorescence microscopy. Mol. Biol. Cell *16*, 3289–3300.

Opdam, F.J., Echard, A., Croes, H.J., van den Hurk, J.A., van de Vorstenbosch, R.A., Ginsel, L.A., Goud, B., and Fransen, J.A. (2000). The small GTPase Rab6B, a novel Rab6 subfamily member, is cell-type specifically expressed and localised to the Golgi apparatus. J. Cell Sci. *113*, 2725–2735.

Patterson, G.H., and Lippincott-Schwartz, J. (2002). A photoactivatable GFP for selective photolabeling of proteins and cells. Science *297*, 1873–1877.

Riechmann, V., and Ephrussi, A. (2001). Axis formation during Drosophila oogenesis. Curr. Opin. Genet. Dev. *11*, 374–383.

Sannerud, R., Saraste, J., and Goud, B. (2003). Retrograde traffic in the biosynthetic-secretory route: Pathways and machinery. Curr. Opin. Cell Biol. *15*, 438–445.

Saraste, J., and Kuismanen, E. (1984). Pre- and post-Golgi vacuoles operate in the transport of Semliki Forest virus membrane glycoproteins to the cell surface. Cell *38*, 535–549.

Schmoranzer, J., Goulian, M., Axelrod, D., and Simon, S.M. (2000). Imaging constitutive exocytosis with total internal reflection fluorescence microscopy. J. Cell Biol. *149*, 23–32.

Shaner, N.C., Campbell, R.E., Steinbach, P.A., Giepmans, B.N., Palmer, A.E., and Tsien, R.Y. (2004). Improved monomeric red, orange and yellow fluorescent proteins derived from Discosoma sp. red fluorescent protein. Nat. Biotechnol. *22*, 1567–1572.

Short, B., Preisinger, C., Schaletzky, J., Kopajtich, R., and Barr, F.A. (2002). The Rab6 GTPase regulates recruitment of the dynactin complex to Golgi membranes. Curr. Biol. *12*, 1792–1795.

Toomre, D., Steyer, J.A., Keller, P., Almers, W., and Simons, K. (2000). Fusion of constitutive membrane traffic with the cell surface observed by evanescent wave microscopy. J. Cell Biol. *149*, 33–40.

Utskarpen, A., Slagsvold, H.H., Iversen, T.G., Walchli, S., and Sandvig, K. (2006). Transport of ricin from endosomes to the Golgi apparatus is regulated by Rab6A and Rab6A'. Traffic *7*, 663–672.

Wang, Y., Liu, X., Biederer, T., and Sudhof, T.C. (2002). A family of RIM-binding proteins regulated by alternative splicing: Implications for the genesis of synaptic active zones. Proc. Natl. Acad. Sci. USA *99*, 14464–14469.

White, J., Johannes, L., Mallard, F., Girod, A., Grill, S., Reinsch, S., Keller, P., Tzschaschel, B., Echard, A., Goud, B., and Stelzer, E.H. (1999). Rab6 coordinates a novel Golgi to ER retrograde transport pathway in live cells. J. Cell Biol. *147*, 743–760.

Young, J., Stauber, T., del Nery, E., Vernos, I., Pepperkok, R., and Nilsson, T. (2005). Regulation of microtubule-dependent recycling at the trans-Golgi network by Rab6A and Rab6A'. Mol. Biol. Cell *16*, 162–177.

Supplemental data

Supplemental Experimental Procedures

siRNAs

Control siRNA and the siRNA against ELKS were described previously (Lansbergen et al., 2006); Rab6 siRNAs were described (Young et al., 2005), and corresponded to the following target regions: 5'- GACATCTTTGATCACCAGA (Rab6#1 siRNA) and 5'- CACCTATCAGGCAACAATT (Rab6#2 siRNA). Kinesin-1 KIF5B and cytoplasmic dynein heavy chain 1 siRNAs were directed against the following sequences: KIF5B#1 5'- GCCTTATGCATTTGATCGG (siRNA 118426, Ambion); KIF5B#2 siRNA, 5'- GCACATCTCAAGAGCAAGT (siRNA 118427, Ambion); DHC#1 5'-CGTACTCCCGTGATTGATG (siRNA 118309, Ambion); DHC#2 5'-GCCAAAAGTTACAGACTTT (siRNA 118311, Ambion).

Mass spectrometry-based protein identification

Gels were stained with the Colloidal Blue Staining Kit (Invitrogen). Gel lanes were cut into slices using an automatic gel slicer and subjected to in-gel reduction with dithiothreitol, alkylation with iodoacetamide and digestion with trypsin (Promega, sequencing grade), essentially as described by Wilm *et al.* (Wilm et al., 1996). NanoLC-MS/MS was performed on an 1100 series capillary LC system (Agilent Technologies) coupled to an LTQ ion trap mass spectrometer (Thermo) operating in positive mode and equipped with a nanospray source. Peptide mixtures were trapped on a ReproSil C18 reversed phase column (Dr Maisch GmbH; column dimensions 1.5 cm × 100 µm, packed in-house) at a flow rate of 8 µl/min. Peptide separation was performed on ReproSil C18 reversed phase column (Dr Maisch GmbH; column dimensions 15 cm × 50 µm, packed in-house) using a linear gradient from 0 to 80% B (A = 0.1 M acetic acid; B = 80% (v/v) acetonitrile, 0.1 M acetic acid) in 70 min and at a constant flow rate of 200 nl/min using a splitter. The column eluent was directly sprayed into the ESI source of the mass spectrometer. Mass spectra were acquired in continuum mode; fragmentation of the peptides was performed in data-dependent mode.

Peak lists were automatically created from raw data files using the Mascot Distiller software (version 2.0; MatrixScience). The Mascot search algorithm (version 2.0, MatrixScience) was used for searching against the NCBInr database (release date: 20th January 2006; taxonomy H. sapiens). The peptide tolerance was typically set to 2 Da and the fragment ion tolerance to 0.8 Da. Only doubly and triply charged peptides were searched for. A maximum number of 2 missed cleavages by trypsin were allowed and carbamidomethylated cysteine and oxidised methionine were set as fixed and variable modifications, respectively. The Mascot score cut-off value for a positive protein hit was set to 100. Individual peptide MS/MS spectra with Mowse scores below 40 were checked manually and either interpreted as valid identifications or discarded.

Yeast two-hybrid analysis

The tail domain of KIF5A, KIF5B, KIF5C, KIF1A and KIF21A were cloned into pBHA (lexA fusion vector) and tested against various deletion mutants of BICD2 constructed in pGAD10 (GAL4 activation domain vector, Clontech). All constructs were generated by PCR-based strategy using the following cDNAs as templates: BICD2 (Hoogenraad et al., 2001), KIF5C (pcDNA3-myc-KIF5C; a gift of K.Verhey, University of Michigan, Ann Arbor, USA) (Verhey et al., 1998), KIF5A (IMAGE clones 1630386/6195468), KIF5B (IMAGE clones 4422906/6165834), KIF1A (gift of E.Kim, Korea Advanced Institute of Science and Technology, Daejeon, Korea (Shin et al., 2003)) and KIF21B (human cDNA KIAA0449, a gift from Kazusa DNA Research Institute, Kisarazu, Japan (Seki et al., 1997)). Yeast two-hybrid analysis was carried out using the L40 yeast strain harboring HIS3 and β-galactosidase as reporter genes as described previously (Niethammer and Sheng, 1998). β-galactosidase activity was detected using colony filter lift assays and scored according to time needed for β-galactosidase reporter to generate visible blue-colored yeast colonies on X-Gal-containing filters.

Fluorescence microscopy of fixed and live cells

Images of fixed cells were collected with a Leica DMRBE microscope equipped with a PL Fluotar 100x 1.3 N.A. oil objective, FITC/EGFP filter 41012 (Chroma) and Texas Red filter 41004 (Chroma) and an ORCA-ER-1394 CCD camera (Hamamatsu). 12-bit images were projected onto the CCD chip at a magnification of 0.1 μm/pixel.

Time-lapse live cell imaging was performed on the inverted microscope Zeiss Axiovert 200M (Zeiss) equipped with a Plan Neofluar 100x 1.3 N.A. oil objective (Zeiss), the X-Cite 120 illuminating system (with a 120W metal halide lamp) (EXFO) and ORCA-ER-1394 CCD camera (Hamamatsu) driven by Improvision Openlab 5.0 software (Improvision). 12-bit images were projected onto the CCD chip at a magnification of 0.063 μm/pixel. For GFP imaging we used Filter Set 10 (Zeiss) with excitation filter BP 450-490, dichroic FT 510 and emission filter BP 515-565. Images were captured at 0.89 s intervals. A typical image series comprised 100 frames, covering a period of 89 s.

Time-lapse live cell imaging with a high temporal resolution, two-color imaging and TIRFM were performed on the inverted research microscope Nikon Eclipse TE2000U (Nikon) with a CFI Apo TIRF 100x 1.49 N.A. oil objective (Nikon), equipped with Cascade 512B EMCCD camera (Roper Scientific) controlled by MetaMorph 6.3 software (Molecular Devices). For TIRFM we used 15 mW 488 nm laser line of argon laser (Melles Griot) and 25 mW 561 nm diode-pumped solid-state laser (Melles Griot). The 16-bit images was projected onto the CCD chip at a magnification of 0.156 μm/pixel with intermediate magnification 1X or a magnification of 0.104 μm/pixel with intermediate magnification 1.5X. For imaging GFP or Venus fluorochrome we used GFP-3035B Filter Set (Semrock) with excitation filter 472/30, dichroic 442-488/502-730 and emission filter 520/35. For imaging RFP or Strawberry fluorochrome we used Y-2E/C Filter Set (Nikon) with excitation filter EX 540-580, dichroic DM 595 and emission filter BA 600-660. For simultaneous imaging of green and red fluorescent signals we used F/TXR 96352 Filter Set (Chroma) together with Optosplit Image Splitter (Cairn Research), equipped with dichroic filter Q565LP, short emitter HQ535/50 and long emitter HQ610/75. Depending on the

task, images were captured in with different time intervals in the range of 0.071s – 0.87s. A typical epifluorescent image series comprised 100-530 frames, covering a period of ~50-300 s depending on the time interval. A typical TIRF image series comprised 2000 frames, covering a period of 142 s. Simultaneous two-color (green and red) TIRF time-lapse live cell imaging were performed on the inverted research microscope Nikon Eclipse TE2000E (Nikon) with a CFI Apo TIRF 100x 1.49 N.A. oil objective (Nikon), equipped with QuantEM EMCCD camera (Roper Scientific) controlled by MetaMorph 7.1 software (Molecular Devices). For excitation we used simultaneously 113 mW 488nm laser line of argon laser (Spectra-Physics Lasers) and 11 mW 561nm diode-pumped solid-state laser (Melles Griot) and Chroma ET-GFP/mCherry filter cube. For emissions separation we used DualView (Optical Insight) with Emitters HQ530/30M and HQ630/50M (Chroma) and beam splitter 565DCXR (Chroma). The 16-bit images were projected onto the CCD chip at a magnification of 0.067 µm/pixel with intermediate magnification 2.5X. Images were captured with exposure of 100 ms with no delay between frames. A typical image series comprised 500 frames, covering a period of 50s.

FRAP assay on the wide-field fluorescent microscope (Fig.S3C,D) was carried out with inverted research microscope Nikon Eclipse TE2000E (Nikon) equipped with FRAP scanning head FRAP L5 D – CURIE (Curie Institute), CFI Apo TIRF 100x 1.49 N.A. oil objective (Nikon), and QuantEM EMCCD camera (Roper Scientific) controlled by MetaMorph 7.1 software (Molecular Devices). For FRAP we used 11 mW 561nm diode-pumped solid-state laser (Melles Griot).

FRAP assay on the confocal microscope shown in Fig. 2G,H was carried out with a Zeiss LSM510Meta system, which included a Zeiss Axiovert 200 inverted microscope equipped with a PlanApo 63x 1.4 N.A. oil objective, controlled by Zeiss LSM510 software version 3.2 SP1 (Zeiss). We used Argon laser 488 nm (3%) and HeNe laser 561 nm (5-10%). The channel mode was: Multi track, Line. The beam path and channel assignment was: beam splitter HFT 405/488/561; Mirror; NFT 565; green channel – filter BP 505-550, red channel – filter LP 585; The 12-bit images was captured with pixel size 0.09 – 0.14 µm.

Cells were kept at 37°C during observation. For VSVG trafficking experiments, cells were incubated at overnight at 39,5°C, 2 hrs at 19°C and 5min - 4 hrs at 37°C prior to imaging. Optimal colocalization between VSVG-YFP and Rab6A was observed after 10 min at 37°C. Recombinant STB labelled with Cy3 (a gift of B. Goud, Institut Curie, Paris, France) was used for STB trafficking experiments as described previously (White et al., 1999).

Image processing

Images of fixed samples were prepared using Adobe Photoshop by converting them to 8 bit and linear adjustment of "Levels"; no image filtering was performed. Images of live cells were subjected to custom-made "2D deconvolution" procedure using MetaMorph software as described previously (Grigoriev et al., 2006). The procedure is based on applying Low Pass filter (MetaMorph) to the image and subtracting the resultant image from the original one (Fig.S7). Further, blur, sharpen and Gaussian filtering was applied using MetaMorph and Adobe Photoshop. The details of image acquisition and adjustment for each individual figure showing live cells and for movies are listed below.

Statistical analysis of the data

Analysis of different parameters was performed by computing the mean value for each cell and then averaging the values for cells within a certain category (such as treatment with a particular siRNA); n for each measurement corresponds to the number of analyzed cells. To evaluate the statistical significance of the observed differences we used the two-tailed Mann-Whitney U test (STATISTICA 5.5, StatSoft Ins.), a nonparametric alternative to the t-test for independent samples, because many of the measured parameters did not show normal distribution. The test was used to evaluate the hypothesis that the given parameter measured in cells treated with a certain siRNA is the same as in control cells. The alpha level was 0.05. In the figures the results of statistical analysis are indicated as follows: n.s. – no statistically significant difference; * - statistically significant with $p<0.05$; ** - statistically significant with $p<0.01$; *** - statistically significant with $p<0.001$.

Figure 3D.
Number of NPY-Venus vesicles per 100 µm² (in fixed cells)

control siRNA	519 vesicles in 20 cells			
Rab6#1 siRNA	555 vesicles in 20 cells	p = 0.0699	p > 0.05	n.s.
Rab6#2 siRNA	778 vesicles in 20 cells	p = 0.3577	p > 0.05	n.s.

Intermediate pause duration

control siRNA	218 pauses in 20 cells			
Rab6#1 siRNA	126 pauses in 19 cells	p = 0.8883	p > 0.05	n.s.
Rab6#2 siRNA	134 pauses in 15 cells	p = 0.2935	p > 0.05	n.s.

Vesicle velocity

control siRNA	328 tracks in 25 cells			
Rab6#1 siRNA	216 tracks in 20 cells	p = 0.0165	p < 0.05	*
Rab6#2 siRNA	169 tracks in 15 cells	p = 9.7650e-3	p < 0.01	**

Track length

control siRNA	328 tracks in 25 cells			
Rab6#1 siRNA	216 tracks in 20 cells	p = 1.0000e-6	p < 0.001	***
Rab6#2 siRNA	169 tracks in 15 cells	p = 2.0000e-6	p < 0.001	***

Figure 3E.
Number of Rab6 vesicles per 100 µm² (in fixed cells)

control siRNA	673 vesicles in 20 cells			
KIF5B#1 siRNA	1547 vesicles in 50 cells	p = 8.75e-4	p < 0.001	***
KIF5B#2 siRNA	1267 vesicles in 50 cells	p = 1.209e-3	p < 0.01	**

Intermediate pause duration

control siRNA	272 pauses in 20 cells			
KIF5B#1 siRNA	96 pauses in 11 cells	p = 0.2477	p > 0.05	n.s.
KIF5B#2 siRNA	85 pauses in 10 cells	p = 0.3116	p > 0.05	n.s.

Vesicle velocity

control siRNA	374 tracks in 21 cells			
KIF5B#1 siRNA	201 tracks in 11 cells	p = 1.7800e-4	p < 0.001	***
KIF5B#2 siRNA	126 tracks in 10 cells	p = 4.2000e-5	p < 0.001	***

Track length

control siRNA	374 tracks in 21 cells			
KIF5B#1 siRNA	201 tracks in 11 cells	p = 1.4000e-5	p < 0.001	***
KIF5B#2 siRNA	126 tracks in 10 cells	p = 1.3000e-5	p < 0.001	***

Figure 4B.
Number of vesicles per 100 µm^2 (in fixed cells)

Rab6, control siRNA	673 vesicles in 20 cells			
Rab6, ELKS siRNA	2945 vesicles in 47 cells	p = 1.0000e-6	p < 0.001	***
NPY, control siRNA	519 vesicles in 20 cells			
NPY, ELKS siRNA	811 vesicles in 20 cells	p = 1.0000e-6	p < 0.001	***

Figure 4E.
Frequency of appearance of vesicles per second

Rab6A, control siRNA	428 vesicles in 14 cells			
Rab6A, ELKS siRNA	321 vesicles in 11 cells	p = 0.8480	p > 0.05	n.s.

Figure 4F.
Vesicle velocity

Rab6A, control siRNA	374 tracks in 21 cells			
Rab6A, ELKS siRNA	171 tracks in 5 cells	p = 0.2287	p > 0.05	n.s.

Figure 4G.
Track length

Rab6A, control siRNA	374 tracks in 21 cells			
Rab6A, ELKS siRNA	171 tracks in 5 cells	p = 0.0550	p > 0.05	n.s.

Figure 4H.
Average velocity of reaching the cell edge

Rab6A, control siRNA	23 vesicles in 6 cells			
Rab6A, ELKS siRNA	27 vesicles in 5 cells	p = 0.5839	p > 0.05	n.s.

Figure 4I.
Terminal pause duration

Rab6A, control siRNA	120 vesicles in 8 cells			
Rab6A, ELKS siRNA	67 vesicles in 6 cells	p = 2.9870e-3	p < 0.01	**
NPY, control siRNA	58 vesicles in 7 cells			
NPY, Rab6#1 siRNA	34 vesicles in 7 cells	p = 2.6780e-3	p < 0.01	**
NPY, Rab6#2 siRNA	36 vesicles in 7 cells	p = 0.0127	p < 0.05	*
NPY, Rab6#2 + ELKS siRNAs	24 vesicles in 6 cells	p = 4.2770e-3	p < 0.01	**
NPY, ELKS siRNA	35 vesicles in 7 cells	p = 1.7470e-3	p < 0.01	**

Figure 4K.
Mean colocalization of NPY-Venus exocytosis events with mRFP-LL5β (in live cells)

control siRNA	266 vesicles in 27 cells			
Rab6#1 siRNA	56 vesicles in 9 cells	p = 9.1000e-4	p < 0. 001	***
Rab6#2 siRNA	49 vesicles in 8 cells	p = 1.0360e-3	p < 0. 01	**

Figure S1B.
Number of displacements

control	753 tracks in 20 cells			
latrunculin	395 tracks in 17 cells	p = 0.2228	p > 0.05	n.s.
nocodazole	112 tracks in 20 cells	p = 1.0000e-8	p < 0.001	***

Figure S6A.
Number of displacements

control	753 tracks in 20 cells			
KIF5B#1	593 tracks in 20 cells	3,20E+1	p < 0.01	**
KIF5B#1+ latrunculin	284 tracks in 17 cells	4,60E+1	p < 0.01	**
KIF5B#1+ nocodazole	47 tracks in 20 cells	1,00E-4	p < 0.001	***
KIF5B#2	337 tracks in 14 cells	6,06E+0	p < 0.001	***
KIF5B#2+ latrunculin	121 tracks in 10 cells	6,01E+0	p < 0.001	***
KIF5B#2+ nocodazole	20 tracks in 10 cells	1,10E-1	p < 0.001	***

Figure S6B.
Number of vesicles (in live cells)

control	753 tracks in 20 cells			
KIF5B#1	593 tracks in 20 cells	1,00E-4	p < 0.001	***
KIF5B#1+ latrunculin	284 tracks in 17 cells	1,00E-4	p < 0.001	***
KIF5B#1+ nocodazole	47 tracks in 20 cells	0.3302	p > 0.05	n.s.
KIF5B#2	337 tracks in 14 cells	6,60E-1	p < 0.001	***
KIF5B#2+ latrunculin	121 tracks in 10 cells	9,00E-1	p < 0.001	***
KIF5B#2+ nocodazole	20 tracks in 10 cells	0.0197	p < 0.05	*

Figure S6C.
Number of displacements

control	753 tracks in 20 cells			
KIF5B#1	593 tracks in 20 cells	3,20E+1	p < 0.01	**
KIF5B#2	337 tracks in 14 cells	6,06E+0	p < 0.001	***
DHC#1	358 tracks in 20 cells	2,00E-2	p < 0.001	***
DHC#2	218 tracks in 20 cells	1,00E-4	p < 0.001	***

Figure S6D.
Number of vesicles (in live cells)

control	753 tracks in 20 cells			
KIF5B#1	593 tracks in 20 cells	1,00E-4	p < 0.001	***
KIF5B#2	337 tracks in 14 cells	6,60E-1	p < 0.001	***
DHC#1	358 tracks in 20 cells	10.000	p > 0.05	n.s.
DHC#2	218 tracks in 20 cells	3,20E+1	p < 0.01	**

Figure S6E
Vesicle velocity

control siRNA	374 tracks in 21 cells			
DHC1 siRNA	138 tracks in 15 cells	p = 3.3000e-5	p < 0.001	***
DHC2 siRNA	152 tracks in 15 cells	p = 1.0000e-6	p < 0.001	***

Table S1. Microtubule motor-related binding partners of Bio-GFP-BICD2-NT identified by mass spectrometry.

Identified proteins	NCBI GI number	Mascot score	% coverage	Identified unique peptides
Bicaudal D homologue 2	21735417	2281	29,7	27
Dynein, cytoplasmic 1, heavy chain 1	119602166	3079	13,5	47
Dynein, cytoplasmic 1, intermediate chain 2	14585873	109	2,3	1
Dynein, cytoplasmic 1, light intermediate chain 2	5453634	139	5,3	3
Dynein, cytoplasmic 1, light intermediate chain 1	119584835	147	7	2
Dynactin 1 (p150 glued)	13259508	824	14	12
Dynactin 2 (dynamitin,p50)	5453629	328	22,2	5
Dynactin 4 (p62)	119582110	134	5,8	2
ARP1 (actin-related protein 1)	5031569	245	13,6	4
Kinesin-1 (kinesin family member 5B)	4758648	139	4,4	3

The table shows microtubule motor-related proteins identified with a significant Mascot score in the pull down with streptavidin beads from an extract of HeLa cells co-expressing Bio-GFP-BICD2-N-terminus (NT) (BICD2 amino acids 1-575) and biotin ligase BirA. BICD2-NT, which includes the first and the second coiled coil segments of BICD2 comprising the motor-binding part of this protein (Hoogenraad et al., 2001; Hoogenraad et al., 2003), was used in this experiment because our previous studies have shown that the BICD2 C-terminus, which binds to Rab6, is likely involved in autoinhibition of BICD2 (Hoogenraad et al., 2001; Hoogenraad et al., 2003; Matanis et al., 2002). Probably due to such autoinhibition, only a few significant hits were found with the full-length Bio-GFP-BICD2 (data not shown). A pull-down from HeLa cells expressing BirA alone was used as a control (only proteins which displayed significantly higher Mascot score in the Bio-GFP-BICD2-NT lane compared to the control lane are listed). For each identified protein, the list is filtered for duplicates and shows only the hits with the highest score and most identified peptides.
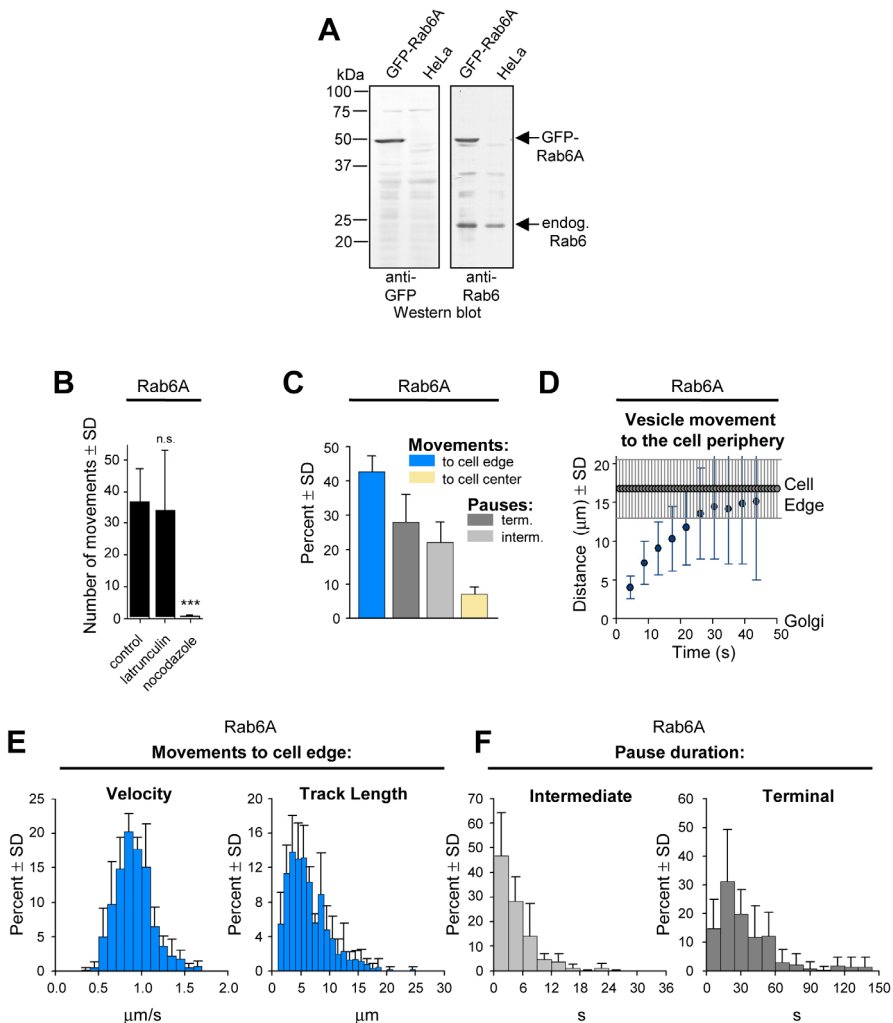
Figure S1. Characterization of the GFP-Rab6A-expressing stable cell line.
A. Western blots of lysates of control HeLa cells or the cells stably expressing GFP-Rab6A with antibodies against GFP and Rab6. Note that the expression level of GFP-Rab6A in the stable cell line is comparable the endogenous Rab6 level. B. Number of GFP-Rab6A vesicle displacements (±SD) longer than 1 µm with a velocity exceeding 0.3 µm/s per 100 µm² per 1 min per 10 vesicles. Quantification was performed in control cells, cells treated for 30 min with 10 µM latrunculin B or for 2 hrs with 10 µM nocodazole. Values significantly different from control are indicated by asterisks (p<0.001, ***; p>0.05, n.s., Mann-Whitney U-test). C-F. Analysis of GFP-Rab6A vesicle trafficking. The majority of the observed GFP-Rab6A vesicles emerged from the Golgi, moved to the cell periphery along curvilinear trajectories with some pauses or occasional short reversals, stopped at the cell periphery, where they could undergo short-range movements, immobilized, paused for some time and disappeared. Complete trajectories (from the moment of appearance until disappearance) were divided into tracks (periods of uninterrupted movement in one direction, typically without deviation from the original course by more than 45-60 degrees in 1 s), intermediate pauses (periods longer than 2 frames (1,14 s) when the vesicles moves with a velocity less than ~0.3 µm/s, preceded and followed by movement) and terminal pauses (pauses preceding vesicle disappearance). A track could terminate with a pause or a reversal (change of direction by typically 135-180 degrees). C. Percentage of time vesicles spent in movements and pauses. Note that

movements toward cell periphery predominated among other states. Quantification is based on measurements of trajectories of 60 vesicles in 6 cells (total number of analyzed frames was 3307). D. Distance from the origin (first position of the vesicle near the Golgi, from which the vesicle was traced). As reversions and intermediate pauses were relatively minor events, vesicles showed gradual displacement toward cell edge. Near the cell edge (the position of which is indicated by grey circles with error bars), terminal pauses were a predominant mode of vesicle behavior, causing a reduction in the speed of movement. Mean cell radius was 16.75 ± 3.77 µm (mean $\pm$ SD; range:10.36-25.93; n=29). The vesicle data set was the same as in (C). E. Characteristics of periphery-directed vesicle movement: distributions of track velocities and track lengths. Whiskers indicate standard deviation for each bin per cell. Velocities were computed by dividing displacements between frames by the interval between frames (pauses were excluded from analysis). Mean velocity was 0.92 ± 0.28 µm/s (mean $\pm$ SD; range: 0.34-3.41; n=374) and mean track length was 6.20 ± 3.73 µm (mean $\pm$ SD; range: 1.09-24.13; n=382). F. Distributions of the intermediate and terminal pause durations. Mean intermediate pause duration was 3.99 ± 4.10 s (mean $\pm$ SD; range: 0.57-30.80; n=272) and mean terminal pause duration was 33.09 ± 25.44 s (mean $\pm$ SD; range: 5.34-135.28; n=120)
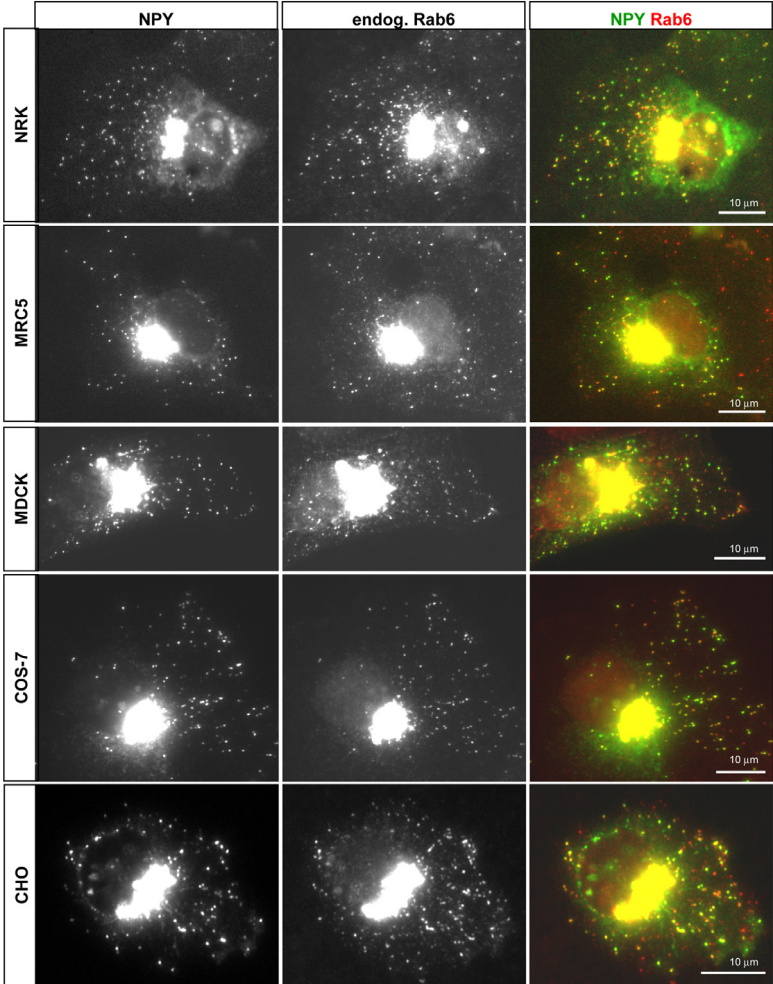
Figure S2. Colocalization of exocytosis marker NPY-Venus with the endogenous Rab6 in different cell lines. Different cell lines (indicated on the left) were transiently transfected with NPY-Venus, fixed and stained for the endogenous Rab6.
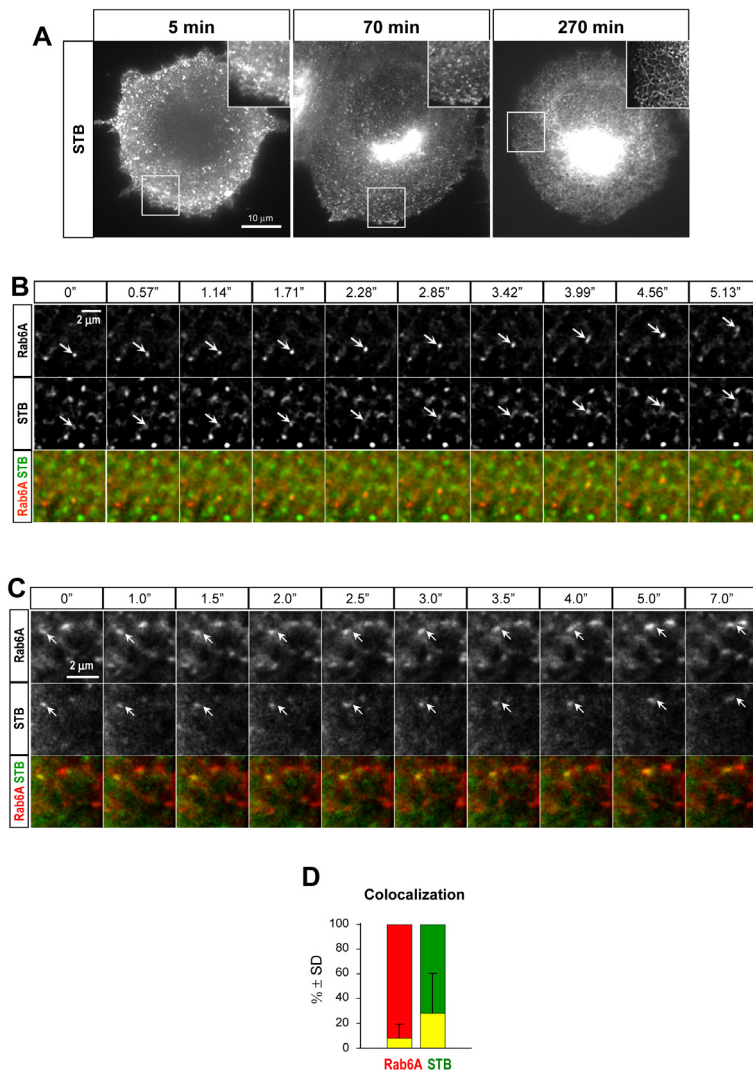
Figure S3. Trafficking of STB.
A. Live images of HeLa cells incubated with Cy3-STB at 4°C for 30 min, and after washing away unbound STB, incubated at 37°C for 5 min (plasma membrane labeling), 70 min (accumulation at the Golgi) and 270 min (toxin is largely redistributed to the ER). B. Frames of a two-color movie of a HeLa cell expressing GFP-Rab6A, incubated with Cy3-STB at 4°C for 30 min, and after washing away unbound STB, incubated for 1hr at 37°C prior to imaging. Note the colocalization of Cy3-STB and GFP-Rab6A on a moving vesicle (shown by arrows). C. Frames of a two-color movie of a HeLa cell expressing GFP-Rab6A, incubated with Cy3-STB at 4°C for 30 min, and after washing away unbound STB, incubated for 1hr at 37°C prior to imaging. The red signal in the lamella (Cy3-STB outside of Golgi) was photobleached for ~20 sec by 561 nm diode laser in order to reveal the weakly labeled Golgi-derived moving structures that were normally masked by plasma membrane staining and/or the background. Note the colocalization of Cy3-STB and GFP-Rab6A on a moving vesicle (shown by arrows). D. Quantification of vesicle colocalization in cells prepared as described in (C). Red and green bars correspond to all counted vesicles (Rab6A and STB, respectively), while yellow parts of each bar correspond to double labeled vesicles. 616 vesicles in 36 cells were counted.
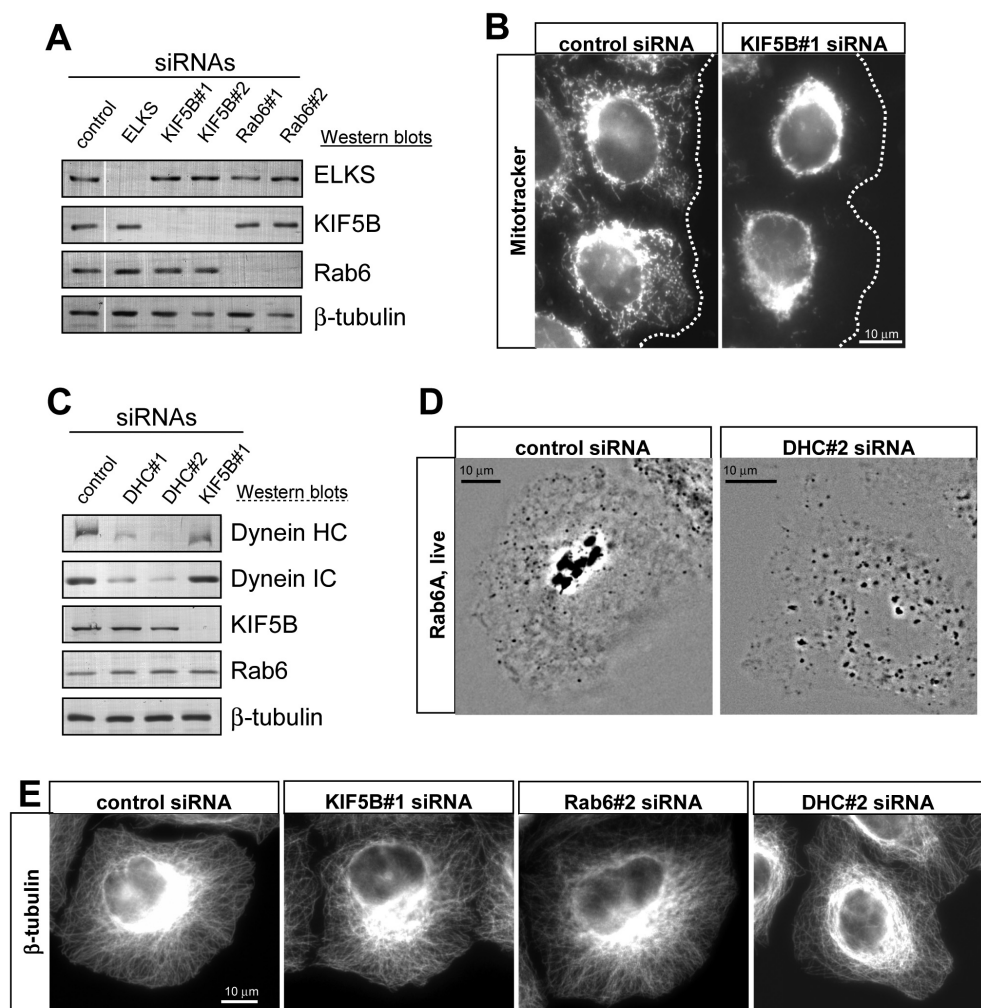
Figure S4. Characterization of Rab6, KIF5B and DHC siRNAs.

A,C. Western blot analysis of the extracts of HeLa cells cultured for 3 days after transfection with the indicated siRNAs. B. HeLa cells were stained with MitoTracker Red CMXRos 3 days after transfection with the indicated siRNAs. In agreement with published data, loss of KIF5B activity causes redistribution of mitochondria to the perinuclear region (Tanaka et al., 1998). Cell edges are indicated with a stippled line. D. Live images of GFP-Rab6A-expressing cells three days after transfection with the indicated siRNAs. Note Golgi dispersion after dynein knockdown. E. HeLa cells were stained for β–tubulin 3 days after transfection with the indicated siRNAs. Note that MT network is not significantly affected by KIF5B or Rab6 siRNA transfection, but is disorganized due to DHC depletion.

A

BICD2 amino acids	Empty vector	KIF5A 353-1031	KIF5A 765-932	KIF5B 770-962	KIF5C 771-955	KIF1A 359-1690	KIF21B 376-1073	KIF21B 1067-1624
1-595	-	+++	+++	++	++	-	-	-
1-345	-	-	-	-	-	-	-	-
336-595	-	+++	+++	++	++	-	-	-
586-820	-	-	-	-	-	-	-	-

B

Figure S5. Analysis of the interaction between BICD2 and kinesin-1 isoforms.
A. Yeast two-hybrid analysis. BICD2 fragments were linked to GAL4 activation domain and tested in a pair wise fashion for interaction with kinesin-1 (KIF5A, B and C), kinesin-3 (KIF1A) and kinesin-4 (KIF21B) tail regions cloned into LexA fusion vector. Interaction strength was scored according to the time needed for β-galactosidase reporter to generate visible blue-colored yeast colonies on X-Gal containing filters in a colony filter lift assay: +++ 0-30 min, ++ 30-60 min, + 60-180 min and - no β-galactosidase activity. B. Co-immunoprecipitation from transfected HEK293 cells. HEK293 cells were co-transfected with GFP-tagged BICD2 or its fragments and myc-tagged full-length KIF5A or KIF5B. Cells were lysed and immunoprecipitations were performed using mouse anti-GFP or mouse anti-myc antibodies. Immunoprecipitates were analyzed by Western blotting using rabbit anti-GFP or anti-myc antibodies.
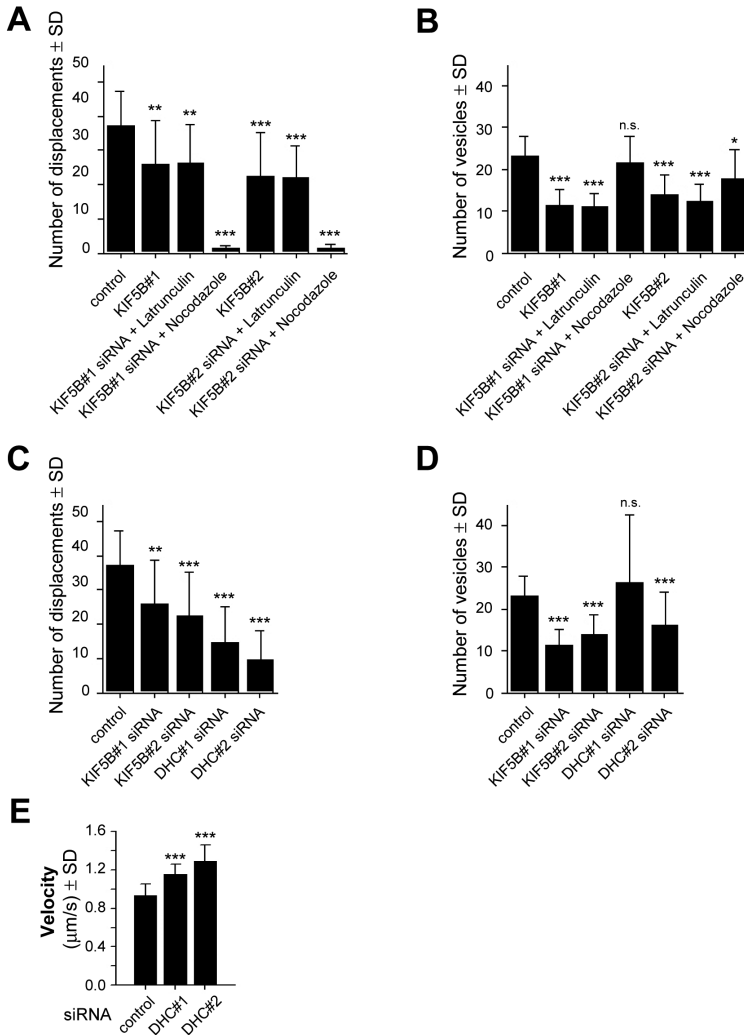
Figure S6. Quantifications of vesicle movement after kinesin-1 and cytoplasmic dynein depletion.
A. Number of GFP-Rab6A vesicle displacements (±SD) longer than 1 μm with a velocity exceeding 0.3 μm/s per 100 μm^2 per 1 min per 10 vesicles. Quantification was performed in cells transfected with the indicated siRNAs that were either untreated or treated for 30 min with 10 μM latrunculin B or for 2 hrs with 10 μM nocodazole (control population is the same as in Fig.S1B). B. Number of GFP-Rab6A vesicles (±SD) per 100 μm^2 in cells described in (A). Note that the exact values slightly deviate from those shown in Fig.3 E, because endogenous Rab6 vesicles in fixed cells were counted in that experiment, while here live cells from the stable GFP-Rab6A-expressing cell line were used. C. Number of GFP-Rab6A vesicle displacements (±SD) longer than 1 μm with a velocity exceeding 0.3 μm/s per 100 μm^2 per 1 min per 10 vesicles in cells transfected with the indicated siRNAs. D. Number of GFP-Rab6A vesicles (±SD) per 100 μm^2 in cells transfected with the indicated siRNAs. Data for control and KIF5B knockdown cells in panels (C,D) are the same as in panels (A,B) and are shown for comparison. E. Velocity of periphery-directed GFP-Rab6A vesicle movement after DHC knockdown. Data for control cells are the same as in Fig.3E. Values significantly different from control are indicated by asterisks (p<0.001, ***; p<0.01, **; p<0.05, *; p>0.05, n.s., Mann-Whitney U-test).
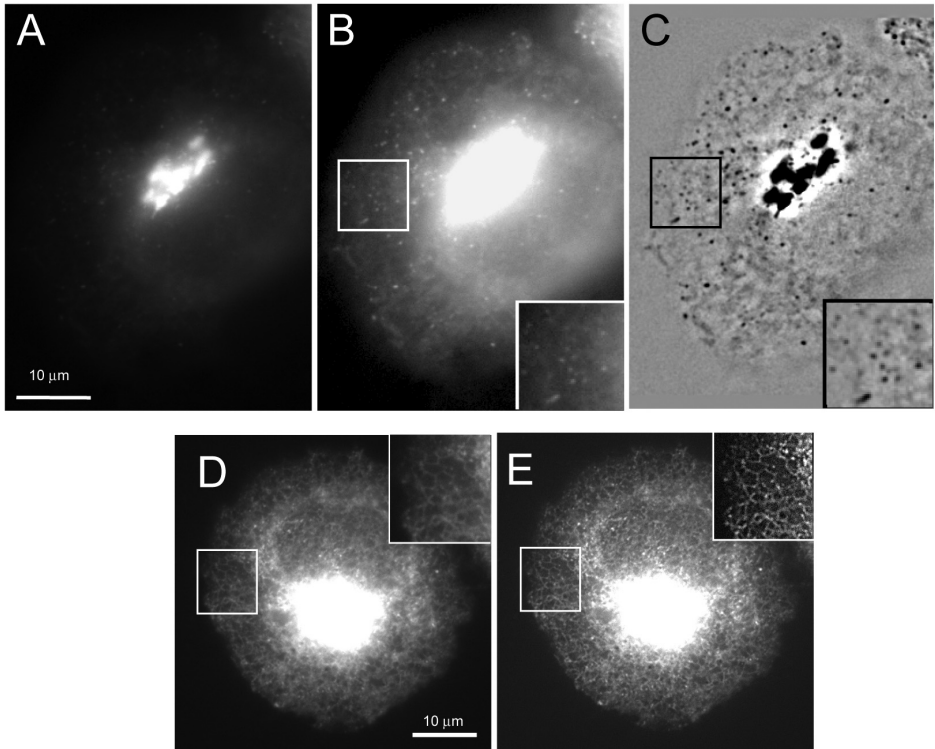
Figure S7. Illustration of live image adjustment procedures.
A-C. Image adjustment procedure for left panel of Fig.S4D. A. Original image, converted to 8 bit and autoscaled.
B. The same image as in (A) after levels adjustment in Adobe Photoshop to visualize the cell margin. C. The same image as in (A) after subtraction of the same image subjected to Low Pass filtration (MetaMorph), application of the Blur filter (MetaMorph) and Unsharp Mask filter (Photoshop). D,E. Image adjustment procedure for the right panel of Fig.S3A. D. Original image, converted to 8 bit and after levels adjustment (Photoshop) to visualize the cell margin. E. The same image after applying Unsharp Mask filter in Adobe Photoshop.

Supplemental references

Grigoriev, I., G. Borisy, et al. (2006). "Regulation of microtubule dynamics in 3T3 fibroblasts by Rho family GTPases." Cell Motil Cytoskeleton 63(1): 29-40.

Hoogenraad, C. C., A. Akhmanova, et al. (2001). "Mammalian Golgi-associated Bicaudal-D2 functions in the dynein-dynactin pathway by interacting with these complexes." Embo J 20(15): 4041-54.

Hoogenraad, C. C., P. Wulf, et al. (2003). "Bicaudal D induces selective dynein-mediated microtubule minus end-directed transport." Embo J 22(22): 6004-15.

Lansbergen, G., I. Grigoriev, et al. (2006). "CLASPs attach microtubule plus ends to the cell cortex through a complex with LL5beta." Dev Cell 11(1): 21-32.

Matanis, T., A. Akhmanova, et al. (2002). "Bicaudal-D regulates COPI-independent Golgi-ER transport by recruiting the dynein-dynactin motor complex." Nat Cell Biol 4(12): 986-92.

Niethammer, M. and M. Sheng (1998). "Identification of ion channel-associated proteins using the yeast two-hybrid system." Methods Enzymol 293: 104-22.

Seki, N., M. Ohira, et al. (1997). "Characterization of cDNA clones in size-fractionated cDNA libraries from human brain." DNA Res 4(5): 345-9.

Shin, H., M. Wyszynski, et al. (2003). "Association of the kinesin motor KIF1A with the multimodular protein liprin-alpha." J Biol Chem 278(13): 11393-401.

Tanaka, Y., Y. Kanai, et al. (1998). "Targeted disruption of mouse conventional kinesin heavy chain, kif5B, results in abnormal perinuclear clustering of mitochondria." Cell 93(7): 1147-58.

Verhey, K. J., D. L. Lizotte, et al. (1998). "Light chain-dependent regulation of Kinesin's interaction with microtubules." J Cell Biol 143(4): 1053-66.

White, J., L. Johannes, et al. (1999). "Rab6 coordinates a novel Golgi to ER retrograde transport pathway in live cells." J Cell Biol 147(4): 743-60.

Wilm, M., A. Shevchenko, et al. (1996). "Femtomole sequencing of proteins from polyacrylamide gels by nano-electrospray mass spectrometry." Nature 379(6564): 466-9.

Young, J., T. Stauber, et al. (2005). "Regulation of microtubule-dependent recycling at the trans-Golgi network by Rab6A and Rab6A'." Mol Biol Cell 16(1): 162-77.

Bicaudal-D2, dynein and kinesin-1 associate with nuclear pore complexes and regulate centrosome positioning during mitotic entry

3

Bicaudal-D2, dynein and kinesin-1 associate with nuclear pore complexes and
regulate centrosome positioning during mitotic entry

65
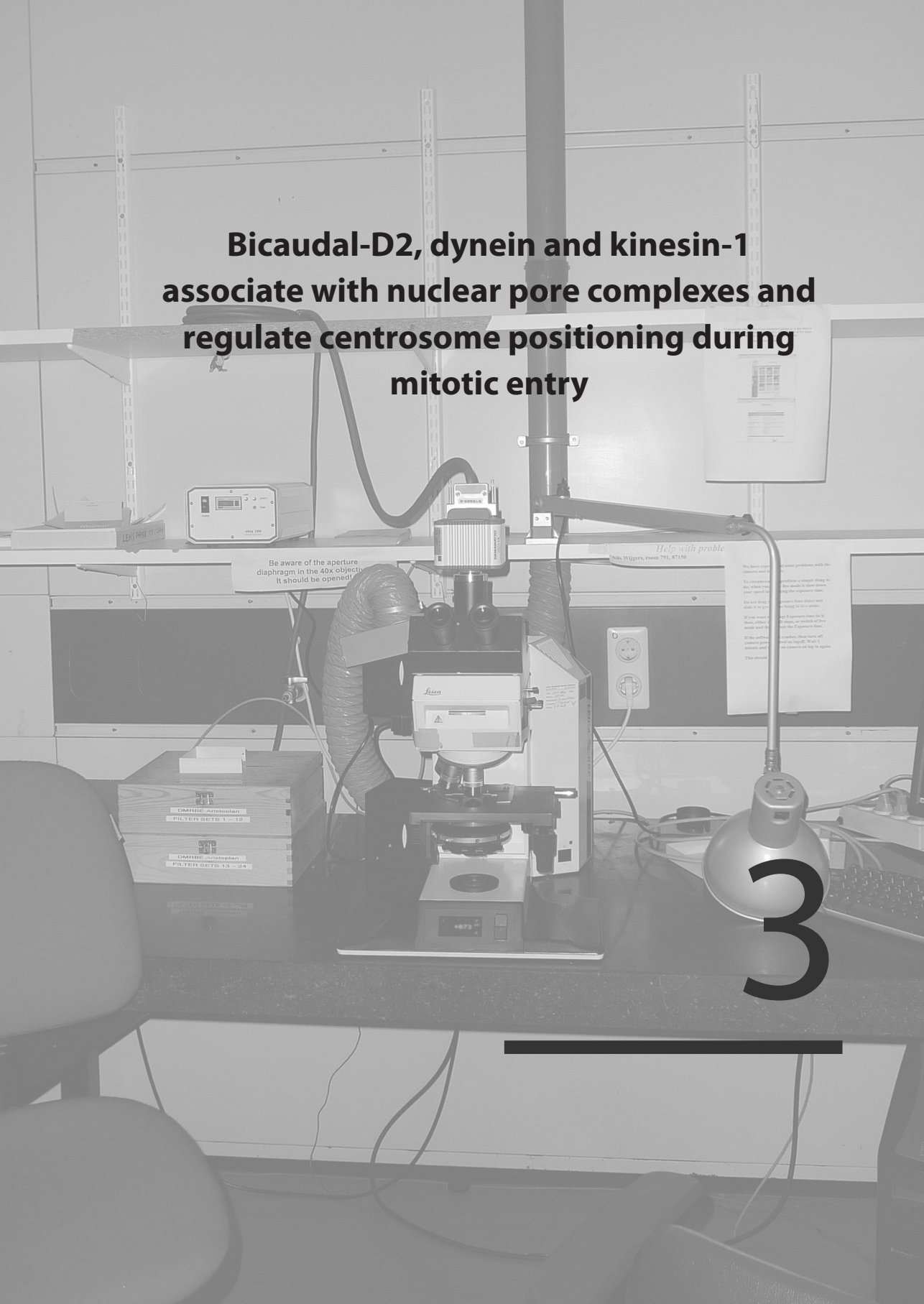
Bicaudal-D2, dynein and kinesin-1 associate with nuclear pore complexes and regulate centrosome positioning during mitotic entry

Daniël Splinter, Marvin E. Tanenbaum, Annette Flotho, Ilya Grigoriev, Dieuwke Engelsma, Nanda Keijzer, Jeroen Demmers, Ka Lou Yu, Maarten Fornerod, Frauke Melchior, Casper Hoogenraad, René H. Medema and Anna Akhmanova

Summary

BICD2 is one of the two mammalian homologues of the Drosophila Bicaudal-D, an evolutionarily conserved adaptor between microtubule motors and their cargo. Here we show that the nuclear pore complex (NPC) component RanBP2 directly binds to BICD2 and recruits it to NPCs of nuclei and annulate lamellae specifically in the G2 phase. Consequently, the two motors that associate with BICD2, kinesin-1 and dynein, promote BICD2-dependent movement of nuclei and annulate lamellae to microtubule plus and minus ends, respectively. A correct balance of forces, generated by these motors not only determines the position of annulate lamellae relative to centrosomes, but is also required to couple the centrosomes to the nuclear envelope prior to mitosis. Based on these results, we propose that BICD2 controls proper positioning of the nucleus relative to the microtubule network before cell division through regulation of kinesin-1 and dynein function.

Introduction

Spatial organization of eukaryotic cells requires active transport of proteins, macromolecular assemblies and membrane organelles along cytoskeletal fibers. Transport is driven by motor proteins, which use actin and microtubules (MTs) as tracks for their movement. Cytoskeletal elements are polarized structures, and each particular motor can move along them only in one direction. For example, MT-based motors include kinesins, which with a few exceptions walk to MT plus ends, and dyneins, which drive minus end-directed transport (Vale, 2003).

Motor-dependent transport machineries display a high degree of complexity. First, the same motor can move multiple cargos. For example, cytoplasmic dynein is responsible for the movement of the majority of membrane organelles, mRNAs and proteins to MT minus ends (Karki and Holzbaur, 1999; Vale, 2003). Second, the same cargo can simultaneously associate with multiple motors of opposite polarity and frequently switch the direction of movement (Gross, 2004; Welte, 2004). Molecular mechanisms responsible for motor recruitment, activation and switching of directions are still poorly understood. Motors are likely to be controlled by cargo-specific adaptor complexes, which often include structural components and small GTPases (Jordens et al., 2005; Karcher et al., 2002). For example, kinesin-1 is recruited to mitochondria by the coiled coil protein Milton acting

together with the Rho-like GTPase Miro (Glater et al., 2006), and the dynein/dynactin complex is attached to late endosomes by a complex containing the adaptor RILP, oxysterol-binding protein-related protein 1L, βIII spectrin and the small GTPase Rab7 (Johansson et al., 2007).

Another example of a well-studied motor adaptor is Bicaudal-D (BICD), which is conserved throughout the animal kingdom (Claussen and Suter, 2005). BICD consists of several coiled coil segments separated by regions expected to be highly flexible. The N-terminal part of BICD binds to cytoplasmic dynein and its accessory factor dynactin; moreover, BICD N-terminus is sufficient to recruit these complexes to organelles (Hoogenraad et al., 2001; Hoogenraad et al., 2003). The C-terminal domain of BICD is the cargo-binding part of the molecule. In mammals and flies, it directly associates with the small GTPase Rab6 (Januschke et al., 2007; Matanis et al., 2002; Short et al., 2002). In mammalian cells, BICD participates in recruitment of dynein-dynactin to Rab6-positive exocytotic vesicles and in their MT minus end-directed transport (Grigoriev et al., 2007; Matanis et al., 2002). The middle portion of BICD weakly binds to kinesin-1 (Grigoriev et al., 2007). The functional role of this link is not yet clear, but it is noteworthy that BICD-bound Rab6 vesicles move mostly in the plus end direction, suggesting that kinesin motor activity on Rab6 vesicles is the predominant one (Grigoriev et al., 2007; Matanis et al., 2002). In Drosophila, BicD participates in dynein-dependent mRNP transport (Bullock and Ish-Horowicz, 2001; Bullock et al., 2006). This function depends on the association between BicD and Egalitarian, a protein that has no clear mammalian counterparts (Bullock et al., 2006; Mach and Lehmann, 1997).

To investigate whether mammalian BICD is involved in other transport routes in addition to Rab6 vesicle trafficking, we searched for partners of the cargo-binding domain of BICD2, one of the two mammalian homologues of the fly BicD (Hoogenraad et al., 2001). We identified a component of the nuclear pore complex (NPC), RanBP2 (Wu et al., 1995; Yokoyama et al., 1995), as the major interacting partner of BICD2 C-terminus. RanBP2 (also known as NUP358) is a large protein, which acts as docking factor in nucleocytoplasmic transport (Gorlich and Kutay, 1999) and as an E3 ligase for posttranslational modification with the ubiquitin-like protein SUMO1 (Pichler et al., 2002). It forms extended fibers at the cytoplasmic side of the NPC and represents a good candidate for a link between the cytoskeleton and the nuclear envelope (NE).

Previous studies showed that cytoplasmic dynein is specifically recruited to the NE in mitotic prophase, where it plays a role in regulating the relative positioning of the nucleus and the centrosomes and participates in NE breakdown during mitotic entry ((Busson et al., 1998; Salina et al., 2002), for review see Hetzer et al., 2005; Rosenblatt, 2005). In C. elegans, dynein is anchored to the NE by the nuclear membrane component SUN-1 and a hook protein ZYG-12 (Malone et al., 2003). In yeast, a dynein light chain is a nucleoporin, but it likely acts at the NPC independently of the dynein motor (Stelter et al., 2007). In mammals, the molecular mechanism of dynein interaction with the NE is not yet clear.

In this study we focus on the function of RanBP2, BICD2, cytoplasmic dynein and kinesin-1 in the positioning of the centrosomes during mitotic entry. We show that BICD2 specifically associates with the NPCs in G2 phase of the cell cycle and participates in the recruitment of the dynein-dynactin complexes to these structures. During prophase, cytoplasmic dynein activity predominates over

Bicaudal-D2, dynein and kinesin-1 associate with nuclear pore complexes and regulate centrosome positioning during mitotic entry

67

kinesin activity, and the centrosomes remain tightly associated with the NE. However, kinesin-1 also plays a role in this process, because it pushes the nucleus and the centrosomes apart when cytoplasmic dynein is inactivated. Furthermore, depletion of the adaptor components of the complex, BICD2 and RanBP2, also causes centrosome detachment from the NE. It appears, therefore, that similar to most other MT motor cargos in animal cells, the prophase cell nucleus is transported bi-directionally by a molecular complex combining MT motors of opposite polarity.

Results

RanBP2 directly binds to BICD2 C-terminus

Our previous studies showed that the individual coiled coil segments of BICD2 display strong association with their binding partners, while the full-length molecule binds to the same proteins less efficiently, suggesting that it may be autoinhibited (Hoogenraad et al., 2001; Hoogenraad et al., 2003; Matanis et al., 2002). Therefore, we used the C-terminal coiled coil segment of BICD2 (Fig.1A) as a bait to search for new BICD2 cargos. We linked this BICD2 fragment to GFP and a biotinylation tag (Bio), a short peptide sequence that can be modified by the addition of biotin when expressed together with the biotin ligase BirA (de Boer et al., 2003). The resulting Bio-GFP-BICD2-CT fusion was transiently expressed together with BirA in HeLa cells, which were used for pull down assays with streptavidin beads. The resulting protein complexes were analyzed by mass spectrometry (Suppl. Table S1).

The most abundant newly identified potential BICD2 partner was the NPC component RanBP2. RanGAP1, which is known to form a tight complex with RanBP2 (Mahajan et al., 1997; Matunis et al., 1996), was also present among the isolated proteins in highly significant amounts (Suppl. Table S1).

The results of the pull down assay were confirmed by co-immunoprecipitation (co-IP) of endogenous RanBP2 and BICD2 from nocodazole arrested HeLa cells (Fig.1B). Next, we investigated if BICD2-CT could directly associate with RanBP2 domains. RanBP2 is a protein of ~350 kDa, which contains a leucine-rich region, four Ran-binding domains, eight zinc finger motifs and a C-terminal cyclophilin A-homologous region (Fig.1A). We generated five RanBP2 fragments, which covered most of the RanBP2 sequence, as fusions to CFP and the plasma membrane targeting palmitoylation motif of GAP-43 (Fig.1A). With the exception of the N-terminal fragment 1, these constructs were expressed well in mammalian cells, where they displayed a strong association with the Golgi apparatus and the plasma membrane, including filopodia (Fig.1F). BICD2-CT expressed in mammalian cells associates with the Golgi and cytoplasmic vesicles, but not with the plasma membrane (Hoogenraad et al., 2001; Matanis et al., 2002). Interestingly, BICD2-CT was specifically recruited to the plasma membrane by RanBP2 fragment 3 but not by other RanBP2 fragments (Fig.1F). The interaction between overexpressed BICD2-CT and RanBP2 fragment 3 was further confirmed by co-IP from HEK293 cells (Fig.1C). This experiment also showed that BICD2-CT does not interact with the GFP-tagged RanGAP1 (Fig.1C). We also employed a yeast two-hybrid assay to show that RanBP2 fragment 3 binds exclusively to the C-terminal part of BICD2 and not to its N-terminal and middle
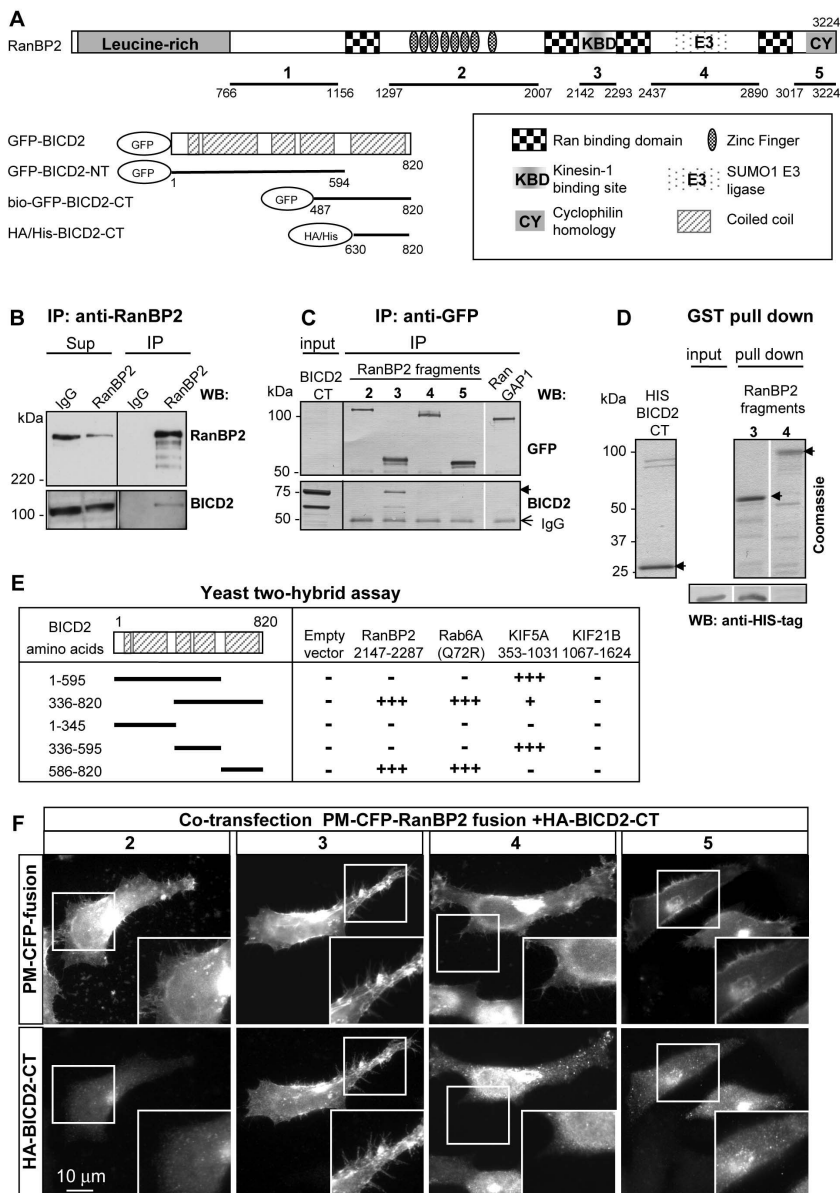
Figure 1. BICD2 interacts directly with RanBP2.

A. Schematic representation of the domains of RanBP2 and BICD2 and their fragments used for binding studies.
B. Co-IP of endogenous RanBP2 and BICD2 from nocodazole-arrested HeLa cells. IPs were performed with antibodies against RanBP2 or the control IgG and analyzed by Western blotting with the indicated antibodies. 3% of the supernatant (Sup) after IP was loaded on gel. C. IPs from HEK293 cells co-transfected with CFP-tagged RanBP2 fragments or GFP-RanGAP1 and mCherry-fused BICD2-CT. IPs were performed using mouse anti-GFP antibodies and analyzed by Western blotting using rabbit anti-GFP or anti-BICD2 antibodies. BICD2-CT and the

Bicaudal-D2, dynein and kinesin-1 associate with nuclear pore complexes and regulate centrosome positioning during mitotic entry

69

IgG bands are indicated by an arrowhead and an arrow. D. GST pull down assays with the indicated RanBP2 fusions and purified HIS-tagged BICD2-CT. The upper panels show Coomassie stained proteins, the bottom panel is a Western blot with anti-HIS tag antibodies. 10% of the input was loaded on gel. E. Yeast two-hybrid analysis. BICD2 fragments were linked to GAL4 activation domain and tested in a pairwise fashion for interaction with RanBP2, GTP-bound Rab6A (Q72R), kinesin-1 (KIF5A) and kinesin-4 (KIF21B) tail regions cloned into LexA fusion vector. Interaction strength was scored according to the time needed for β-galactosidase reporter to generate visible blue-colored yeast colonies on X-Gal containing filters: +++ 0-30 min, ++ 30-60 min, + 60-180 min and - no β-galactosidase activity. F. HeLa cells were co-transfected with the indicated plasma membrane targeted CFP-RanBP2 fusions and HA-tagged BICD2-CT, fixed with paraformaldehyde and stained with anti-HA antibodies. CFP fluorescence was visualized directly.

segments (Fig.1E). This is similar to the previously described interaction between BICD2 and Rab6 (Hoogenraad et al., 2001; Matanis et al., 2002), and is in contrast to kinesin-1 KIF5A, which associates with the middle portion of BICD2 (Grigoriev et al., 2007) (Fig.1E). The interaction between BICD2 and RanBP2 is direct, since BICD2-CT and RanBP2 segment 3, purified from bacteria, specifically bind to each other in a glutathione S-transferase (GST) pull-down assay (Fig.1D). Remarkably, the same RanBP2 fragment was previously shown to interact directly with kinesin-1 isoforms KIF5B and KIF5C (Cai et al., 2001; Cho et al., 2007), supporting the notion that it is involved in MT motor recruitment.

BICD2 and RanBP2 colocalize at the NE and annulate lamellae in G2 phase

We next investigated if endogenous BICD2 and RanBP2 colocalize in HeLa cells. Previously, we have shown that BICD2 predominantly localizes to the Golgi apparatus and Rab6-positive cytoplasmic vesicles (Hoogenraad et al., 2001; Matanis et al., 2002). However, a careful examination of the endogenous BICD2 distribution showed that BICD2 specifically associates with the nuclear envelope in a subset of cells, largely overlapping with the RanBP2 staining (Fig.2A). We hypothesized that this heterogeneity of BICD2 staining pattern was caused by cell cycle regulation. Indeed, all cells that showed BICD2 accumulation at the NE were positive for cyclin B1, and vice versa, indicating that BICD2 associates with the NE in the G2 phase (Fig. 2A).

We next examined whether this localization was RanBP2-dependent. RanBP2 could be specifically depleted from HeLa cells without affecting the expression of BICD2 (Suppl. Figure S1). BICD2 showed no accumulation on the NE of cyclin B1-positive cells if they were RanBP2-depleted (Fig. 2B), confirming that RanBP2 is required for BICD2 recruitment to the NE. To obtain further evidence that BICD2 specifically associates with NPCs, we made use of the fact that rapidly proliferating cells, such as HeLa, contain cytoplasmic stacks of NPCs known as annulate lamellae (AL) (Kessel, 1992). AL are usually more difficult to detect in G2 cells, when they start to disassemble (Cordes et al., 1996), however, MT-active agents induce their enlargement (Kessel, 1992). We could readily observe the association of endogenous BICD2 with the AL in cyclin B1 positive, but not in cyclin B1-negative cells treated with the MT-destabilizing drug nocodazole (Fig. 2C). Furthermore, we could observe specific association of GFP-tagged BICD2-CT and the full length BICD2 with the individual NPCs on the NE of nocodazole-treated cells that were pre-extracted with a Triton X-100-containing buffer to
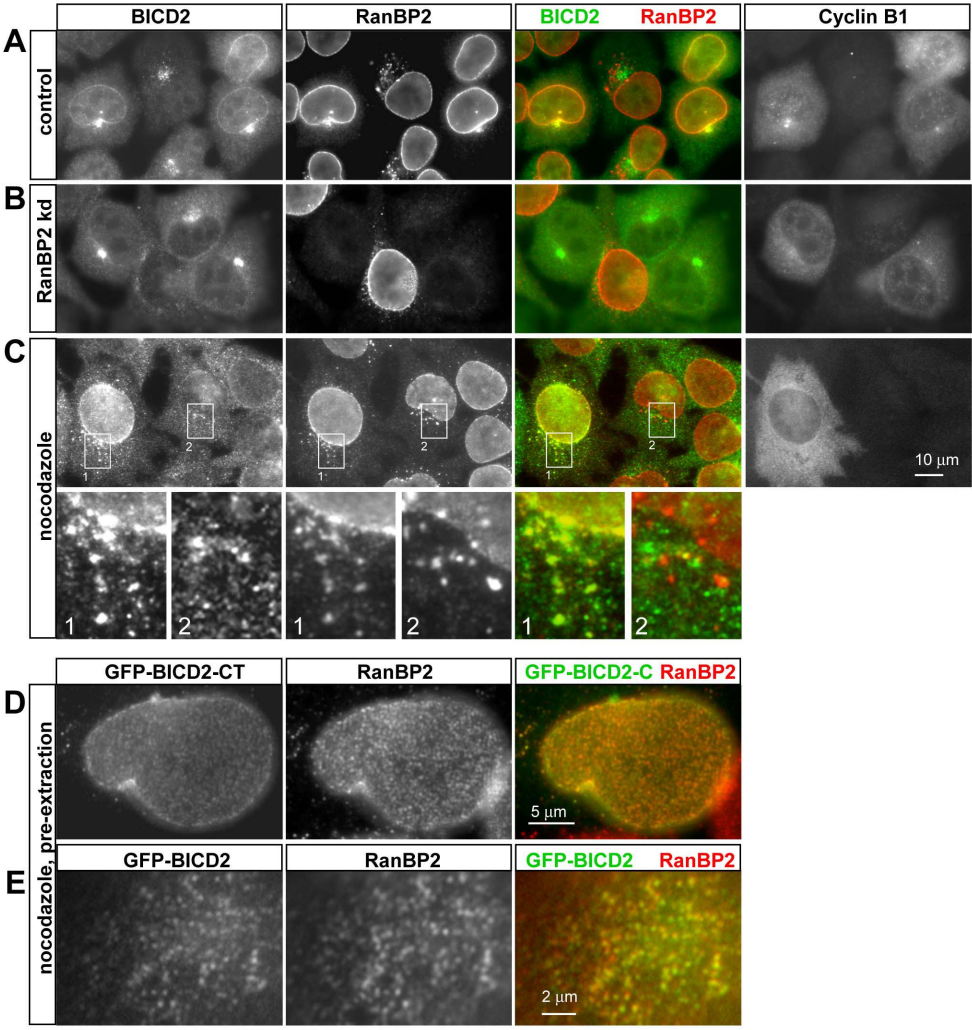
Figure 2. BICD2 associates with the NE and AL in G2 phase in a RanBP2-dependent manner.

A, B. HeLa cells were transfected with a control siRNA (A) or a mixture of RanBP2 siRNAs #1 and #2 (B), fixed with paraformaldehyde 3 days later and stained for endogenous BICD2, RanBP2 and cyclin B1. C. HeLa cells were treated with 10 µM nocodazole for 1 hr and stained as described for A. D, E. HeLa cells were transfected with the indicated GFP fusions, treated with 10 µM nocodazole, pre-extracted in a buffer with 0.5% Triton X-100, fixed with paraformaldehyde and stained for RanBP2. In the overlays, BICD2 is shown in green and RanBP2 in red.

Bicaudal-D2, dynein and kinesin-1 associate with nuclear pore complexes and regulate centrosome positioning during mitotic entry

71

reduce the cytoplasmic pool of the GFP-BICD2 fusions (Fig. 2D,E). Taken together, these data indicate that BICD2 associates with NPC in G2 cells in a RanBP2-dependent manner.

BICD2 and dynein/dynactin complex are recruited to the NE and AL in G2 phase

Although previous studies showed that BICD2 strongly colocalizes with Rab6 on the Golgi apparatus and cytoplasmic vesicles (Matanis et al., 2002; Short et al., 2002), careful examination demonstrated that this was not the case in G2 cells where BICD2 accumulated at the NE (Fig. 3A and data not shown). This conclusion was confirmed by staining of nocodazole-treated cells, where the dispersion of the Golgi and enlargement of the AL permitted better distinction of protein localization in cytoplasmic structures (Fig. 3B). In the cells where BICD2 associated with Rab6-bound membranes, it did not stain the NE or the AL. However, in the cells where BICD2 localized to the NE and AL, it displayed virtually no colocalization with Rab6 (Fig. 3B). Combined with the results described above, these observations indicate that BICD2 switches from Rab6-bound membranes to the NPCs in G2 phase cells.

We next investigated whether the localization of MT motor complexes correlates with that of BICD2. In untreated cells, dynein is diffusely distributed, while dynactin is predominantly located at the MT plus ends and the centrosomes (data not shown). However, in nocodazole-treated cells, a prominent colocalization of dynactin (visualized with the antibodies against its large subunit p150^{Glued}) with BICD2 can be detected in cytoplasmic structures (Hoogenraad et al., 2001). Interestingly, dynactin co-localized with BICD2 both on Rab6 and RanBP2-positive membranes, suggesting that the association of BICD2 with dynactin remains unchanged even when it switches from Rab6 to RanBP2 (Fig. 3C). Dynein staining pattern in nocodazole-treated cells displayed a lot of variation; however, we could detect its recruitment to the NE in G2, in agreement with previously published data (Fig. 3D) (Busson et al., 1998; Salina et al., 2002). Since both BICD2 and RanBP2 were shown to bind to kinesin-1, we also attempted to investigate the localization of its isoforms, but were unable to find antibodies that worked well in immunofluorescent staining experiments.

AL positioning reflects the forces exerted on them by kinesin and dynein

We reasoned that if BICD2 and the associated MT motors are specifically recruited to the NPCs in G2, they could generate forces affecting intracellular localization of these structures. To investigate these forces, we first analyzed the distribution of AL, which are relatively small and are likely to provide a sensitive readout for the balance of MT motors on the NPCs. In control cells, AL are predominantly located around the Golgi apparatus in G1 and S-phase; in G2 they shift towards the centrosome and gradually disappear ((Cordes et al., 1996), Fig. 2A, 3A, 4B and data not shown). Previously, we used the C-terminus of BICD2 as a dominant negative mutant to uncouple dynein/dynactin complex from Rab6 vesicles (Matanis et al., 2002). Interestingly, the same construct induced relocalization of AL to the cell periphery (towards MT plus ends; Fig.4A). An even more extreme AL accumulation in the cell corners was observed after the depletion of the dynactin large subunit p150^{Glued} or dynein heavy chain (DHC) (Fig. 4B). In contrast, depletion of the kinesin-1 isoform KIF5B
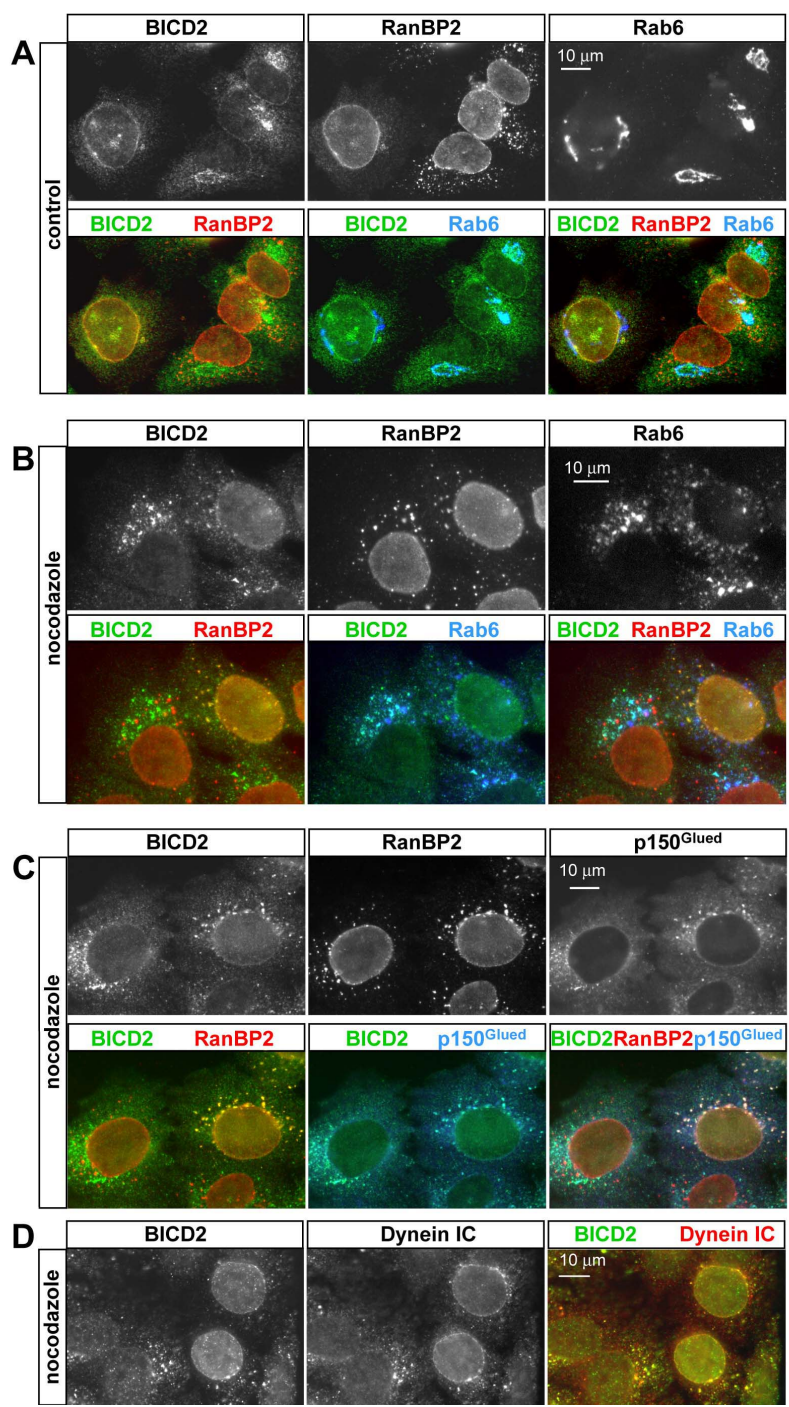
Figure 3 BICD2 and dynactin switch between Rab6 and RanBP2-positive membranes., legend on page 73

Bicaudal-D2, dynein and kinesin-1 associate with nuclear pore complexes and regulate centrosome positioning during mitotic entry

73

Figure 3. BICD2 and dynactin switch between Rab6 and RanBP2-positive membranes.

Control HeLa cells or HeLa cells treated with 10 μM nocodazole for 1 hr were fixed with paraformaldehyde and stained for the indicated endogenous proteins. Dynactin is visualized with an antibody to its large subunit p150^{Glued} and dynein with an antibody to its intermediate chain (IC). Colors used for the overlays are indicated above the corresponding images.

caused a very strong accumulation of AL near the centrosome, where MT minus ends are located (Fig. 4B). In both cases, BICD2 remained strongly enriched at the AL and the NE, indicating that its association with the NPCs is independent of these MT motors (Fig. 4B). AL redistribution in dynein or kinesin-depleted cells was only observed in cyclin B1-positive cells, indicating that it is specific for cells in G2. We conclude that the steady state distribution of AL in HeLa cells in G2 phase is controlled by both dynein and kinesin-1.

To investigate the timing of AL relocalization in more detail, we generated a cell line stably expressing GFP-tagged RanGAP1. GFP-RanGAP1 localized to the cytoplasm, NE and AL, similar to the endogenous protein; it had no significant impact on cell growth and division (data not shown). The expression levels of the fusion protein exceeded the endogenous RanGAP1 level by approximately a factor of four; however, the amount of SUMOylated RanGAP1, which is likely to be RanBP2- and NPC-bound (Mahajan et al., 1997; Matunis et al., 1996), was not significantly altered compared to control cells (Fig.4C; compare bands 1 and 3). In the stable cell line, this pool was predominantly represented by the GFP-tagged RanGAP1; therefore the GFP-RanGAP1 fusion serves as a good marker of the NE and AL (Fig.4C).

Time lapse live cell imaging of GFP-RanGAP1 expressing cells over a period of ~24 hours showed that AL were loosely distributed in the central part of the cell throughout G1 and S-phase; during these stages this pattern was independent of the presence of dynein or kinesin-1 (Fig. 4D; Suppl. Movies 1-3). However, strong accumulation of AL near the nucleus was observed in G2 cells after KIF5B depletion (3 hours ± 30 min before NE breakdown, measured in 18 cells, Fig. 4D; Suppl. Movie 2), suggesting that the motor-dependent forces that act on the NPC are engaged in G2. The timing of this motor activity switch correlated well with the duration of G2 phase and, therefore, the timing of BICD2 relocalization to the NPC (Fig.2A). It is possible that during G2, dynein is recruited by BICD2 to the NPCs and, in the absence of kinesin-1 (KIF5B), it efficiently transports AL towards the centrosome. In contrast, knockdown of either dynein or dynactin resulted in displacement of AL towards the cell periphery (Fig.4D, Suppl. Movie 3 and data not shown). Interestingly, the peripheral displacement of AL after dynein or dynactin knockdown occurred at a later stage than their displacement towards the nucleus after KIF5B knockdown, ~1 hour ± 30 min before mitotic onset (measured in 6 and 10 cells, respectively), indicating that additional MT motor recruitment and/or activation steps involving kinesin-1 take place shortly before mitotic entry. Taken together, these data show that dynein and kinesin-1-dependent forces that act on the NPCs are tightly regulated during the cell cycle.
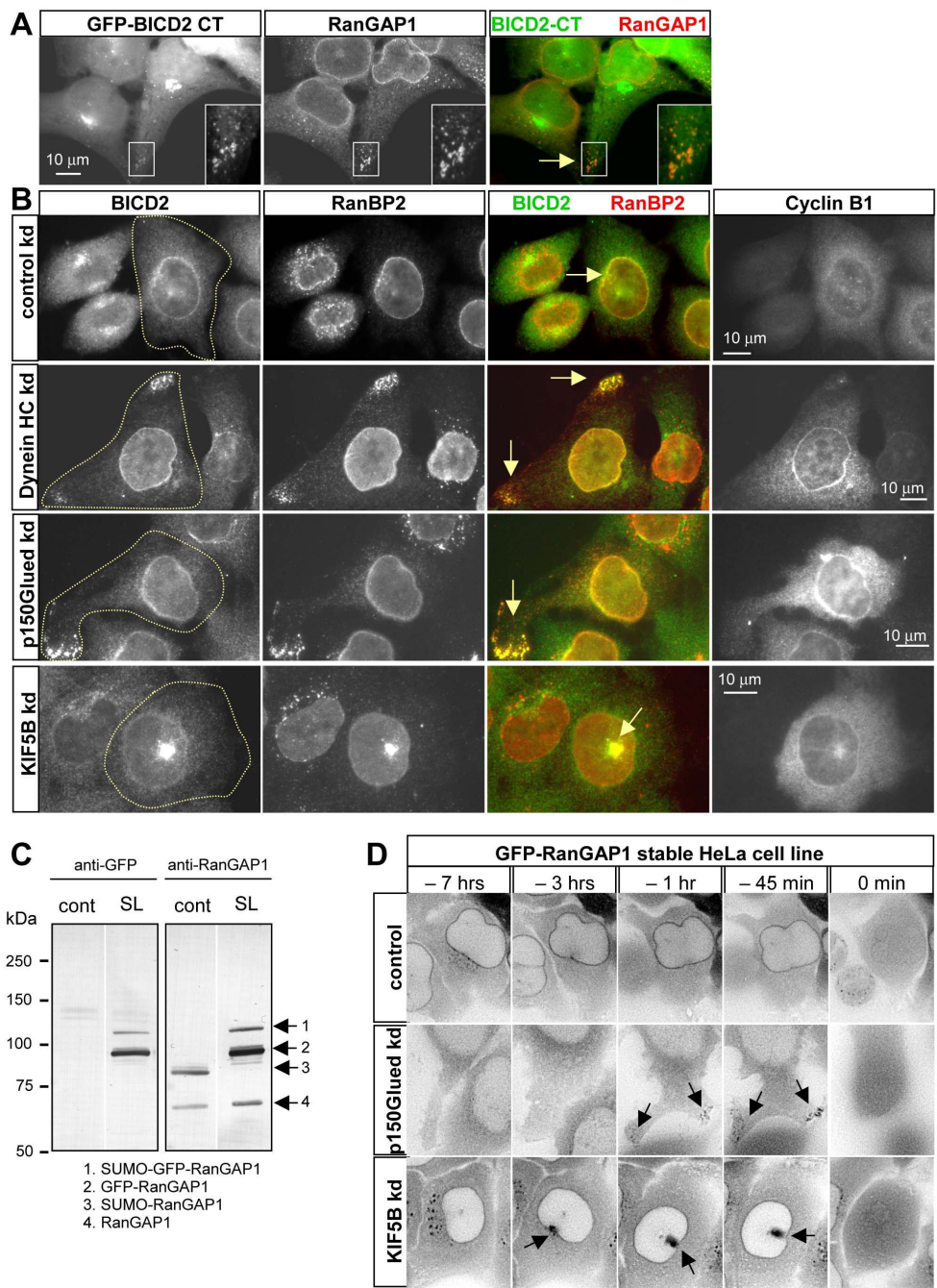
Figure 4 Dynein and kinesin-1 control the localization of AL in the G2 phase, legend on page 75

Bicaudal-D2, dynein and kinesin-1 associate with nuclear pore complexes and regulate centrosome positioning during mitotic entry

75

Figure 4. Dynein and kinesin-1 control the localization of AL in G2 phase.
A. HeLa cells were transfected with GFP-BICD2-CT, fixed with paraformaldehyde and stained for RanGAP1. The inset shows the enlargement of the boxed area.B. HeLa cells were transfected with the control, DHC#1, p150Glued, or KIF5B#1 siRNAs, fixed with paraformaldehyde 3 days later and stained for endogenous BICD2, RanBP2 and cyclin B1. In the overlays, BICD2 is shown in green and RanBP2 in red. The outline of the cyclin B1-positive cell is indicated. C. Western blots prepared with equal amounts of extracts of control HeLa cells or the stable GFP-RanGAP1 HeLa cell line and incubated with antibodies against GFP or RanGAP1.D. GFP-RanGAP1 stable HeLa cell line was imaged with a 2 or 3 min time interval two days after transfection with the control, p150Glued, or KIF5B#1 siRNAs. 0 min indicates the first frame after NE breakdown. Contrast is inverted. Arrows show the accumulation of AL at the cell periphery or the cell center.

BICD2 participates in motor recruitment to NPCs

Since BICD2 can directly bind both the NPCs and the dynein/dynactin complex, we next investigated whether BICD2 is required to recruit dynein and dynactin to the NPCs. Indeed, we observed a significant decrease in the number of cells that displayed strong dynactin staining at the NE and AL after BICD2 knockdown, indicating that BICD2 is required for dynactin association with the NPCs (Fig.5A,B, Suppl. Fig. S2). To confirm these results, we investigated BICD2 and dynactin localization in another human cell line, U2OS. Also in these cells we observed relocalization of BICD2 to the NE in G2 phase (data not shown) and a reduction of dynactin staining at the NE of G2 cells after BICD2 knockdown (Suppl. Fig.S3). Importantly, this decrease in dynactin-positive cells was not due to differences in cell cycle progression, since BICD2 depletion did not affect the proportion of cyclin B1 positive cells (Fig.5C,D). Together, these results suggest that, indeed, BICD2 is required to recruit dynein/dynactin to the NPCs, although it should be noted that we were unable to quantify dynein localization in cells due to variable and high cytoplasmic staining in late G2 cells.

In agreement with an important role of BICD2 in motor recruitment to the NPCs, the shift of AL to the cell center or the cell periphery caused by kinesin-1 or dynein depletion was strongly inhibited by co-transfection of BICD2-specific siRNAs, but not by control siRNAs or siRNAs against BICD1 or Rab6 (Fig.5C,E and data not shown). BICD2 knockdown did not alleviate other phenotypes induced by dynein depletion, such as the mitotic arrest, indicating that the observed effect on AL redistribution is specific. These results demonstrate that BICD2 is required for the G2-specific force generation at the AL by both kinesin-1 and dynein.

Dynein and kinesin-1 control relative positioning of the nucleus and the centrosomes before mitotic onset

Since dynein and kinesin-1 start to exert forces on the NPCs in G2 phase, we wondered how these forces would affect the relative position of the nucleus and centrosomes upon mitotic entry. We found that dynein inactivation frequently caused rapid relocalization of the nucleus from the cell center into one of the cell corners shortly before NE breakdown. This effect is nicely illustrated by the behavior of the nuclei in the binucleate cell in Fig. 6A (presence of two nuclei is likely a result of mitotic defects due to dynein depletion in the preceding cell division). The two nuclei remain close
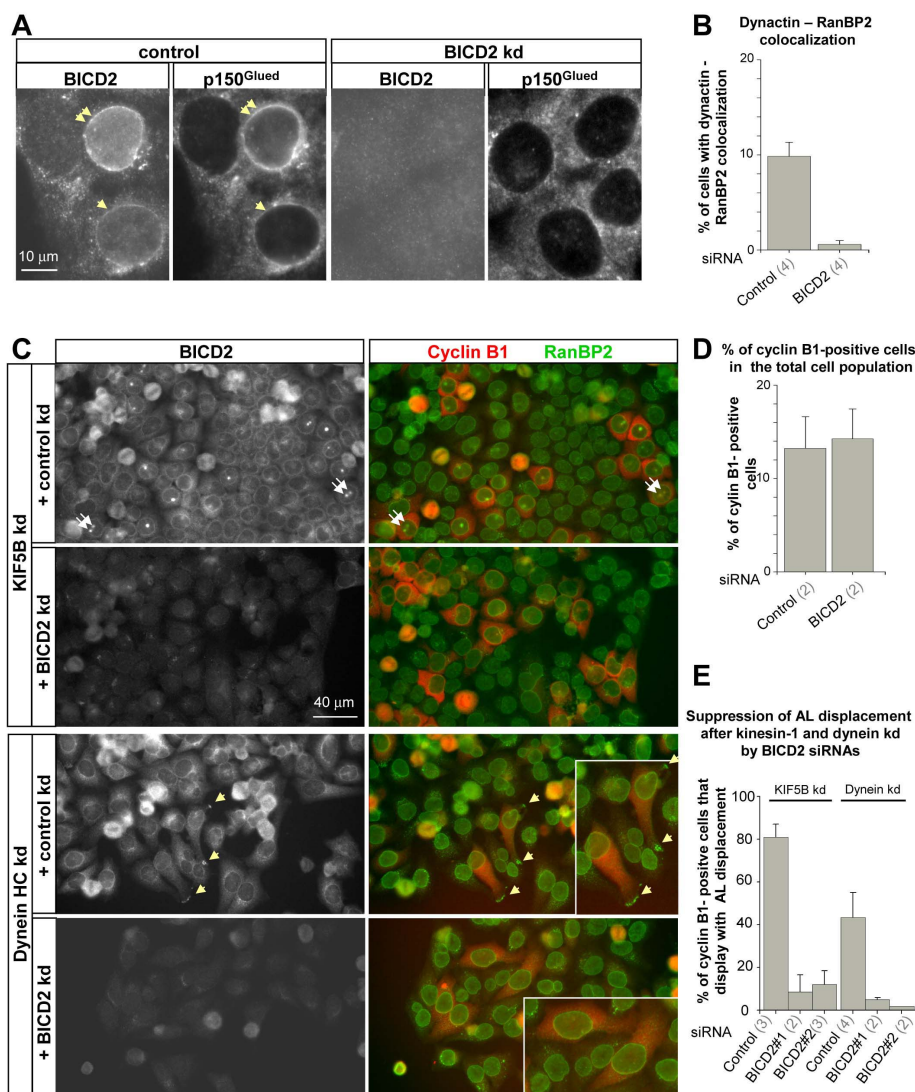
Figure 5. BICD2 is required for targeting dynein/dynactin to the NE and relocalization of AL caused by the knockdown of dynein or kinesin-1. A. HeLa cells were transfected with the control or BICD2A#1 siRNA, fixed with cold methanol followed by paraformaldehyde three days later and stained for BICD2 and dynactin (p150[Glued]). B. Percentage of HeLa cells showing strong accumulation of p150[Glued] at the RanBP2-positive NE and AL in control or BICD2-depleted cells three days after siRNA transfection.. C. HeLa cells were transfected with the KIF5B#1 or DHC#1 siRNAs in combination with the control or BICD2#1 siRNAs, incubated with 10 μM nocodazole for 1 hr, fixed with paraformaldehyde 3 days later and stained for BICD2, RanBP2 (green in overlay) and cyclin B1 (red in overlay). Insets show enlargement of cyclin B1-positive dynein-depleted cells. Accumulations of AL at the two separated centrosomes in kinesin-1-depleted cells and at the cell periphery in dynein-depleted cells are indicated by arrows. D. Percentage of cyclin B1-positive HeLa cells three days after transfection with the control

Bicaudal-D2, dynein and kinesin-1 associate with nuclear pore complexes and regulate centrosome positioning during mitotic entry

77

or BICD2-specific siRNAs. E. Percentage of HeLa cells showing AL displacement after transfection with KIF5B siRNAs or dynein heavy chain siRNAs in combination with the control siRNA or the siRNAs against BICD2. Cells with AL accumulation in the cell center or the cell periphery were scored in KIF5B or dynein knockdown cells, respectively. Error bars represent standard deviation (SD). The number of experiments is indicated in parentheses below each graph. ~300 cells per experiment were counted in panels B and D, and ~30-40 cells in panel E.

to the cell center during interphase, but are pushed into the opposite cell corners ~30 min before NE breakdown (Fig. 6A; Suppl. Movie 4). Also in cells with a single nucleus, the latter frequently appeared to be pushed to one of the cell corners prior to mitotic onset in dynein or dynactin knockdown cells (data not shown). Nuclear movement occurred somewhat later than peripheral displacement of AL in dynein/dynactin knockdown cells. It is possible that the motor activity at the NPCs gradually increases in the course of G2 progression; since the nucleus is a very large cargo its displacement requires more force than the movement of AL in the cytoplasm. Alternatively, discrete regulatory steps controlling nuclear positioning are involved.

Pushing a relatively large nucleus into a flattened corner of a cultured cell would require force, which is most likely generated by kinesin motors attached to the nucleus and moving to MT plus ends. To prove this, we first investigated the positioning of the nucleus, MTs and centrosomes in control and dynein-depleted cells. Since the perinuclear MT cytoskeleton is very dense and therefore difficult to analyze in the HeLa cells that we used, we switched to U2OS cells, a human cell line with a more sparse and centrosome-centered MT array. In control cells, the centrosomes were always located very close to the NE, both before and after their separation (Fig. 6B,C). In contrast, in dynein-depleted cells the nucleus and the centrosomes were frequently found in the opposite cell corners during prophase (Fig. 6B,C). A significant proportion of MT minus ends was still focused at the centrosomes (Fig.6B); moreover, the centrosomes were still able to separate. Centrosome separation at a considerable distance from the nucleus was also observed in dynein or dynactin-depleted HeLa cells, indicating that it does not rely on the association with the NE (Fig. 6D, Suppl. Movies 5-7).

Based on our experiments with the AL, the most likely candidate to create a pushing force on the nucleus in the absence of dynein is kinesin-1. Indeed, the effect of dynein depletion on the relative nuclear-centrosome positioning could be suppressed by the co-depletion of KIF5B (Fig.6E). Furthermore, overexpression of KIF5B was by itself sufficient to displace the centrosomes from the nuclei (Fig.6F), supporting the notion that the relative localization of the nucleus and the MT organizing centers is regulated by a balance in the antagonistic activities of kinesin-1 and cytoplasmic dynein, with the latter being predominant in untreated cells.

BICD2 and RanBP2 are required for maintenance of the association between the NE and the centrosomes in prophase cells

Since BICD2 is required for motor recruitment and/or activation at the NPCs in G2 phase, we next investigated whether its depletion has an influence on the relative positioning of the centrosomes and nuclei. Similar to HeLa, U2OS cells express both BICD2 and BICD1, which can be
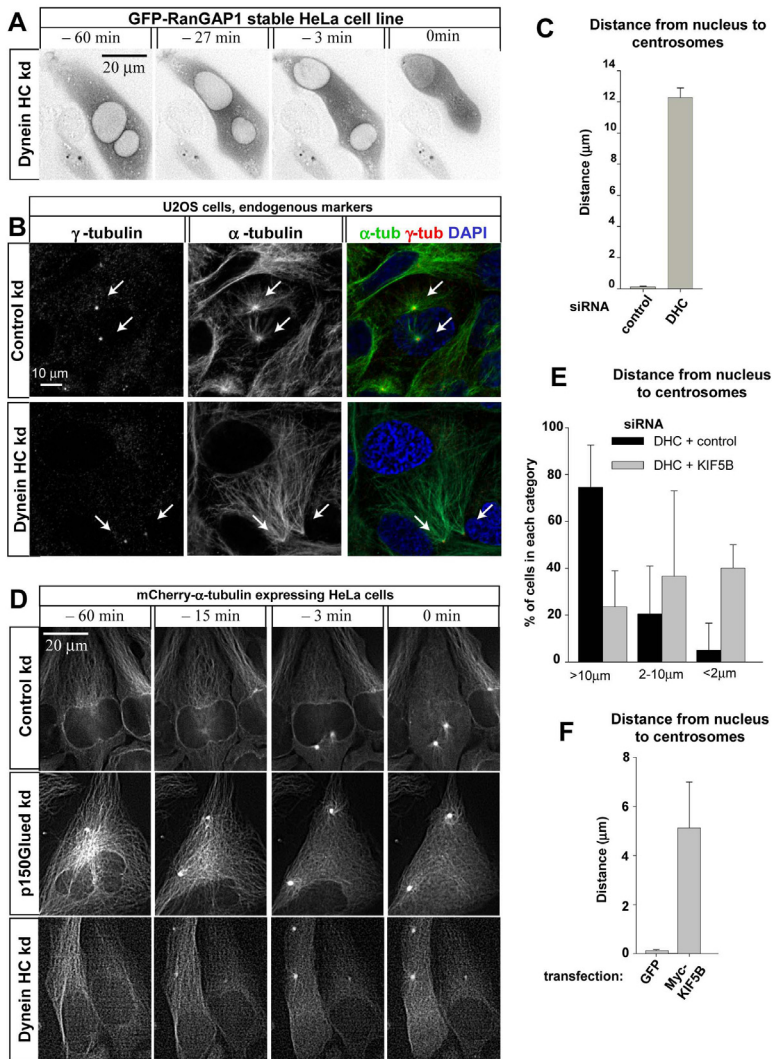
Figure 6. Opposing activities of dynein and kinesin-1 regulate nuclear positioning before mitotic entry. A. GFP-RanGAP1 stable HeLa cell line was imaged with a 3 min time interval two days after transfection with the DHC#2 siRNA. 0 min indicates the first frame after NE breakdown. Contrast is inverted. B, C. U2OS cells were transfected with the control or DHC#3 siRNAs, fixed with cold methanol and stained for α-tubulin (green in overlay) and γ-tubulin (red in overlay), as well as DNA (DAPI, blue in overlay). Representative images are shown in B, and the distance between the nucleus and the centrosomes in prophase cells is shown in C. D. mCherry-α-tubulin stable HeLa cell line was imaged with a 2 or 3 min time interval two days after transfection with the control, p150[Glued] or DHC#2 siRNAs. 0 min indicates the first frame after NE breakdown. E. Percentage of prophase U2OS cells displaying a large (>10 μm), intermediate (2-10 μm) and short distance between the nucleus and the centrosomes 3 days after simultaneous transfection with the siRNAs DHC#3 and control, or DHC#3 and KIF5B#1. F. Distance between the nucleus and the centrosomes in cells overexpressing myc-tagged KIF5B. Error bars represent SD. 20-30 cells were counted in 3 independent experiments in C and F, and in 4 experiments in E.

Bicaudal-D2, dynein and kinesin-1 associate with nuclear pore complexes and regulate centrosome positioning during mitotic entry

79

depleted by a number of different siRNAs without affecting the expression of RanBP2 or MT motors (Fig. 7A and data not shown).

 Depletion of BICD2 induced the detachment of the centrosomes from the nucleus in prophase U2OS cells; similar to dynein knockdown, also in these conditions MT minus ends remained focused at the centrosomes (Fig. 7B,C(a)). Cells with simultaneous knockdown of BICD1 and BICD2 displayed a phenotype similar to that of single BICD2 depletion, indicating that BICD1 does not contribute much to centrosome positioning (Fig. 7C(a)). A similar phenotype was also observed in cells overexpressing BICD2-CT, which is expected to uncouple dynein/dynactin from BICD2 cargo (Matanis et al., 2002) (Fig.7B,C(b)). Interestingly, RanBP2 depletion, which prevents BICD2 recruitment to the NE (Fig. 2B) also caused an increase in the distance between the nuclei and the centrosomes (Fig.7C(c)). Importantly, the distance between the centrosomes and the nucleus in BICD2 or RanBP2 knockdown cells was much smaller than in the case of dynein knockdown (compare Fig. 6C to Fig. 7C). This suggests that there is no severe imbalance between the forces exerted by dynein and kinesin-1 at the NE under these conditions. Based on the previously described data on the AL positioning (Fig. 5C, E), it seems very likely that the activities of both motors at the NE are low when either RanBP2 or BICD2 are depleted.

Why do centrosomes detach from the NE after BICD2 knockdown? It is possible that the increased distance between the centrosome and nucleus might merely be a consequence of inter-centrosomal separation. We recently found that the plus-end directed kinesin-5 Eg5, known to slide antiparallel MTs (Kapitein et al., 2005), pushes centrosomes apart during prophase (Tanenbaum et al., submitted). Thus, Eg5-dependent sliding forces might drive the centrosomes away from the nucleus when it becomes uncoupled from dynein and kinesin-1 due to BICD2 depletion. In line with this idea, inhibition of Eg5 with S-trityl-L-cysteine (STLC) significantly suppressed centrosome detachment caused by BICD2 depletion, indicating that Eg5 is at least in part responsible for pushing the centrosomes away from NE in BICD2-depleted prophase cells (Fig.7C (d)).

Finally, to prove that BICD2 can exert a direct effect on centrosome positioning through its localization at the nuclear envelope, we constructed a fusion protein in which we attached the N-terminal portion of BICD2, including the dynein and kinesin-1 binding sites, to the C-terminal KASH (Klarsicht, ANC-1, Syne Homology) domain-containing region of nesprin-3, which is targeted to the NE by SUN proteins (Ketema et al., 2007). This fusion localized specifically to the NE and enhanced the accumulation of dynactin to the NE (Fig.7D). Importantly, the expression of the BICD2-nesprin-3 fusion completely suppressed centrosome detachment in RanBP2-depleted prophase cells, even at very low expression levels (Fig. 7C(e)). Taken together, these results support the view that BICD2 can recruit dynein/dynactin to the NE and regulate the relative localization of the nucleus and the centrosomes.

A

Control · BICD2#1 · BICD2#2 · BICD1#1 · BICD1#2 · BICD1#3 · BICD2#1+BICD1#1 · BICD2#2+BICD1#2

BICD1 — BICD1 / BICD2

BICD2

p150^Glued

KIF5B

DIC

RanBP2

B

BICD1/BICD2 kd

γ-tubulin | α-tubulin | α-tub γ-tub DAPI

10 μm

GFP-BICD2-CT

γ-Tubulin | GFP-BICD2-CT | CT γ-tub DAPI

C

Distance from nucleus to centrosomes

(a) BICD1/2 kd · (b) BICD2-CT ox · (c) RanBP2 kd · (d) BICD2 kd Eg5 inhibition · (e) rescue of RanBP2 kd

Distance (μm)

siRNA

Control (4) · BICD2#1 (12) · BICD2#1+BICD1#1 (4) · BICD2#2 (12) · BICD2#2+BICD1#1 (4) · GFP-BICD2-CT (2) · Control (3) · RanBP2#1 (3) · RanBP2#3 (3) · BICD2#1 (12) · BICD2#1+STLC (9) · BICD2#2 (12) · BICD2#2+STLC (9) · GFP (3) · GFP-BICD2-NT-nesprin (3)

D

GFP-BICD2-NT-nesprin3-CT

10 μm

p150Glued

E

G1 and S phase | G2 phase
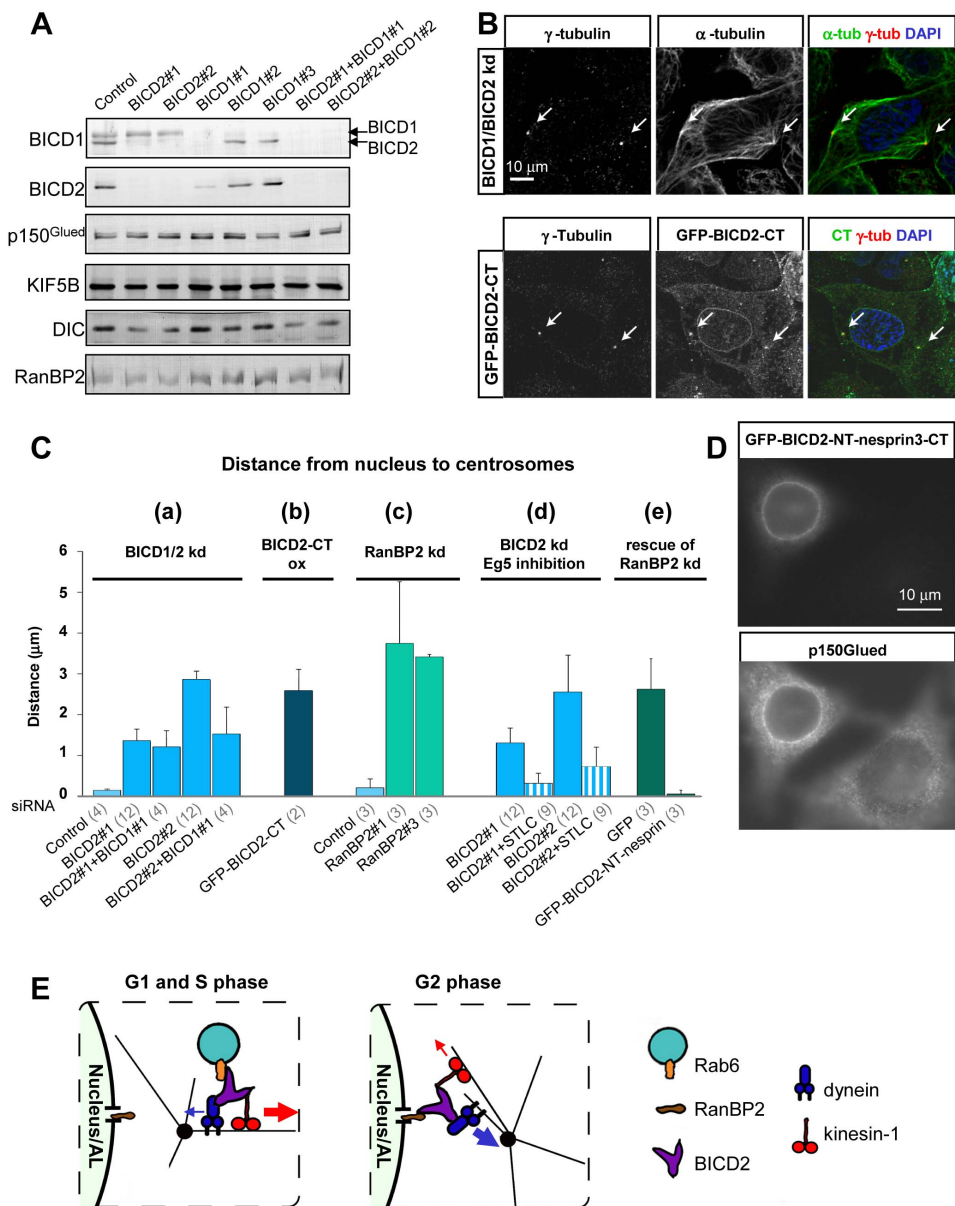
Nucleus/AL

Rab6
RanBP2
BICD2
dynein
kinesin-1

Figure 7. Depletion of BICD2 and RanBP2 causes centrosome detachment in prophase U2OS cells.
A. Western blots with the indicated antibodies were performed with equal amounts of extracts of U2OS cells 3 days after transfection with the indicated siRNAs. Note that BICD1 antibody cross-reacts with BICD2 (arrows). B. U2OS cells were transfected with BICD1#1 and BICD2#1 siRNAs (upper panel) or with GFP-BICD2-CT, fixed with cold methanol and stained for α-tubulin (green in overlay) and γ-tubulin (red in overlay), as well as DNA (DAPI, blue in overlay). C. The distance between the nucleus and the centrosomes in prophase U2OS cells under

Bicaudal-D2, dynein and kinesin-1 associate with nuclear pore complexes and regulate centrosome positioning during mitotic entry

81

different conditions. (a). Cells were transfected with the indicated siRNAs against BICD1 and BICD2. (b). Cells were transfected with GFP-BICD2-CT. (c). Cells were transfected with the indicated siRNAs against RanBP2. (d). Cells were transfected with the indicated siRNAs against BICD2, and either untreated or incubated with 4 µM STLC, an Eg5 inhibitor. (e). The effect of RanBP2 knockdown (induced with the RanBP2#3 siRNA) was rescued by expression of the GFP-BICD2-NT-nesprin-3 fusion but not by GFP alone. Error bars represent SD; the number of experiments for each condition is shown in parentheses below the graph; 20-30 cells were counted per experiment. D. HeLa cells were transfected with GFP-BICD2-NT-nesprin-3 fusion, fixed with paraformaldehyde and stained for p150[glued]. Note the recruitment of dynactin to the NE in the transfected cell. E. A model of the concerted action of BICD2, dynein and kinesin-1 on Rab6 vesicles and NPCs in different phases of the cell cycle. In G1 and S phase, BICD2, dynein and kinesin-1 associate with Rab6 vesicles; kinesin-1 activity predominates in this complex. In G2, BICD2 with the associated motors accumulates at the NPCs, where the dynein-mediated movement predominates.

Discussion

During cell division the MT cytoskeleton and membrane organelles undergo a severe reorganization, which proceeds in a highly regulated manner. In many cell types, the two centrosomes move apart while maintaining their attachment to the NE. This helps to form the bipolar mitotic spindle around the chromosomes that are released after NE breakdown. In this study, we have identified molecular mechanisms important for the relative positioning of the nucleus and the centrosomes before mitotic onset. We show that the dynein/dynactin adaptor BICD2 is specifically recruited to the NPC in G2 phase through a direct interaction with the NPC component RanBP2. In line with previously published data (reviewed by (Hetzer et al., 2005; Rosenblatt, 2005)), we find that cytoplasmic dynein is the major player responsible for the nucleo-centrosomal attachment, but, unexpectedly, we find that kinesin-1 also participates in this process by antagonizing the dynein function. Furthermore, our data indicates that BICD2 and RanBP2 are involved in linking MT motors to the NPCs, and we show that their depletion causes centrosome detachment from the nucleus.

Our previous studies showed that BICD2 associates with MT motors through its N-terminus and the middle portion, while the C-terminus is the cargo-binding site (Grigoriev et al., 2007; Hoogenraad et al., 2003; Matanis et al., 2002). Here we identified a new cargo for BICD2, the nucleoporin RanBP2, which binds to the same domain of BICD2 as the small GTPase Rab6. Our data suggest that the interaction of BICD2 with the two cargos is temporally regulated during the cell cycle: during G1 and S phase, BICD2 appears to associate predominantly with Rab6, while in G2 it binds mostly to the NPC (Fig. 7E). It is currently unclear how this switch is controlled, but it is likely that mitotic kinases are involved.

Both during Rab6 vesicle trafficking and in nuclear positioning, BICD2 participates in transport processes that involve the opposing functions of cytoplasmic dynein and kinesin-1. The predominating motor in the two processes is different: Rab6 vesicles are exocytotic carriers that preferentially move to MT plus ends, while the nucleus and AL are mainly pulled by dynein (Fig. 7E). This indicates that although BICD2 strongly binds to dynein and dynactin and can induce selective MT minus-directed transport when artificially tethered to cargo (Hoogenraad et al., 2003), BICD2

participation by itself is insufficient to shift the balance in favor of dynein; therefore, additional factors are likely to be involved.

Importantly, we have shown here that BICD2 is needed both for dynein and kinesin-1-mediated force generation on the NPCs, suggesting that it is an essential component of both motor complexes (Fig.7E). While it may appear strange that the two opposite polarity motors act together in processes which mostly depend on only one of them, this arrangement seems to represent a fundamental property of MT motor systems most likely required to allow flexibility and permit regulation of cargo distribution (Gross, 2004; Welte, 2004). Our study shows that even the positioning of a very large cargo, such as the cell nucleus, is no exception to this rule.

The mechanism underlying kinesin-1 recruitment to BICD2-bound NPCs is unlikely to be explained solely by the binding between BICD2 and kinesin-1 (Grigoriev et al., 2007), since RanBP2 can directly bind to kinesin-1 as well (Cai et al., 2001; Cho et al., 2007). Intriguingly, both BICD2 and kinesin-1 interact with the same region of RanBP2; whether these interactions are cooperative and what consequences this has on the architecture of the motor complex remains to be determined.

It is likely that additional tightly regulated components of the motor recruitment and/or activation machinery, such as dynein accessory factors, are involved in nuclear positioning; this view is strongly supported by the observed timing of binding and transport steps. BICD2 associates with the NPCs early in G2; this results in dynein activation that is sufficient to cause strong AL accumulation around the centrosome in the absence of kinesin-1 at ~3.5 hrs before NE envelope breakdown. At a later stage (1.5-0.5 hrs before NE breakdown), additional motor activation likely takes place; this is reflected by the peripheral displacement of the AL, the nucleus and the centrosomes in dynein-depleted cells. Furthermore, Eg5 becomes active during prophase and pushes centrosomes apart. The forces induced by Eg5-dependent centrosome separation are kept in check by the complex of RanBP2-BICD2-dynein that prevents centrosome detachment from the nucleus while allowing centrosomes to part.

What is the function of the complex molecular events described in this study? The normal geometry of the mitotic apparatus at the onset of mitosis is likely to promote efficient kinetochore attachment to MT plus ends. The interaction of dynein with the NPCs through BICD2 could also help to tear apart the nuclear envelope (Beaudouin et al., 2002; Salina et al., 2002), a possibility that was not addressed by us here. It should be noted that the significant redundancy of mechanisms controlling mitotic progression allows the cell to compensate for deviations at the early mitotic stages. In line with this idea, cells depleted of BICD2 and kinesin-1 do not exhibit significant mitotic abnormalities (Tanenbaum, unpublished data), and the mitotic phenotypes caused by RanBP2 and dynein knockdown are likely due to their involvement in subsequent steps of cell division (Joseph et al., 2004; Karki and Holzbaur, 1999; Maiato et al., 2004; Salina et al., 2003). Further, dynein-mediated coupling between the nucleus, MTs and the centrosome plays an important role in differentiated cells, such as migrating neurons (Tsai and Gleeson, 2005). In flies, BicD is involved in MT and dynein/dynactin-dependent positioning of the oocyte and photoreceptor nuclei (Claussen and Suter, 2005) and it would be interesting to know if it plays a similar role in differentiated mammalian cells.

Bicaudal-D2, dynein and kinesin-1 associate with nuclear pore complexes and regulate centrosome positioning during mitotic entry

83

Experimental Procedures

Expression constructs and siRNAs

We used the following previously described expression vectors: GFP-BICD2 (Hoogenraad et al., 2001), HA-BICD2-CT (Matanis et al., 2002); myc-KIF5B (Grigoriev et al., 2007); BirA (Driegen et al., 2005) (a gift of D. Meijer, Erasmus MC, Rotterdam, The Netherlands); mCherry-α-tubulin (Shaner et al., 2004) (a gift of R. Tsien, UCSD, San Diego, USA). Biotinylation and GFP-tagged BICD2 C-terminus (Bio-GFP-BICD2-CT, BICD2 amino acids 487-820, accession number CAC51393) was generated in pEGFP-C2 (Clontech) by cloning at the NheI and AgeI sites in front of the GFP a linker encoding the amino acid sequence MASGLNDIFEAQKIEWHEGGG. CFP-tagged RanBP2 fragments with the N-terminal palmitoylation signal derived from GAP-43 were generated in a modified version of the pECFP-N1 vector (Clontech) by a PCR based strategy. GFP-BICD2-NT-nesprin-3 fusion was generated by attaching the amino acids 582-975 of nesprin-3 (accession number NP_001036164, (Wilhelmsen et al., 2005); a gift of A. Sonnenberg, Netherlands Cancer Institute, Amsterdam) to the C-terminus of GFP-BICD2-NT (amino acids 1-594 of BICD2 (Hoogenraad et al., 2003)). GFP-RanGAP1 was generated in pEGFP-C1 by inserting into it the BglII-SmaI fragment of KIAA1835 (accession number AB058738, a gift of Kazusa DNA Research Institute, Japan).

We used the following siRNAs: KIF5B#1, 5'- GCCUUAUGCAUUUGAUCGG (siRNA 118426, Ambion), KIF5B#2, 5'- GCACAUCUCAAGAGCAAGU (siRNA 118427, Ambion); DHC#1 5'- CGUACUCCCGUGAUUGAUG (siRNA 118309, Ambion); DHC#2 5'- GCCAAAAGUUACAGACUUU (siRNA 118311, Ambion), DHC#3 5'-GGAUCAAACAUGACGGAAU, RanBP2#1 5'-GGACAGUGGGAUUGUAGUG (Joseph et al., 2004); RanBP2#2 5'- CACAGACAAAGCCGUUGAA; RanBP2#3 Dharmacon SMARTpool; p150[Glued] 5' GUAUUUGAAGAUGGAGCAG; BICD2#1 5' GGAGCUGUCACACUACAUG; BICD2#25'- GGUGGACUAUGAGGCUAUC; BICD1#1 5'- CCUUAAUGCCAUAAUCCGG; BICD1#2 5'- GCAAAGAGCCAAUGAAUAU; BICD1#3 5'- GCAACUGUCUCGUCAAAGA. As a control we used a previously described scrambled CLASP1 siRNA, the siRNA against luciferase (Grigoriev et al., 2008) or the siRNA to GAPD (control Dharmacon SMARTpool).

Pull downs, IP, identification of BICD2-CT binding partners by mass spectrometry and yeast two-hybrid analysis

Bio-GFP-BICD2-CT and BirA were transiently co-expressed in HeLa cells; cells were lysed in a buffer containing 100 mM NaCl, 20 mM Tris-HCl, pH 7.5, 1 % Triton X-100 and protease inhibitors (Complete, Roche). Streptavidin pull down assays, mass spectrometry analysis and IP from HEK293 cells overexpressing different protein fusions were performed as described by (Grigoriev et al., 2007). For the IP of endogenous proteins, HeLa cells were arrested with 75 ng/mL nocodazole for 18 h, washed with PBS, lyzed with digitonin in the buffer containing 20 mM HEPES pH 7.3, 110 mM potassium acetate, 2 mM magnesium acetate, 1 mM EGTA, 1 mM DTT and protease and phosphatase inhibitors; lysates were centrifuged at 100000xg for 1h and IP was carried out using standard procedures. 6XHIS-tagged BICD2-CT (amino acids 630-820) was generated in pET28a. GST fusions of RanBP2 fragments 3 and 4 (amino acids 2147-2287 and 2447-2887, accession number

NP_006258) were generated in pGEX-3X. Protein purification and GST pull down assays were carried out as described by Lansbergen et al., 2006.

For yeast two-hybrid assays, different bait constructs were prepared in pBHA (lexA fusion vector) and tested against various BICD2 fragments cloned into pGAD10 (GAL4 activation domain vector, Clontech) as described by Grigoriev et al., 2007.

Cell culture and transfection of plasmids and siRNAs

HeLa, HEK293 and U2OS cells were cultured as described previously (Mimori-Kiyosue et al., 2005; Tanenbaum et al., 2006). PolyFect (Qiagen), Lipofectamine 2000 (Invitrogen) or FuGENE 6 (Roche) reagents were used for plasmid transfection. Stable HeLa clones expressing fluorescent proteins were selected using Fluorescence Activated Cell Sorting and cultured in the presence of 0.4 mg/ml G418 (Roche). Synthetic siRNAs were transfected into HeLa cells plated at 20% confluence using HiPerFect (Qiagen) at the final concentration 5 nM; cells were analyzed by 3 days after transfection. U2OS cells were transfected with HiPerFect during plating at ~20% confluence using 10 nM siRNAs; a second transfection with the same siRNA concentration was performed one or two days later and the cells were analyzed 3 or 4 days after plating.

Antibodies, immunofluorescent staining and Western blotting

We used affinity purified goat polyclonal antibodies against RanBP2 and RanGAP1 (Hutten et al., 2008; Pichler et al., 2002), rabbit polyclonal antibodies against GFP (Abcam), BICD1 and BICD2 (Hoogenraad et al., 2001; Matanis et al., 2002), DHC and KIF5B (Santa Cruz), mouse monoclonal antibody against Rab6 (which recognizes Rab6A and Rab6A′, a gift of A. Barnekow, University of Muenster, Germany), α- and β-tubulin (Sigma), DIC (Chemicon and Sigma), cyclin B1 (Santa Cruz), p150[Glued] (BD Biosciences). For secondary antibodies we used Alexa 350, Alexa 488 and Alexa 594-conjugated goat antibodies against rabbit, rat and mouse IgG, donkey antibodies against sheep IgG (Molecular Probes), AMCA-labeled rat anti-mouse, FITC-labeled donkey anti-rabbit and anti-mouse antibodies (Jackson ImmunoResearch Laboratories). Cell fixation and staining procedures were described previously (Hoogenraad et al., 2001). Briefly, we used the following fixations; 4% paraformaldehyde in PBS (15 min at room temperature), -20°C methanol (10 min), or -20°C methanol (10 min) immediately followed by 4% paraformaldehyde in PBS (15 min at room temperature). For pre-extraction of live cells we used the following buffer: 60 mM PIPES, 25 mM HEPES, 10 mM EGTA, 0.5% Triton X-100, 4 mM $MgSO_4$, pH 7.5. Western blotting was performed as described previously (Mimori-Kiyosue et al., 2005).

Fluorescence microscopy and image analysis

Images of fixed cells with the exception of Fig.6B and 7B were collected with a Leica DMRBE microscope equipped with a PL Fluotar 100x 1.3 N.A. or 40x 1.00-0.50 N.A. oil objectives, FITC/EGFP filter 41012 (Chroma) and Texas Red filter 41004 (Chroma) and an ORCA-ER-1394 CCD camera (Hamamatsu). Images in Fig.6B and 7B were acquired on a confocal Zeiss LSM510 META (CarlZeiss)

Bicaudal-D2, dynein and kinesin-1 associate with nuclear pore complexes and regulate centrosome positioning during mitotic entry

85

with a Plan Apochromat 63x 1.4 N.A. objective. Z-planes were acquired with 1µm intervals. Images are maximum intensity projections of all Z-planes.

Time-lapse live cell imaging was performed on the inverted research microscope Nikon Eclipse TE2000E (Nikon) with a CFI Plan Fluor 40x 1.30 N.A. oil objective (Nikon), equipped with CoolSNAP-HQ2 CCD camera (Roper Scientific) controlled by MetaMorph 7.1 software (Molecular Devices). For excitation we used HBO 103 W/2 Mercury Short Arc Lamp (Osram) and Chroma ET-GFP (49002) or Chroma ET-DsRed (49005) filter sets. 16-bit images were projected onto the CCD chip at a magnification of 0.1563 mm/pixel. Image analysis was performed by using MetaMorph software. Cells were kept at 37°C during observation.

Images were prepared for publication using Adobe Photoshop. The images of fixed cells were modified by adjustments of levels and contrast. Live images were modified by adjustments of levels and contrast and applying Unsharp Mask and Gaussian Blur filters.

Acknowledgements

References

Beaudouin, J., Gerlich, D., Daigle, N., Eils, R., and Ellenberg, J. (2002). Nuclear envelope breakdown proceeds by microtubule-induced tearing of the lamina. Cell *108*, 83-96.

Bullock, S.L., and Ish-Horowicz, D. (2001). Conserved signals and machinery for RNA transport in Drosophila oogenesis and embryogenesis. Nature *414*, 611-616.

Bullock, S.L., Nicol, A., Gross, S.P., and Zicha, D. (2006). Guidance of bidirectional motor complexes by mRNA cargoes through control of dynein number and activity. Curr Biol *16*, 1447-1452.

Busson, S., Dujardin, D., Moreau, A., Dompierre, J., and De Mey, J.R. (1998). Dynein and dynactin are localized to astral microtubules and at cortical sites in mitotic epithelial cells. Curr Biol *8*, 541-544.

Cai, Y., Singh, B.B., Aslanukov, A., Zhao, H., and Ferreira, P.A. (2001). The docking of kinesins, KIF5B and KIF5C, to Ran-binding protein 2 (RanBP2) is mediated via a novel RanBP2 domain. J Biol Chem *276*, 41594-41602.

Cho, K.I., Cai, Y., Yi, H., Yeh, A., Aslanukov, A., and Ferreira, P.A. (2007). Association of the kinesin-binding domain of RanBP2 to KIF5B and KIF5C determines mitochondria localization and function. Traffic *8*, 1722-1735.

Claussen, M., and Suter, B. (2005). BicD-dependent localization processes: from Drosophilia development to human cell biology. Ann Anat *187*, 539-553.

Cordes, V.C., Reidenbach, S., and Franke, W.W. (1996). Cytoplasmic annulate lamellae in cultured cells: composition, distribution, and mitotic behavior. Cell Tissue Res *284*, 177-191.

de Boer, E., Rodriguez, P., Bonte, E., Krijgsveld, J., Katsantoni, E., Heck, A., Grosveld, F., and Strouboulis, J. (2003). Efficient biotinylation and single-step purification of tagged transcription factors in mammalian cells and transgenic mice. Proc Natl Acad Sci U S A *100*, 7480-7485.

Driegen, S., Ferreira, R., van Zon, A., Strouboulis, J., Jaegle, M., Grosveld, F., Philipsen, S., and Meijer, D. (2005). A generic tool for biotinylation of tagged proteins in transgenic mice. Transgenic Res *14*, 477-482.

Glater, E.E., Megeath, L.J., Stowers, R.S., and Schwarz, T.L. (2006). Axonal transport of mitochondria requires milton to recruit kinesin heavy chain and is light chain independent. J Cell Biol *173*, 545-557.

Gorlich, D., and Kutay, U. (1999). Transport between the cell nucleus and the cytoplasm. Annu Rev Cell Dev Biol *15*, 607-660.

Grigoriev, I., Gouveia, S.M., van der Vaart, B., Demmers, J., Smyth, J.T., Honnappa, S., Splinter, D., Steinmetz, M.O., Putney, J.W., Jr., Hoogenraad, C.C., *et al.* (2008). STIM1 is a MT-plus-end-tracking protein involved in remodeling of the ER. Curr Biol *18*, 177-182.

Grigoriev, I., Splinter, D., Keijzer, N., Wulf, P.S., Demmers, J., Ohtsuka, T., Modesti, M., Maly, I.V., Grosveld, F., Hoogenraad, C.C., *et al.* (2007). Rab6 regulates transport and targeting of exocytotic carriers. Dev Cell *13*, 305-314.

Gross, S.P. (2004). Hither and yon: a review of bi-directional microtubule-based transport. Phys Biol *1*, R1-11.

Hetzer, M.W., Walther, T.C., and Mattaj, I.W. (2005). Pushing the envelope: structure, function, and dynamics of the nuclear periphery. Annu Rev Cell Dev Biol *21*, 347-380.

Hoogenraad, C.C., Akhmanova, A., Howell, S.A., Dortland, B.R., De Zeeuw, C.I., Willemsen, R., Visser, P., Grosveld, F., and Galjart, N. (2001). Mammalian Golgi-associated Bicaudal-D2 functions in the dynein-dynactin pathway by interacting with these complexes. Embo J *20*, 4041-4054.

Hoogenraad, C.C., Wulf, P., Schiefermeier, N., Stepanova, T., Galjart, N., Small, J.V., Grosveld, F., de Zeeuw, C.I., and Akhmanova, A. (2003). Bicaudal D induces selective dynein-mediated microtubule minus end-directed transport. Embo J *22*, 6004-6015.

Hutten, S., Flotho, A., Melchior, F., and Kehlenbach, R.H. (2008). The Nup358-RanGAP Complex Is Required for Efficient Importin {alpha}/{beta}-dependent Nuclear Import. Mol Biol Cell *19*, 2300-2310.

Januschke, J., Nicolas, E., Compagnon, J., Formstecher, E., Goud, B., and Guichet, A. (2007). Rab6 and the secretory pathway affect oocyte polarity in Drosophila. Development *134*, 3419-3425.

Johansson, M., Rocha, N., Zwart, W., Jordens, I., Janssen, L., Kuijl, C., Olkkonen, V.M., and Neefjes, J. (2007). Activation of endosomal dynein motors by stepwise assembly of Rab7-RILP-p150Glued, ORP1L, and the receptor betalll spectrin. J Cell Biol *176*, 459-471.

Jordens, I., Marsman, M., Kuijl, C., and Neefjes, J. (2005). Rab proteins, connecting transport and vesicle fusion. Traffic *6*, 1070-1077.

Joseph, J., Liu, S.T., Jablonski, S.A., Yen, T.J., and Dasso, M. (2004). The RanGAP1-RanBP2 complex is essential for microtubule-kinetochore interactions in vivo. Curr Biol *14*, 611-617.

Kapitein, L.C., Peterman, E.J., Kwok, B.H., Kim, J.H., Kapoor, T.M., and Schmidt, C.F. (2005). The bipolar mitotic kinesin Eg5 moves on both microtubules that it crosslinks. Nature *435*, 114-118.

Karcher, R.L., Deacon, S.W., and Gelfand, V.I. (2002). Motor-cargo interactions: the key to transport specificity. Trends Cell Biol *12*, 21-27.

Karki, S., and Holzbaur, E.L. (1999). Cytoplasmic dynein and dynactin in cell division and intracellular transport. Curr Opin Cell Biol *11*, 45-53.

Kessel, R.G. (1992). Annulate lamellae: a last frontier in cellular organelles. Int Rev Cytol *133*, 43-120.

Ketema, M., Wilhelmsen, K., Kuikman, I., Janssen, H., Hodzic, D., and Sonnenberg, A. (2007). Requirements for the localization of nesprin-3 at the nuclear envelope and its interaction with plectin. J Cell Sci *120*, 3384-3394.

Bicaudal-D2, dynein and kinesin-1 associate with nuclear pore complexes and
regulate centrosome positioning during mitotic entry

87

Lansbergen, G., Grigoriev, I., Mimori-Kiyosue, Y., Ohtsuka, T., Higa, S., Kitajima, I., Demmers, J., Galjart, N., Houtsmuller, A.B., Grosveld, F., *et al.* (2006). CLASPs attach microtubule plus ends to the cell cortex through a complex with LL5beta. Dev Cell *11*, 21-32.

Mach, J.M., and Lehmann, R. (1997). An Egalitarian-BicaudalD complex is essential for oocyte specification and axis determination in Drosophila. Genes Dev *11*, 423-435.

Mahajan, R., Delphin, C., Guan, T., Gerace, L., and Melchior, F. (1997). A small ubiquitin-related polypeptide involved in targeting RanGAP1 to nuclear pore complex protein RanBP2. Cell *88*, 97-107.

Maiato, H., Sampaio, P., and Sunkel, C.E. (2004). Microtubule-associated proteins and their essential roles during mitosis. Int Rev Cytol *241*, 53-153.

Malone, C.J., Misner, L., Le Bot, N., Tsai, M.C., Campbell, J.M., Ahringer, J., and White, J.G. (2003). The C. elegans hook protein, ZYG-12, mediates the essential attachment between the centrosome and nucleus. Cell *115*, 825-836.

Matanis, T., Akhmanova, A., Wulf, P., Del Nery, E., Weide, T., Stepanova, T., Galjart, N., Grosveld, F., Goud, B., De Zeeuw, C.I., *et al.* (2002). Bicaudal-D regulates COPI-independent Golgi-ER transport by recruiting the dynein-dynactin motor complex. Nat Cell Biol *4*, 986-992.

Matunis, M.J., Coutavas, E., and Blobel, G. (1996). A novel ubiquitin-like modification modulates the partitioning of the Ran-GTPase-activating protein RanGAP1 between the cytosol and the nuclear pore complex. J Cell Biol *135*, 1457-1470.

Mimori-Kiyosue, Y., Grigoriev, I., Lansbergen, G., Sasaki, H., Matsui, C., Severin, F., Galjart, N., Grosveld, F., Vorobjev, I., Tsukita, S., *et al.* (2005). CLASP1 and CLASP2 bind to EB1 and regulate microtubule plus-end dynamics at the cell cortex. J Cell Biol *168*, 141-153.

Pichler, A., Gast, A., Seeler, J.S., Dejean, A., and Melchior, F. (2002). The nucleoporin RanBP2 has SUMO1 E3 ligase activity. Cell *108*, 109-120.

Rosenblatt, J. (2005). Spindle assembly: asters part their separate ways. Nat Cell Biol *7*, 219-222.

Salina, D., Bodoor, K., Eckley, D.M., Schroer, T.A., Rattner, J.B., and Burke, B. (2002). Cytoplasmic dynein as a facilitator of nuclear envelope breakdown. Cell *108*, 97-107.

Salina, D., Enarson, P., Rattner, J.B., and Burke, B. (2003). Nup358 integrates nuclear envelope breakdown with kinetochore assembly. J Cell Biol *162*, 991-1001.

Shaner, N.C., Campbell, R.E., Steinbach, P.A., Giepmans, B.N., Palmer, A.E., and Tsien, R.Y. (2004). Improved monomeric red, orange and yellow fluorescent proteins derived from Discosoma sp. red fluorescent protein. Nat Biotechnol *22*, 1567-1572.

Short, B., Preisinger, C., Schaletzky, J., Kopajtich, R., and Barr, F.A. (2002). The Rab6 GTPase regulates recruitment of the dynactin complex to Golgi membranes. Curr Biol *12*, 1792-1795.

Stelter, P., Kunze, R., Flemming, D., Hopfner, D., Diepholz, M., Philippsen, P., Bottcher, B., and Hurt, E. (2007). Molecular basis for the functional interaction of dynein light chain with the nuclear-pore complex. Nat Cell Biol *9*, 788-796.

Tanenbaum, M.E., Galjart, N., van Vugt, M.A., and Medema, R.H. (2006). CLIP-170 facilitates the formation of kinetochore-microtubule attachments. Embo J *25*, 45-57.

Tsai, L.H., and Gleeson, J.G. (2005). Nucleokinesis in neuronal migration. Neuron *46*, 383-388.

Vale, R.D. (2003). The molecular motor toolbox for intracellular transport. Cell *112*, 467-480.

Welte, M.A. (2004). Bidirectional transport along microtubules. Curr Biol *14*, R525-537.

Wilhelmsen, K., Litjens, S.H., Kuikman, I., Tshimbalanga, N., Janssen, H., van den Bout, I., Raymond, K., and Sonnenberg, A. (2005). Nesprin-3, a novel outer nuclear membrane protein, associates with the cytoskeletal linker protein plectin. J Cell Biol *171*, 799-810.

Wu, J., Matunis, M.J., Kraemer, D., Blobel, G., and Coutavas, E. (1995). Nup358, a cytoplasmically exposed nucleoporin with peptide repeats, Ran-GTP binding sites, zinc fingers, a cyclophilin A homologous domain, and a leucine-rich region. J Biol Chem *270*, 14209-14213.

Yokoyama, N., Hayashi, N., Seki, T., Pante, N., Ohba, T., Nishii, K., Kuma, K., Hayashida, T., Miyata, T., Aebi, U., *et al.* (1995). A giant nucleopore protein that binds Ran/TC4. Nature *376*, 184-188.

Supplemental table and figures

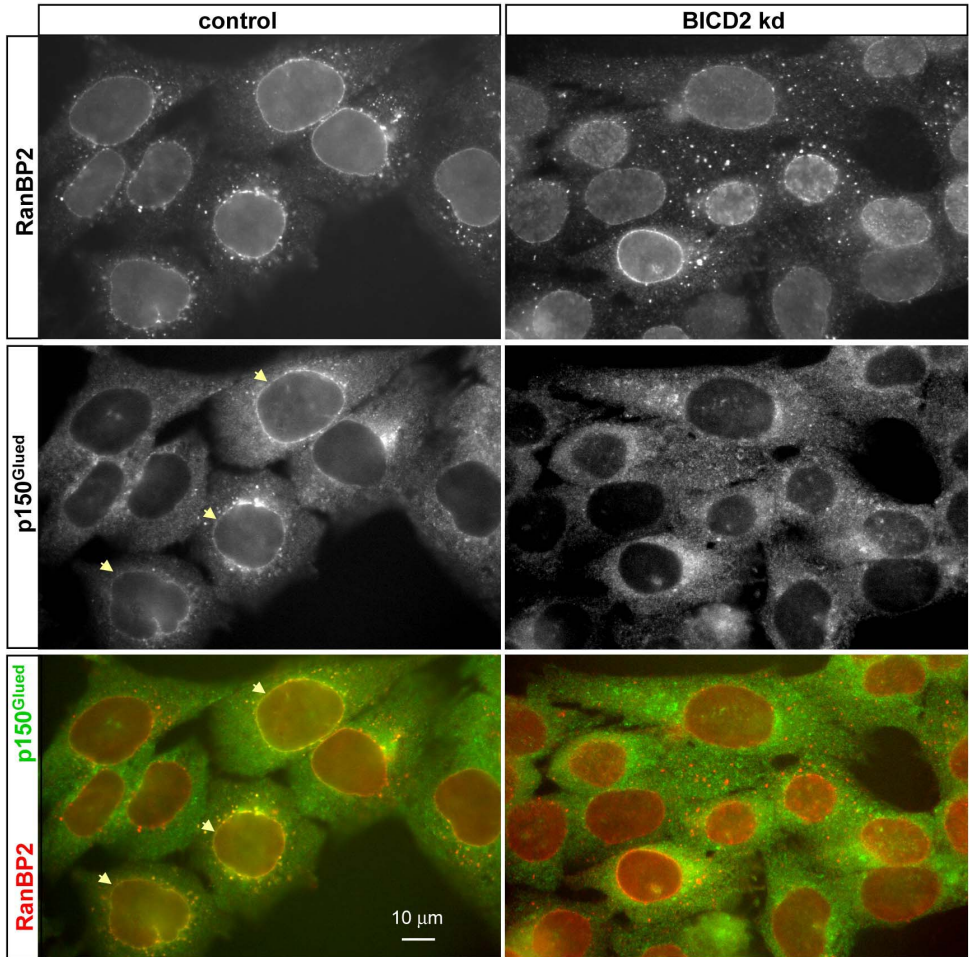**Table S1. Binding partners of Bio-GFP-BICD2-NT identified by mass spectrometry.**

Identified Proteins	NCBI GI Number	% coverage	Unique peptides	Mascot Score
Ran binding protein2	gi|62088546	10,4	23	1489
Bicaudal-D homolog 2	gi|51479166	21,1	16	1254
Kinesin family member 1C	gi|40254834	13,1	12	826
LL5β	gi|27650425	14,3	13	799
Myosin IC	gi|46430642	13,7	11	763
Non-muscle myosin, heavy polypeptide 9	gi|12667788	7,1	10	737
Ran GTPase activating protein 1	gi|119580824	15,4	8	720
Kinesin family member 1B α	gi|41393559	10,2	9	579
CLIP-associating protein 2	gi|57863301	6,6	7	512
EVI-5 homolog	gi|3093476	5,6	4	293
Nucleoporin 93kDa	gi|41281437	5,5	3	179
Centrosomal protein 170kDa	gi|109255230	2,2	3	170

The table shows the proteins identified with a significant Mascot score in the pull down with streptavidin beads from an extract of HeLa cells co-expressing Bio-GFP-BICD2-CT (BICD2 amino acids 487-820) and biotin ligase BirA. A pull-down from HeLa cells expressing BirA alone was used as a control (only proteins which displayed significantly higher Mascot score in the Bio-GFP-BICD2-CT lane compared to the control lane are listed). For each identified protein, the list is filtered for duplicates and shows only the hits with the highest score and most identified peptides.
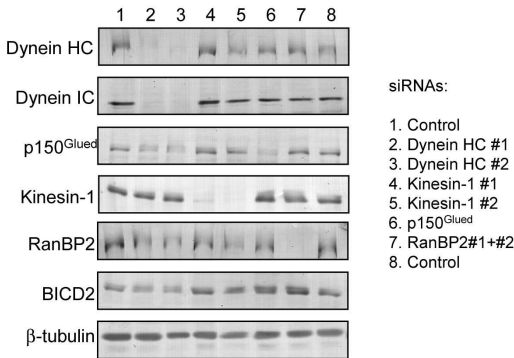

Supplemental Figure 1. Protein depletion in HeLa cells.
Western blots with the indicated antibodies were performed with equal amounts of extracts of HeLa cells 3 days after transfection with the indicated siRNAs.

Bicaudal-D2, dynein and kinesin-1 associate with nuclear pore complexes and regulate centrosome positioning during mitotic entry

89

Supplemental Figure 2. BICD2 depletion causes loss of dynactin from the NE in HeLa cells.

HeLa cells were transfected with the control or BICD2-specific siRNAs, incubated with 10 μM nocodazole for 1 hr, fixed with cold methanol followed by paraformaldehyde and stained for RanBP2 (red in overlay) and dynactin (p150[Glued], green in overlay). Cells with clear accumulation of p150[Glued] at the NE and AL are indicated by arrowheads.
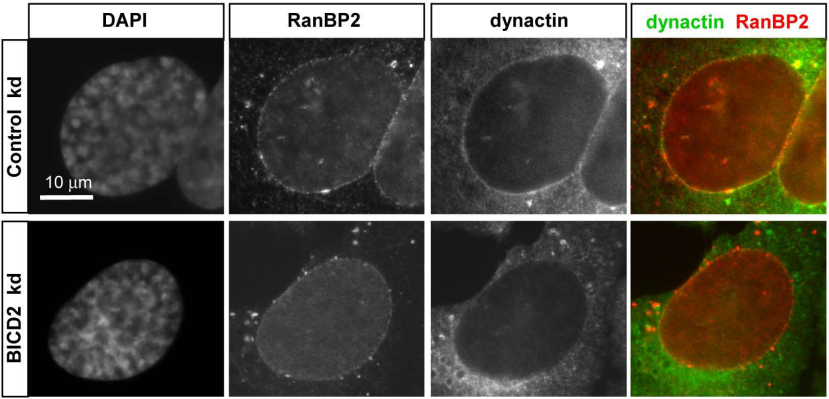
Supplemental Figure 3. BICD2 depletion causes loss of dynactin from the NE in U2OS cells.
U2OS cells were transfected with the control or BICD2-specific siRNAs, incubated with 10 µM nocodazole for 1 hr, fixed with cold methanol followed by paraformaldehyde and stained for RanBP2 (red in overlay), p150^{Glued} (green in overlay). G2 phase were selected based on the presence of condensed chromatin visualized by DAPI staining.

Bicaudal-D regulates the interaction between dynein and dynactin complexes

4

Bicaudal-D2 regulates the interaction between dynein and dynactin complexes

Daniël Splinter, David S. Razafsky, Jeroen Demmers, Nanda Keijzer, Casper C. Hoogenraad, Stephen J. King and Anna Akhmanova

Abstract

Cytoplasmic dynein is a motor responsible for moving a large variety of organelles and macromolecules to the minus ends of the microtubules. Dynein-dependent transport depends on dynactin, a protein complex that stimulates dynein processivity and participates in binding dynein to cargo. Dynein and dynactin directly interact with each other but molecular mechanisms controlling this association are poorly understood. Here we show that the N-terminal part of Bicaudal-D, an evolutionary conserved adaptor molecule involved in microtubule-based mRNA transport in flies and vesicle trafficking in mammals, forms a triple complex with dynein and dynactin in vitro and in cells. In vitro motility assays show that Bicaudal-D N-terminus promotes a stable interaction between dynein and dynactin without significantly affecting dynein velocity or the run length. We provide evidence that the Bicaudal-D N-terminus associates with both the dynein heavy chain and the dynactin subunit p150[Glued]. The full length Bicaudal-D protein is less efficient in stabilizing dynein-dynactin interaction than the N-terminal part alone; moreover, full length Bicaudal-D inhibits dynein-dynactin motility. This suggests that the capacity to associate with dynein and dynactin is attenuated by the cargo-binding C-terminal part of Bicaudal-D2, which may regulate motility by preventing unproductive movement of the triple complex in the absence of appropriate cargo.

Introduction

Cytoplasmic dynein is a motor responsible for the majority of microtubule-based transport processes directed to the minus ends of microtubules (Vale, 2003). It associates with multiple cargos including single proteins, macromolecular complexes, mRNP particles, small vesicles of different types and large organelles such mitochondria and the Golgi apparatus (Gibbons, 1996; Holzbaur and Vallee, 1994; King, 2000). Cytoplasmic dynein is a large complex, which includes two heavy chains of ~500 kDa, and a number of intermediate, light intermediate and light chains (Hook and Vallee, 2006; King et al., 2002). Dynein heavy chains (DHCs) belong to the AAA+ family of ATPases, they contain the C-terminal motor domain with six AAA ATPase units and a microtubule binding stalk, and the N-terminal domain, which binds to other components of the complex and is responsible for dimer formation and cargo interaction (Hook and Vallee, 2006; Wickstead and Gull, 2007). Dynein intermediate chains (DICs; 60-140 kDa), light intermediate chains (LICs; 30-60 kDa) and light chains (LCs; 8-30 kDa) participate in regulating dynein activity and binding to cargo (King et al., 2002; Wickstead and Gull, 2007).

All types of cytoplasmic dynein motility depend on dynactin, another megadalton complex that is involved in binding dynein to cargo and control of dynein processivity (Holleran et al., 2001; Schroer, 2004). Dynactin contains two structural domains: a projecting arm, which includes the microtubule-binding subunit p150[Glued], and the actin-like cargo-binding filament, which is mainly composed of the actin-related protein Arp1 and the protein complexes that cap the filament on the two ends (Schroer, 2004). Dynein and dynactin directly bind to each other through the interaction between p150[Glued] and the DIC (Karki and Holzbaur, 1999; Vaughan and Vallee, 1995). DIC consists of the N-terminal coiled coil region and C-terminal WD-repeats; it is the N-terminal part of the molecule that is involved in binding to p150[Glued] (Karki and Holzbaur, 1999; Vaughan and Vallee, 1995; Vaughan et al., 2001). p150[Glued] is a dimer which contains two N-terminal microtubule-binding domains, and two coiled coil regions separated by a protein sequence of undetermined structure (Waterman-Storer et al., 1995). Detailed analysis of DIC- p150[Glued] interaction in solution showed that the p150[Glued] N-terminal coiled coil domain (CC1, residues 217-548) associates with DIC (King et al., 2003).

Dynein and dynactin co-purify from brain extracts; however, in cultured cells only a weak association between the two complexes is detected by immunoprecipitation (Gill et al., 1991). A considerable pool of dynactin is found at the growing microtubule ends, while only a small proportion of dynein molecules associates with microtubule tips in normal conditions (Vaughan et al., 1999). These data suggest that the two complexes exist as separate pools that come together to induce motility, and that additional factors that control dynein-dynactin association with cargo may also control the interaction of the two complexes.

A well-studied adaptor for cytoplasmic dynein on specific cargos is the evolutionary conserved coiled coil protein Bicaudal-D (see Claussen and Suter, 2005 for review). In flies, Bicaudal-D controls dynein-mediated movement of mRNPs during oogenesis and embryogenesis (Bullock and Ish-Horowicz, 2001; Bullock et al., 2006; Clark et al., 2007). The mammalian homologues of Bicaudal-D, BICD1 and BICD2, participate in vesicle transport: their C-terminal cargo-binding coiled coil segment specifically associates with the small GTPase Rab6, which is present at the Golgi and exocytotic vesicles (Grigoriev et al., 2007; Hoogenraad et al., 2001; Matanis et al., 2002; Short et al., 2002). Our previous studies showed that the N-terminal portion of BICD2 (BICD2-NT) co-precipitates both dynein and dynactin and, when artificially tethered to different cargos, rapidly induces their microtubule minus-end directed transport by recruiting dynein and dynactin (Hoogenraad et al., 2001; Hoogenraad et al., 2003).

Since dynein and dynactin interact with each other, BICD2 may bind to only one or to both complexes. In order to get insight into how BICD2 regulates dynein motility, we investigated the interaction between BICD2, dynein and dynactin, by combining cell biological and biochemical approaches with *in vitro* reconstitution. We show that BICD2-NT stabilizes the interaction between dynein and dynactin without having a significant effect on the motility of individual dynein motors. The C-terminal cargo-binding portion of BICD2 (BICD2-CT) may have an attenuating effect on the formation of the triple complex between dynein, dynactin and BICD2-NT. Thus BICD2 may regulate recruitment of motile dynein complexes with cargo binding.

Results and Discussion

BICD2-NT stabilizes dynein-dynactin interaction in cells

Our previous study showed that when BICD2-NT (containing the N-terminal and the middle coiled coil segments of the molecule, amino acids 1-575, Fig.1A) is artificially tethered to membrane organelles, it induces their rapid dynein-dependent transport to microtubule minus ends (Hoogenraad et al., 2003). Full length BICD2 (BICD2-FL) showed the same effect, but acted less efficiently, suggesting that the C-terminal part of the molecule may inhibit BICD2 interaction with the motors (Hoogenraad et al., 2003). In line with these observations, GFP-tagged BICD2-NT efficiently precipitated both dynein and dynactin (detected with antibodies against DIC and p150[Glued]) from overexpressing HeLa cells, while a much weaker co-precipitation was observed with GFP-BICD2-FL (Fig.1B). To determine which complex BICD2-NT primarily binds, we performed immunoprecipitations of dynein and dynactin, using DIC and p150[Glued] antibodies. Remarkably, GFP-BICD2-NT was efficiently
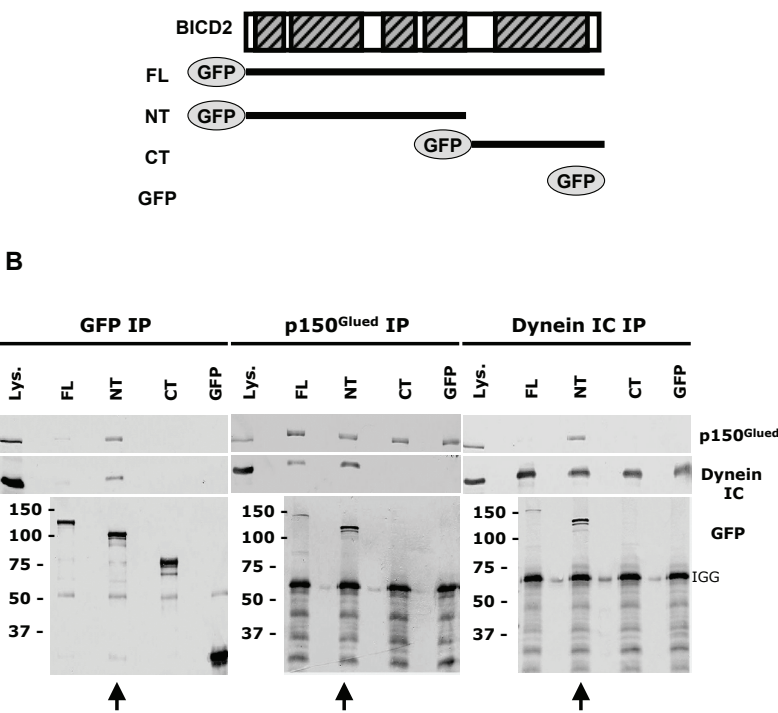

Figure 1. BICD2-NT overexpression stabilizes dynein-dynactin complex in cells.
A. Schematic representation of BICD2 structure and GFP fusion constructs. B. Immunoprecipitation assays with antibodies against GFP dynactin (p150) and dynein (DIC) were performed upon extracts from HeLa cells overexpressing the indicated GFP-BICD2 fusions or GFP alone. Western blotting was performed with the indicated antibodies to determine if protein was pulled down. 2% of the cell lysate used for the immunoprecipitation was loaded as a control. The lanes containing BICD2-NT are indicated by arrows.

co-precipitated with both complexes (Fig.1B). Moreover, the amount of dynein and dynactin complexes co-precipitating with each other was significantly increased in cells overexpressing GFP-BICD2-NT, as compared to cells overexpressing GFP-BICD2-CT, GFP-BICD2-FL or GFP alone (Fig.1B). These results suggest that high levels of BICD2-NT stabilize the interaction between dynein and dynactin in cells.

Purified BICD2-NT, dynein and dynactin form a triple complex in vitro

To investigate the mechanism of dynein-dynactin complex stabilization by BICD2 we purified the full length BICD2 and its N-terminal fragment from overexpressing HEK293T cells (Fig.2A). Dynein and dynactin complexes were purified from bovine brain as described previously (Fig. 2B, C, (Bingham et al., 1998; Mallik et al., 2005)). Next, we used sucrose density gradient centrifugation to investigate the interaction between BICD2, dynein and dynactin complexes. As expected, both dynein and dynactin were present in fractions corresponding to ~20S whereas the much smaller BICD2-NT and BICD2-FL molecules were found in the lighter fractions (Fig.2D). Interestingly, when we combined dynein, dynactin and BICD2-NT, a considerable proportion of all three components shifted to the high-density fractions, indicating that a stable triple complex was formed (Fig.2D). No stable triple complex formation could be observed with the BICD2-FL, consistent with the co-precipitation data showing that BICD2-FL is less efficient at stabilizing the triple complex. No shift in sedimentation behavior was observed when BICD2-NT or BICD2-FL were combined with dynein or dynactin alone, indicating that stable complex formation requires the presence of all three components, BICD2-NT, dynein and dynactin.

BICD2-NT binds to p150^{Glued} and dynein heavy chain

Both dynein and dynactin contain multiple subunits that might serve as binding partners for BICD2-NT. To gain insight into the architecture of the triple complex, we prepared an N-terminally biotinylated version of BICD2-NT (Fig.2A), mixed it with purified dynein and dynactin in conditions promoting triple complex assembly (based on the experiments described above), and cross-linked the resulting complexes with very low doses of chemical cross-linking reagent Bis[sulfosuccinimidyl]glutarate. The resulting cross-linked complexes were solubilized in denaturing conditions. Subsequently, the biotinylated BICD2-NT (together with the cross-linked polypeptides) was isolated by streptavidin pull-down and subjected to mass spectrometry analysis. As a control, we performed mass spectrometry of purified dynein and dynactin samples used as input in this experiment.

As expected, all known dynein and dynactin subunits could be identified by mass spectrometry in the preparations of purified complexes (Table 1A, B). Interestingly, only a small subset of these subunits was recovered in the pull down with BICD2-NT after cross-linking and denaturation: these included the p150^{Glued} subunit of dynactin and the complex of dynein heavy chain with LIC (LIC1 and LIC2, Table 1C). The latter result is not surprising, because DHC and LIC1/2 are known to bind to each other very tightly and to form a stable subcomplex (King et al., 2002).

Next, we used yeast two hybrid assays to dissect the interaction between p150^{Glued} and BICD2-NT. We could detect an interaction between amino acids 1-260 of BICD2 and residues 200-548 of
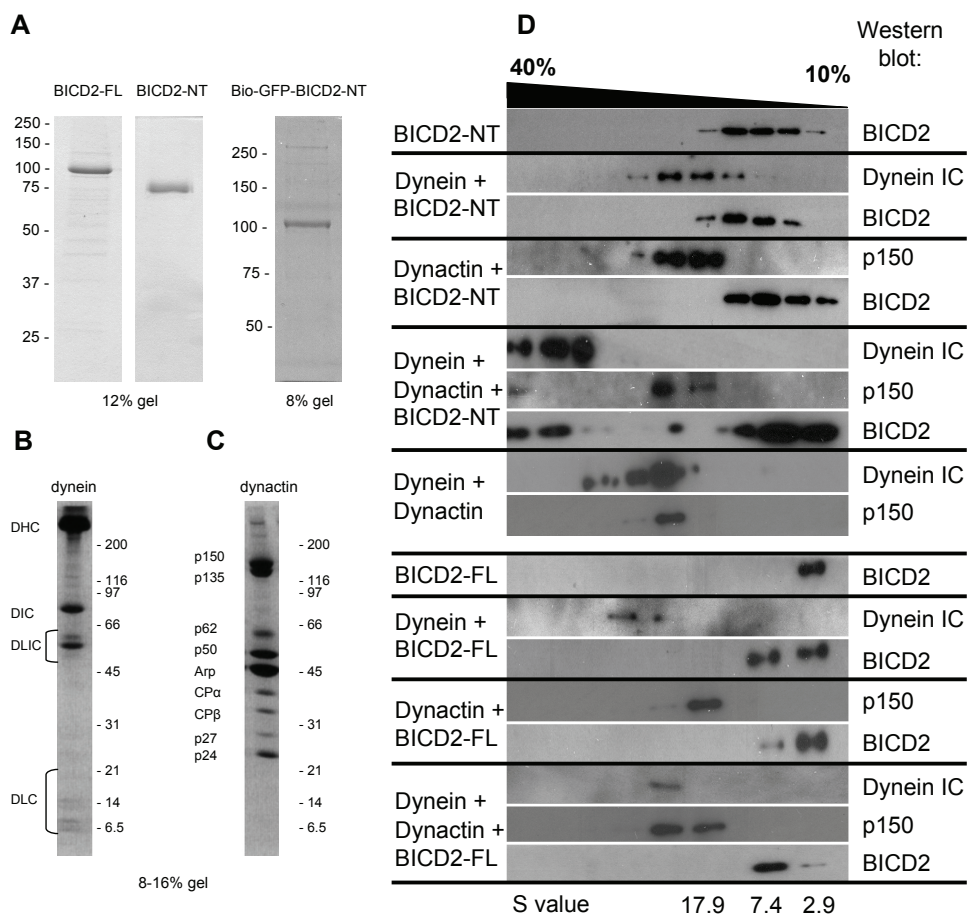
Figure 2. Purified BICD2-NT, dynein and dynactin form a triple complex in vitro.

A-C. Coomassie-stained gels showing purified BICD2-NT (with and without biotinylation and GFP-tag) and BICD2-FL (A), bovine brain dynein (B) and bovine brain dynactin (C). D. Combinations of purified BICD2-NT, BICD2-FL, dynein, and/or dynactin were sedimented as indicated onto 10–40% sucrose gradients. Individual gradient fractions (denser fractions to the left) were subjected to Western blotting with antibodies to BICD2, dynactin (p150[Glued]) and dynein (DIC). S values of sedimentation markers are shown at the bottom.

Table 1A

Score	NCBI GI number	Description	Da	Coverage (%)	Unique Pept.
3890	gi|149642611	dynactin 1 (p150Glued)	137458	45.2	41
1478	gi|5031569	ARP1	42701	54.5	16
1185	gi|77736063	dynactin 2 (p50)	44495	35.7	14
1177	gi|119914141	cytoplasmic dynein heavy chain	548197	5.8	19
933	gi|28603770	capping protein beta	34176	27.6	12
822	gi|61316470	capping protein alpha 2	33073	55.6	9
712	gi|73953656	dynactin p62	54023	29.3	9
262	gi|115497348	cytoplasmic dynein intermediate chain 2	68734	9.5	3
178	gi|119892302	kinesin family member 21A	187179	1.5	2
151	gi|115497064	dynactin 3 (p22)	21292	15.1	3
130	gi|115497256	dynactin 6 (p27)	21061	14.2	2
68	gi|164420721	dynactin 5 (p24)	20698	8.2	2
63	gi|76640631	dynein light intermediate chain 2	54392	2.4	1

Table 1B

Score	NCBI GI number	Description	Da	Coverage (%)	Unique Pept.
16600	gi|119914141	cytoplasmic dynein heavy chain	548197	50.5	199
1593	gi|114051407	cytoplasmic dynein light intermediate chain 1	56800	49.6	22
956	gi|76640631	cytoplasmic dynein light intermediate chain 2	54392	32.3	14
840	gi|11276091	cytoplasmic dynein intermediate chain 1	73222	22.7	10
732	gi|74004544	cytoplasmic dynein intermediate chain 2	69215	27.7	9
321	gi|18777767	cytoplasmic dynein light chain 2A	10983	74.0	4
108	gi|5730085	cytoplasmic dynein, light chain, Tctex	12672	14.2	1
75	gi|157074188	Arp1	42382	2.7	1
47	gi|77736063	dynactin 2 (p50)	44495	2.2	1

Table 1B

Score	NCBI GI number	Description	Da	Coverage (%)	Unique Pept.
8026	gi|119914141	Cytoplasmic dynein heavy chain	548197	29.3	124
718	gi|149642611	Dynactin 1 (p150Glued)	137458	8.4	9
513	gi|18139547	BICD2	93562	8.9	7
366	gi|114051407	Cytoplasmic dynein light intermediate chain 1	56800	12.6	7
365	gi|76640631	Cytoplasmic dynein light intermediate chain 2	54392	15.2	6

Table 1. Mass spectrometry analysis of dynein and dynactin subunits associated with BICD2-NT
A. Mass spectrometry analysis of purified bovine dynactin
B. Mass spectrometry analysis of purified bovine dynein
C. Mass spectrometry analysis of Bio-GFP-BICD2-NT/dynein/dynactin complex after cross-linking with low doses of Bis[sulfosuccinimidyl] glutarate and isolated by pull-down with streptavidin beads in denaturing conditions.

human p150[Glued], which corresponds to the N-terminal CC1 coiled coil region of the molecule (Table 2). It should be noted that previously we failed to detect this interaction using a *Xenopus* p150[Glued], possibly due to insufficient conservation of BICD2-p150[Glued] interaction interface between frogs and mammals (Hoogenraad et al., 2001). The CC1 region of p150[Glued] was already implicated in interaction with dynein because it also binds to DIC (King et al., 2003). This part of p150[Glued] is expected to be highly elongated and represents a good candidate for the location of additional interactions that could strengthen dynein-dynactin association.

So far, we have not been able to detect an interaction between LIC1/2 and BICD2-NT; therefore, we favor the idea that BICD2 interacts with the DHC and are currently generating a collection of yeast two hybrid constructs with multiple DHC fragments to test this idea.

	Empty vector	BICD2 1-260	BICD2 336-820	BICD2 586-820	DIC1 1-257	DIC1 254-628
Empty vector	-	-	-	-	-	-
p150Glued 200-548	-	+	-	-	+	-
p150Glued 305-811	-	-	-	-	-	-

Table 2. Yeast two-hybrid analysis of BICD2-NT- p150[Glued] interaction
p150[Glued] fragments were cloned into LexA fusion vector and tested in a pair wise fashion for interaction with BICD2 or DIC1 fragments linked to GAL4 activation domain. Interaction was scored as positive if the β-galactosidase reporter generated visible blue-colored yeast colonies on X-Gal containing filters in a colony filter lift assay within four hours.

Effects of BICD2-NT and BICD2-FL on dynein motility in vitro

To investigate how the formation of the triple BICD2-dynein-dynactin complex affects dynein motility we set up an *in vitro* assay where bead motility along microtubules was critically dependent on dynein-dynactin interaction. Dynactin was attached to the surface of polybead carboxylate microspheres using antibodies to the Arp1 subunit (Fig 3). Beads prepared in this way without dynein displayed no motility on taxol-stabilized microtubules when analyzed in a microscope-based motility assay. Purified dynein was then added in low stoichiometric concentration to ensure that bead motility events would reflect the behavior of single active dynein motors that could only bind to the beads via dynein-dynactin based interactions (Fig 3). As a control, the addition of dynein to the Arp1 antibody-coated beads in the absence of dynactin produced absolutely no motility (Figs. 3; 4A). These results demonstrate that in this experimental system, dynein is only capable of moving the beads when it is linked to them via dynactin.

We compared the frequency, velocity and the run lengths of the motility events observed for Arp1
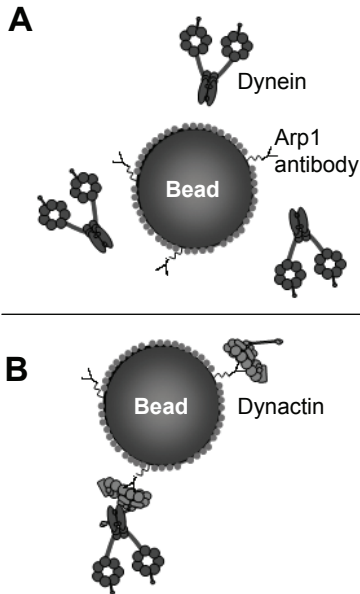
A

B

Figure 3. Schematic representation of the beads used in the motility assays.
Antibodies (Y) to the Arp 1 subunit of dynactin were cross-linked to the bead surface followed by the addition of casein (small circles) to completely block the bead surface. A. In the absence of dynactin, dynein has no way to bind to the bead surface. B. If dynactin is present on the bead surface, dynein can bind to the bead and transport the bead along a microtubule.

antibody/dynactin coated beads in the presence of dynein alone and in combination with purified BICD2-NT or BICD2-FL. The addition of BICD2-NT had no effect on the movement velocity or run length (Fig.4B,C); however, the frequency of motility events was very significantly increased (Fig. 4A, D). These data support the idea that BICD2-NT promotes a stable interaction between dynein and dynactin that is capable of processive motility.

In contrast to BICD2-NT, BICD2-FL only slightly increased the frequency of motility events (Fig.4A,D). Interestingly, although BICD2-FL had no effect on dynein velocity, it did cause a significant decrease in the length of the runs (Fig.4B,C). This suggests that the C-terminal portion of BICD2 has an inhibitory effect on dynein motility. One possibility is that the C-terminus of BICD2 causes the premature release of dynein from the dynactin-coated beads. It is tempting to speculate that this property could be used to regulate the formation of the triple dynein-dynactin-BICD2-NT complex with the cargo binding by BICD2-CT. This BICD2-dependent regulation might prevent unproductive dynein movement in the absence of correct cargo association. The addition of appropriate BICD2 cargo, such as GTP-bound Rab6, to the motility assays would be needed to test this model.

Taken together, our data show that the N-terminal coiled coil domains of BICD2 act to bring together dynein and dynactin into a motile complex. This helps to explain why the overexpression of BICD2-NT acts as a dynein inhibitor (Hoogenraad et al., 2001; Vlug et al., 2005): it is expected to tie up dynein and dynactin in motile but cargo-unbound assemblies. BICD2-NT overexpression is thus phenotypically similar but mechanistically different from overexpression of p50 dynamitin, which inhibits dynein motility by physically disrupting the dynactin complex and separating functional dynein motors from cargoes (Echeverri et al., 1996; Melkonian et al., 2007).
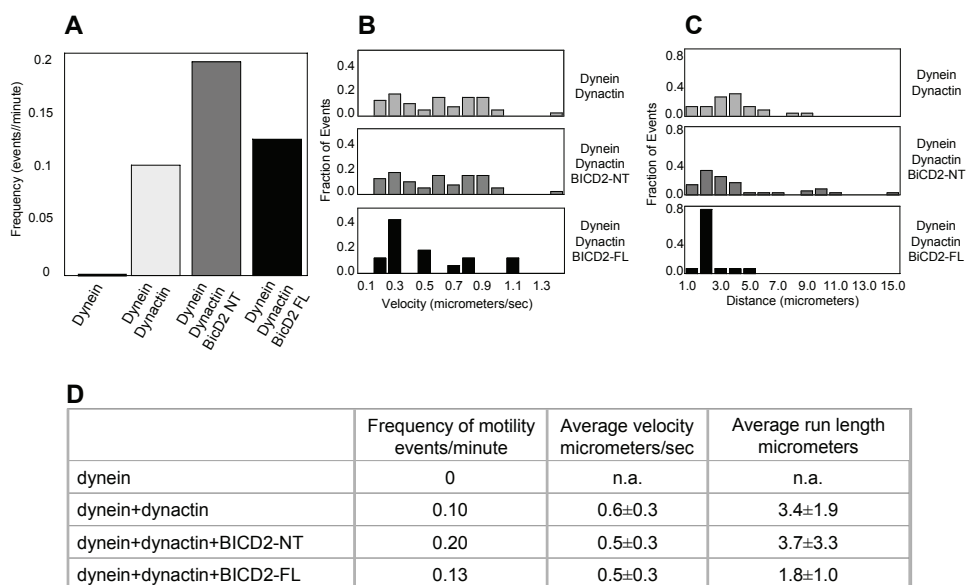
Figure 4. Dynein motility assays. Beads were incubated with the indicated proteins and visualized by differential interference contrast microscopy in a microscope flow chamber.
A. Frequency of motility events.
B. Histograms of bead movement velocities.
C. Histograms of bead run lengths.
D. Bead motility statistics.

	Frequency of motility events/minute	Average velocity micrometers/sec	Average run length micrometers
dynein	0	n.a.	n.a.
dynein+dynactin	0.10	0.6±0.3	3.4±1.9
dynein+dynactin+BICD2-NT	0.20	0.5±0.3	3.7±3.3
dynein+dynactin+BICD2-FL	0.13	0.5±0.3	1.8±1.0

Our previous immunoprecipitation results suggested that the dynein binding site is located in the N-terminal coiled coil segment of BICD2 (residues 1-271, (Hoogenraad et al., 2001)). Yeast two-hybrid assays described here indicate that the dynactin binding site is likely located in the same portion of the BICD2 molecule (residues 1-260). Using mitochondria and peroxisome relocalization assays (Hoogenraad et al., 2003) we mapped the minimal dynein-recruiting region of BICD2 to amino acids 25-400, supporting the idea that the primary dynein and dynactin interaction sites are located in the N-terminal coiled coil segment of BICD2 (D. Splinter, unpublished data). However, optimal relocalization of mitochondria and peroxisomes to microtubule minus ends was induced by a longer N-terminal portion of the BICD2 molecule (residues 1-575); that is why we used this fragment in our *in vitro* work. An additional complexity is created by the fact that this 575 aa BICD2 fragment also contains the binding site for kinesin-1 (residues 336-595) (Grigoriev et al., 2007). The interaction between BICD2 and kinesin-1 is much weaker than the interaction with dynein-dynactin, yet BICD2-associated cargos, such as Rab6 vesicles, move bi-directionally (Grigoriev et al., 2007; Matanis et al., 2002). It would therefore be interesting to investigate if the addition of kinesin-1 and Rab6 cargo to the *in vitro* motility assay would result in bi-directional motility of cargoes and thus model the bi-directional movement observed for the majority of dynein cargos *in vivo*.

Materials and Methods

Immunoprecipitation from Hela cells

HeLa cells were cultured as described previously (Grigoriev et al., 2007); 70% confluent HeLa cells were transfected with constructs expressing GFP-BICD2 fusions or GFP alone using Lipofectamine 2000 (Invitrogen). One day after transfection cells were lysed in a buffer containing 20 mM Tris-HCl, pH 8.0, 100 mM KCl, 1% Triton X-100 and protease inhibitors (Complete, Roche). Immunoprecipitations were performed with mouse monoclonal antibodies against GFP (Roche), p150[Glued] (BD Biosciences) and DIC (Chemicon) as described previously (Hoogenraad et al., 2001). The same antibodies were used for Western blotting, with the exception of GFP, which was detected with rabbit polyclonal antibodies (Abcam).

Protein Purifications

The expression vectors for Bio-GFP-TEV-BICD2-FL and NT were created by first introducing a linker between the GFP and BICD2 sequences containing SpeI, HindIII and EcoRI restriction sites in the Bio-GFP-BICD2-FL and NT vectors, which were described previously (Grigoriev et al., 2007). Two tobacco etch virus (TEV) protease sites flanked by four glycine residues to ensure flexibility were inserted between the GFP and BICD2 open reading frames, by cloning at the SpeI and HindIII sites a linker encoding the amino acid sequence GGGGENLYFQGGGGGGENLYFQGGGGG.

Bio-GFP tagged and untagged BICD2-FL and NT has been purified from HEK293T cells. 70% confluent HEK293T cells were co-transfected with the constructs Bio-GFP-TEV-BICD2-FL and BirA or Bio-GFP-TEV-BICD2-NT and BirA using Lipofectamine 2000. One day after transfection cells were lysed in a buffer containing 20 mM Tris-HCl, 100 mM KCl, 1% Triton X-100 and protease inhibitors (Complete, Roche). Proteins were isolated using M280 streptavidin beads (Invitrogen) as described by Grigoriev et al., 2007. Beads were washed with a high salt buffer 20mM Tris-HCl pH 8.0, 500mM KCl and 0.05% Tween 20 and a low salt buffer containing 20mM Tris-HCl pH 8.0, 150 mM KCl and 0.05% Tween 20 and cut off the beads in a buffer containing 5 µg/ml 6xHistidine (HIS)- tagged TEV protease, 20 mM imidazole, 1% glycerol, 0.05% NP-40 10 mM DTT, 20 mM Tris-HCl pH 8.0 and 150 mM KCl. TEV protease was removed with Ni-beads (Qiagen) and the purified protein was concentrated using 3 kDa Vivaspin columns (Satorius). Bio-GFP tagged BICD2-FL and BICD2-NT was purified with Mutein beads (Roche) according to the protocol of the manufacturer; purified protein was concentrated with 3 kDa Vivaspin columns (Satorius).

Bovine brain tubulin was flash-frozen in liquid nitrogen after purification by two rounds of polymerization-depolymerization cycling followed by Whatman P11 cellulose phosphate (Florham Park, NJ) chromatography (Sloboda and Rosenbaum, 1982). Bovine brain dynactin and cytoplasmic dynein were purified as previously described (Bingham et al., 1998; Mallik et al., 2005).

Sucrose Gradients

Bovine brain dynein was incubated with equimolar amounts of bovine brain dynactin and BICD2 (FL or NT) for three hours on ice and then layered onto a 10-40% sucrose gradient

supplemented with 1mM DTT, 0.5mM ATP, and 0.05% nonyl phenoxylpolyethoxylethanol. Samples were centrifuged in an SW50.1 rotor at 27,000 rpm for 15 hours at 4°C. 500µL fractions were collected and western blots were probed for DIC, p150[Glued], and BICD2 (antibody #2293; (Hoogenraad et al., 2001)).

Analysis of BICD2-NT binding partners in dynein and dynactin by cross-linking

Bio-GFP tagged BICD2-NT was incubated with equimolar amounts of bovine brain dynein and dynactin for three hours on ice in a buffer containing 80 mM PIPES, 1 mM MgCl2, 1 mM EGTA, 50 mM NaCl 1mM DTT, 0.5mM ATP, and 0.05% nonyl phenoxylpolyethoxylethanol, pH 6.8. Bis[sulfosuccinimidyl] glutarate (Pierce) was added in a end concentration of 0.5 mM and quenched after 30 minutes with NH4HCO3. Formed complexes were denatured with 0.5% SDS followed by 5 minutes at 65oC in a buffer containing 20 mM Tris-HCl, pH 8.0, 400 mM KCl and 0.5% Triton X-100. Streptavidin pull down was performed as described previously (Grigoriev et al., 2007).

Mass spectrometry-based protein identification

Mass spectrometry analysis was performed essentially as described by (Grigoriev et al., 2007). Peak lists were automatically created from raw data files using the Mascot Distiller software (version 2.0; MatrixScience). The Mascot search algorithm (version 2.0, MatrixScience) was used for searching against the NCBInr database (release date: NCBInr_20080502.fasta; taxonomy B. taurus). The peptide tolerance was typically set to 2 Da and the fragment ion tolerance to 0.8 Da. Only doubly and triply charged peptides were searched for. A maximum number of 2 missed cleavages by trypsin were allowed and carbamidomethylated cysteine and oxidised methionine were set as fixed and variable modifications, respectively. The Mascot score cut-off value for a positive protein hit was set to 100. Individual peptide MS/MS spectra with Mowse scores below 40 were checked manually and either interpreted as valid identifications or discarded.

Yeast two-hybrid analysis

The p150[Glued] fragments were cloned into pBHA (lexA fusion vector) and tested against various deletion mutants of BICD2 or DIC1 constructed in pGAD10 (GAL4 activation domain vector, Clontech). All constructs were generated by PCR-based strategy using the following cDNAs as templates: mouse BICD2 (Hoogenraad et al., 2001), mouse DIC1 (Image clone 1480265), human p150[Glued] (Smith et al., 2006). Yeast two-hybrid analysis was carried out using the L40 yeast strain harboring HIS3 and β-galactosidase as reporter genes as described previously (Niethammer and Sheng, 1998). β-galactosidase activity was detected using colony filter lift assays.

In vitro motility assay

The monoclonal antibody 45A raised against the Arp1 subunit of dynactin was mixed with Sulfo-NHS and 1-Ethyl-3-[3-dimethylaminopropyl]carbodiimide Hydrochloride (EDC) in the presence of 0.21µm diameter polybead carboxylate microspheres (Polysciences, Warrington,

PA) and incubated at room temperature overnight. The cross-linking reaction was quenched by the addition of excess glycine. The beads were washed four times to remove all traces of cross-linking chemicals and sonicated to disperse aggregated beads. The beads were stored at 4°C in a rotator until needed. Flow cells were prepared as previously described Culver-Hanlon et al., 2006 with the following adaptations. 45A antibody cross-linked beads were incubated with casein for at least 30 minutes at room temperature prior to use to block the bead surface. All combinations of dynein, dynactin, and BICD2 were incubated together in equimolar ratios on ice for at least 30 minutes prior to their addition to the casein-blocked beads. In the absence of dynactin, no dynein motility events were observed in ~2.5 hours of experiments when all combinations of dynein and BicD2 were added to these beads (Fig 3). Computer-based tracking of the recorded images was performed as previously described (Culver-Hanlon et al., 2006).
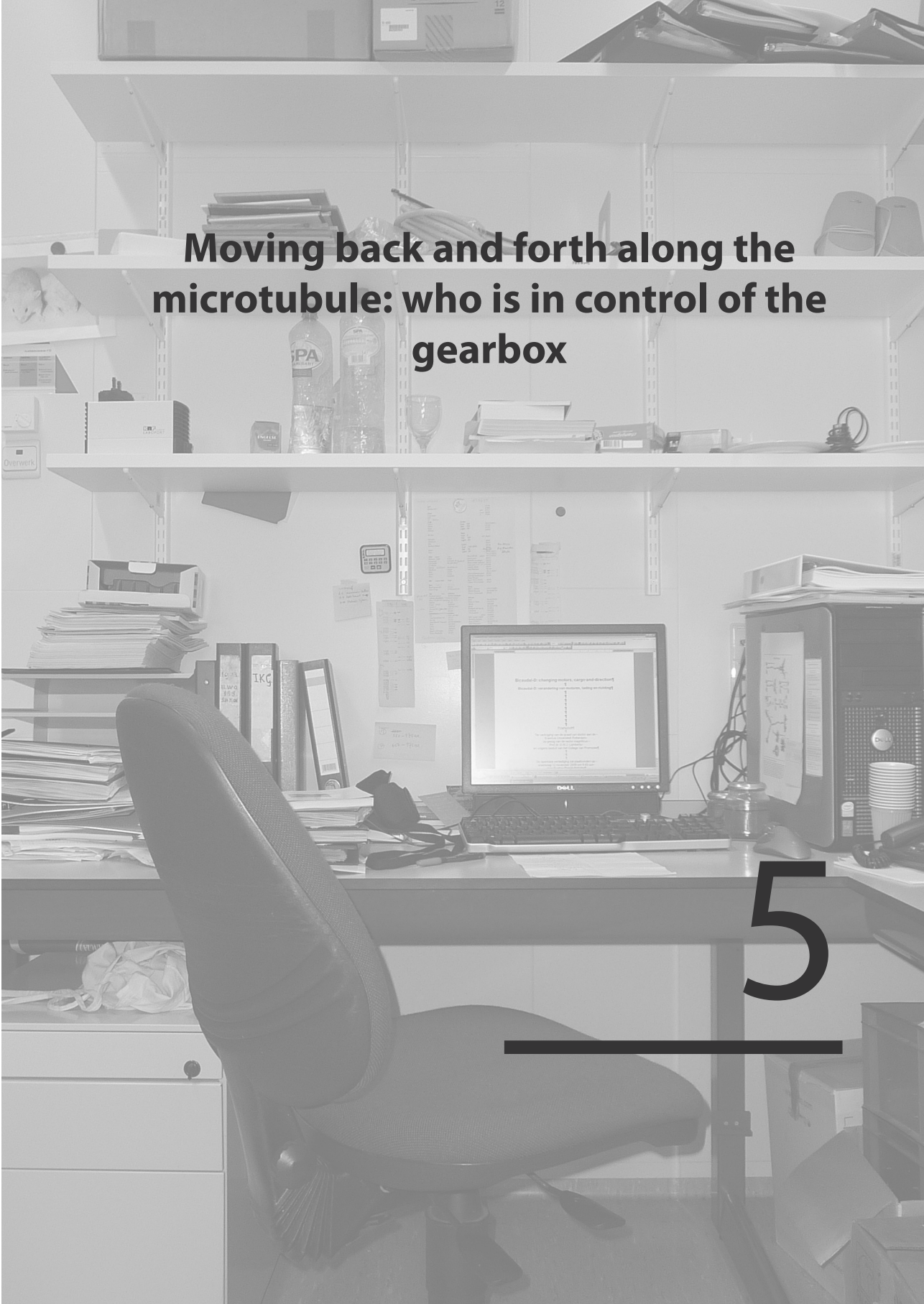
References

Bingham, J.B., S.J. King, and T.A. Schroer. 1998. Purification of dynactin and dynein from brain tissue. Methods Enzymol. 298:171-84.

Bullock, S.L., and D. Ish-Horowicz. 2001. Conserved signals and machinery for RNA transport in Drosophila oogenesis and embryogenesis. Nature. 414:611-6.

Bullock, S.L., A. Nicol, S.P. Gross, and D. Zicha. 2006. Guidance of bidirectional motor complexes by mRNA cargoes through control of dynein number and activity. Curr Biol. 16:1447-52.

Clark, A., C. Meignin, and I. Davis. 2007. A Dynein-dependent shortcut rapidly delivers axis determination transcripts into the Drosophila oocyte. Development. 134:1955-65.

Claussen, M., and B. Suter. 2005. BicD-dependent localization processes: from Drosophilia development to human cell biology. Ann Anat. 187:539-53.

Culver-Hanlon, T.L., S.A. Lex, A.D. Stephens, N.J. Quintyne, and S.J. King. 2006. A microtubule-binding domain in dynactin increases dynein processivity by skating along microtubules. Nat Cell Biol. 8:264-70.

Echeverri, C.J., B.M. Paschal, K.T. Vaughan, and R.B. Vallee. 1996. Molecular characterization of the 50-kD subunit of dynactin reveals function for the complex in chromosome alignment and spindle organization during mitosis. J Cell Biol. 132:617-33.

Gibbons, I.R. 1996. The role of dynein in microtubule-based motility. Cell Struct Funct. 21:331-42.

Gill, S.R., T.A. Schroer, I. Szilak, E.R. Steuer, M.P. Sheetz, and D.W. Cleveland. 1991. Dynactin, a conserved, ubiquitously expressed component of an activator of vesicle motility mediated by cytoplasmic dynein. J Cell Biol. 115:1639-50.

Grigoriev, I., D. Splinter, N. Keijzer, P.S. Wulf, J. Demmers, T. Ohtsuka, M. Modesti, I.V. Maly, F. Grosveld, C.C. Hoogenraad, and A. Akhmanova. 2007. Rab6 regulates transport and targeting of exocytotic carriers. Dev Cell. 13:305-14.

Holleran, E.A., L.A. Ligon, M. Tokito, M.C. Stankewich, J.S. Morrow, and E.L. Holzbaur. 2001. beta III spectrin binds to the Arp1 subunit of dynactin. J Biol Chem. 276:36598-605.

Holzbaur, E.L., and R.B. Vallee. 1994. DYNEINS: molecular structure and cellular function. Annu Rev Cell Biol. 10:339-72.

Hoogenraad, C.C., A. Akhmanova, S.A. Howell, B.R. Dortland, C.I. De Zeeuw, R. Willemsen, P. Visser, F. Grosveld, and N. Galjart. 2001. Mammalian Golgi-associated Bicaudal-D2 functions in the dynein-dynactin pathway by interacting with these complexes. Embo J. 20:4041-54.

Hoogenraad, C.C., P. Wulf, N. Schiefermeier, T. Stepanova, N. Galjart, J.V. Small, F. Grosveld, C.I. de Zeeuw, and A. Akhmanova. 2003. Bicaudal-D induces selective dynein-mediated microtubule minus end-directed transport. Embo J. 22:6004-15.

Hook, P., and R.B. Vallee. 2006. The dynein family at a glance. J Cell Sci. 119:4369-71.

Karki, S., and E.L. Holzbaur. 1999. Cytoplasmic dynein and dynactin in cell division and intracellular transport. Curr Opin Cell Biol. 11:45-53.

King, S.J., M. Bonilla, M.E. Rodgers, and T.A. Schroer. 2002. Subunit organization in cytoplasmic dynein subcomplexes. Protein Sci. 11:1239-50.

King, S.J., C.L. Brown, K.C. Maier, N.J. Quintyne, and T.A. Schroer. 2003. Analysis of the dynein-dynactin interaction in vitro and in vivo. Mol Biol Cell. 14:5089-97.

King, S.M. 2000. The dynein microtubule motor. Biochim Biophys Acta. 1496:60-75.

Mallik, R., D. Petrov, S.A. Lex, S.J. King, and S.P. Gross. 2005. Building complexity: an in vitro study of cytoplasmic dynein with in vivo implications. Curr Biol. 15:2075-85.

Matanis, T., A. Akhmanova, P. Wulf, E. Del Nery, T. Weide, T. Stepanova, N. Galjart, F. Grosveld, B. Goud, C.I. De Zeeuw, A. Barnekow, and C.C. Hoogenraad. 2002. Bicaudal-D regulates COPI-independent Golgi-ER transport by recruiting the dynein-dynactin motor complex. Nat Cell Biol. 4:986-92.

Melkonian, K.A., K.C. Maier, J.E. Godfrey, M. Rodgers, and T.A. Schroer. 2007. Mechanism of dynamitin-mediated disruption of dynactin. J Biol Chem. 282:19355-64.

Niethammer, M., and M. Sheng. 1998. Identification of ion channel-associated proteins using the yeast two-hybrid system. Methods Enzymol. 293:104-22.

Schroer, T.A. 2004. Dynactin. Annu Rev Cell Dev Biol. 20:759-79.

Short, B., C. Preisinger, J. Schaletzky, R. Kopajtich, and F.A. Barr. 2002. The Rab6 GTPase regulates recruitment of the dynactin complex to Golgi membranes. Curr Biol. 12:1792-5.

Sloboda, R.D., and J.L. Rosenbaum. 1982. Purification and assay of microtubule-associated proteins (MAPs). Methods Enzymol. 85 Pt B:409-16.

Smith, D.C., R.A. Spooner, P.D. Watson, J.L. Murray, T.W. Hodge, M. Amessou, L. Johannes, J.M. Lord, and L.M. Roberts. 2006. Internalized Pseudomonas exotoxin A can exploit multiple pathways to reach the endoplasmic reticulum. Traffic. 7:379-93.

Vale, R.D. 2003. The molecular motor toolbox for intracellular transport. Cell. 112:467-80.

Vaughan, K.T., S.H. Tynan, N.E. Faulkner, C.J. Echeverri, and R.B. Vallee. 1999. Colocalization of cytoplasmic dynein with dynactin and CLIP-170 at microtubule distal ends. J Cell Sci. 112:1437-47.

Vaughan, K.T., and R.B. Vallee. 1995. Cytoplasmic dynein binds dynactin through a direct interaction between the intermediate chains and p150Glued. J Cell Biol. 131:1507-16.

Vaughan, P.S., J.D. Leszyk, and K.T. Vaughan. 2001. Cytoplasmic dynein intermediate chain phosphorylation regulates binding to dynactin. J Biol Chem. 276:26171-9.

Vlug, A.S., E. Teuling, E.D. Haasdijk, P. French, C.C. Hoogenraad, and D. Jaarsma. 2005. ATF3 expression precedes death of spinal motoneurons in amyotrophic lateral sclerosis-SOD1 transgenic mice and correlates with c-Jun phosphorylation, CHOP expression, somato-dendritic ubiquitination and Golgi fragmentation. Eur J Neurosci. 22:1881-94.

Waterman-Storer, C.M., S. Karki, and E.L. Holzbaur. 1995. The p150Glued component of the dynactin complex binds to both microtubules and the actin-related protein centractin (Arp-1). Proc Natl Acad Sci U S A. 92:1634-8.

Wickstead, B., and K. Gull. 2007. Dyneins across eukaryotes: a comparative genomic analysis. Traffic. 8:1708-21.

Moving back and forth along the microtubule: who is in control of the gearbox

5

Moving back and forth along the microtubule: who is in control of the gearbox

5.1 Introduction

Active transport of vesicles, organelles and multimolecular complexes is essential for the maintenance and function of complex cellular systems. In order to route cargos to their destination and maintain organelle structure, eukaryotic cells deploy molecular motors. These motors operate on both microtubules and actin filaments, which provide access for cargoes to almost every part of the cytoplasm. The superfamily of myosin motors operates on the actin filaments. Among microtubule-based motors, most kinesins move towards the plus ends of the microtubules, while dyneins move towards the minus ends. Small GTPases from the Rab and Arf families are known to recruit coat proteins and facilitate transport of vesicles and organelles. They target cargos to their destination by recruiting motor proteins and facilitate docking at the acceptor compartments. Various organelles and membranous structures have been shown to move bidirectionally along the microtubule network. Some cargos can even switch between actin filaments and microtubules. In the recent years progress has been made in understanding the mechanistic working of motors, the identification of Rab GTPases and their effector proteins on organelles and vesicles and characterisation of cellular signals that might control transport directionality and destination. In this discussion several well-explored examples of GTPases and their motor interactions will be discussed and compared with the Rab6-Bicaudal-D system, the main subject of this thesis.

5.2 Motor binding and transport models

Microscopic observations of live cells demonstrate bidirectional motility of organelles and vesicles. Mitochondria are known to move towards sites where local energy consumption is needed (Hollenbeck, 1996; Chada and Hollenbeck, 2003; Hollenbeck and Saxton, 2005). Melanosomes in melanocytes and in fish and *Xenopus* melanophores display bidirectional movements controlled by cAMP levels (Rodionov et al., 2003). Similar behaviour was also shown for endosomes (Hollenbeck, 1993; Valetti et al., 1999; Murray et al., 2000). To explain the bidirectional behaviour of these and other structures three models have been proposed (Fig.1).

The first model explains bidirectionality by suggesting that only motors of a certain polarity bind to a cargo at any given time. Cellular components might change the properties of the motor-adaptor complexes, and removal of the motors attached to the cargo will open new binding sites for motors of opposite direction. This very simple model is contradicted by the observation that both kinesin and dynein motors associate simultaneously with various cargos (Rogers et al., 1997; Ligon et al., 2004; Pilling et al., 2006).

More plausible are the "tug-of-war" and "coordination" models which both describe a situation where dynein and kinesin are simultaneously bound to a cargo (Rogers et al., 1997; Gross et al., 2002; Welte, 2004; Pilling et al., 2006).

In the "tug-of-war" model, motors of both minus-end and plus-end directionality are bound to a

cargo at the same time. The number of motors and the force they create will be decisive for the direction of the cargo transport. The back and forth movement of most vesicles and organelles can be explained by motor loss or changes in activities of motors of a certain polarity, causing the opposing motors to take the lead (Muller et al., 2008).

The "coordination" theory also assumes that motors of opposite polarity simultaneously bind to a cargo. In this model vesicle movement is directed by regulated on and off switching of groups of similarly directed motors (Gross et al., 2002; Welte, 2004). The "coordination" theory is strengthened by accumulating evidence that disruption of one set of motors causes transport defects in both directions. This might be explained by the formation of large protein complexes of regulatory factors, like Rab GTPases and motors on a cargo (Martin et al., 1999; Deacon et al., 2003; Kural et al., 2005).
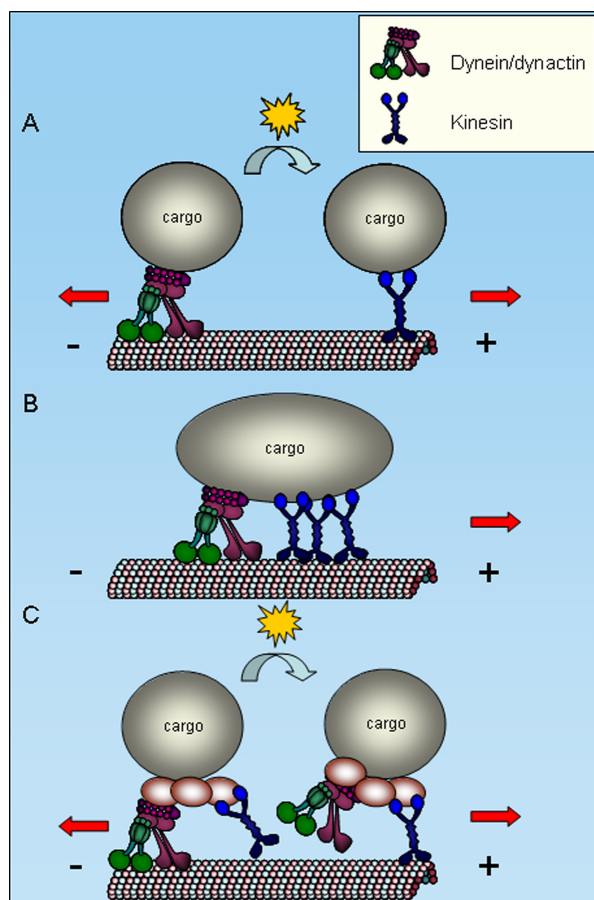
Figure 1. Three possible mechanisms of bidirectional transport. Plus-end motors are shown in blue, dynein in green and dynactin in purple. (A) A single type of motor is attached to a cargo and after a certain signal the motor is replaced by a motor with opposite polarity. (B) Motors of opposite polarity are always attached to cargo and work against each other. The direction of cargo movement depends on the relative strength or number of competing motors. (C) Opposing motors are simultaneously attached to the cargo, but the coordination machinery ensures that when one motor is actively engaged on the microtubule, the opposing motor is turned off. Stochastic processes or cellular signals turn on and off groups of motors and direct the cargo towards its destination (Welte, 2004).

5.3 Role of Rab GTPases in transport

Small GTPases of the Rab family play a vital role in the regulation, directionality and destination specificity of cellular cargos (Chavrier and Goud, 1999; Zerial and McBride, 2001). Rab GTPases are members of the Rho/Rac family and over 60 Rab family members are known today with numerous and sometime tissue specific isoforms (Pereira-Leal and Seabra, 2000; Schultz et al., 2000). Rab proteins and other G proteins exist in two states, a GTP and GDP state, and function as a switch. The switching of GTPases is controlled by guanine nucleotide exchange factors (GEFs), which accelerate the conversion of Rab-GDP into Rab-GTP. Rab-GTP proteins recruit effector proteins, which assist them in fulfilling their various functions in membrane trafficking. Specific GTPase activating proteins (GAPs) inactivate the Rab-GTP complexes and recycle Rab proteins back into GDP-bound state (Pfeffer, 2001; Segev, 2001).

Rab proteins regulate transport of vesicles and organelles in for example the endosomal and lysosomal pathways and specify regions at the Golgi complex and Endoplasmic Reticulum (ER). Several Rab proteins have been well studied and some of their GAPs, GEFs and effector proteins are known (Grosshans et al., 2006).

5.4 Recycling and degradation routes

The endosomal and lysosomal pathways regulate membrane transport between plasma membrane and various intracellular compartments. Endocytosed material, membrane proteins and lipids are either recycled and returned to the plasma membrane or processed further to be degraded in the lysosomes. The processing, sorting and transport of the membranous structures and their content is under tight control of Rab GTPases and their effector proteins and requires an intact microtubule network (Goltz et al., 1992; Bananis et al., 2003; Bananis et al., 2004) (Fig.2).

Endocytosed material is taken up in vesicles, which are transported towards the early endosomal compartment under the control of Rab5 (Zerial and McBride, 2001). Rab5 recruits various effector proteins to the early endosomes. These effector proteins play a role in membrane fusion and vesicle transport. The Rabaptin-5-Rabex complex activates Rab5 and recruits Vps34, a phosphatidylinositol-3-OH kinase, which, in turn, generates PI(3)P (Horiuchi et al., 1997; Christoforidis et al., 1999). Two other Rab5 effector proteins, EEA1 and Rabenosyn-5, are then able to bind to the same membranes via PI(3)P, providing a platform for the interaction with SNARE proteins (Christoforidis et al., 1999; Simonsen et al., 1999).

Rab5 positive endosomes are known to move along actin filaments and bidirectionally on the microtubules (Nielsen et al., 1999; Aschenbrenner et al., 2003). Several motors have been described to bind Rab5 positive membranes. The microtubule plus end directed motor Kinesin-3 (Kif16b), for example, is involved in the movement of Rab5-positive vesicles. This kinesin does not bind directly to Rab5, but is also recruited via the effector protein Vps34 and binds PI(3)P, similar to EEA1 and Rabenosyn-5 (Hoepfner et al., 2005).

Other *in vitro* experiments with early endocytotic vesicles prepared from mouse liver show microtubule based movement based on both Kinesin-1 (Kif5b) and the minus end directed motor Kinesin-14 (KifC1) (Nath et al., 2007).

Rab5-GTP has also been shown to bind Huntingtin, which recruits the Huntingtin Associated Protein 40 (HAP40). The Huntingtin-HAP40 complex is involved in actin-based transport at the cell periphery, possibly via Myosin-VI (Aschenbrenner et al., 2003; Pal et al., 2006). GTP hydrolysis by Rab5 might lead to the dissociation of HAP40 from the Huntingtin-Rab5 complex that allows Huntingtin to recruit new motor complexes and switch from short distance transport on the actin filaments to long distance transport along the microtubules. One of the Huntingtin interacting partners is Huntingtin Associated Protein 1 (HAP1), which binds both Kinesin-1 and p150[glued], a part of the dynactin complex, which is an accessory factor of cytoplasmic dynein (Engelender et al., 1997; McGuire et al., 2006). The Rab5-Huntingtin complex might regulate both actin and microtubule based transport by recruiting HAP1 and other still unknown components. The variety of motors involved in movement of the endosomal vesicles suggests that some of these motors might be cell type specific.

In the early endosomal compartment membrane proteins are sorted and recycled via the short-loop recycling pathway under the control of Rab4. The short-loop recycling pathway is important for returning receptors and transporters such as glucose transporter GLUT4 to the plasma membrane. A direct interaction between Rab4 and Kinesin-2 (Kif3) has been reported which is influenced by insulin (Imamura et al., 2003). Interestingly, Rab4 has also been connected to dynein intermediate chain suggesting that Rab4 is capable of binding both plus and minus end motor complexes (Bielli et al., 2001). It should be mentioned that the major flux of Rab4-positive vesicles is towards the plus ends of the microtubules.

Another part of the early endosomal compartment is formed by Rab7-positive patches, which will mature into late endosomes (Popoff et al., 1996; Bucci et al., 2000). Rab7 is very well characterised and recently several groups showed in detail its binding to dynein/dynactin motor complexes via the Rab7-interacting lysosomal protein (RILP) (Cantalupo et al., 2001). The recruitment of RILP to Rab7-GTP is important for the maturation of phagosomes and the fusion of late endosomal and lysosomal structures (Harrison et al., 2003). Rab7-GTP binds RILP which will recruit dynactin to the Rab7 coated vesicles through an interaction with p150[glued] (Jordens et al., 2001). This interaction alone is insufficient to form motile structures. A second effector protein, oxysterol-binding protein–related protein 1L (ORP1L) is required. The Rab7-RILP-ORP1L complex recruits βIII spectrin which enhances the binding of dynein (Johansson et al., 2007). This whole cascade of events results in a processive dynein/dynactin motor complex that is firmly bound to the lipid membrane and transports Rab7-coated vesicles towards the minus ends of the microtubules where they fuse with the late endosomal compartments. Other content of the late endosomal compartments will be degraded in the lysosomes, which are also under the control of Rab7.
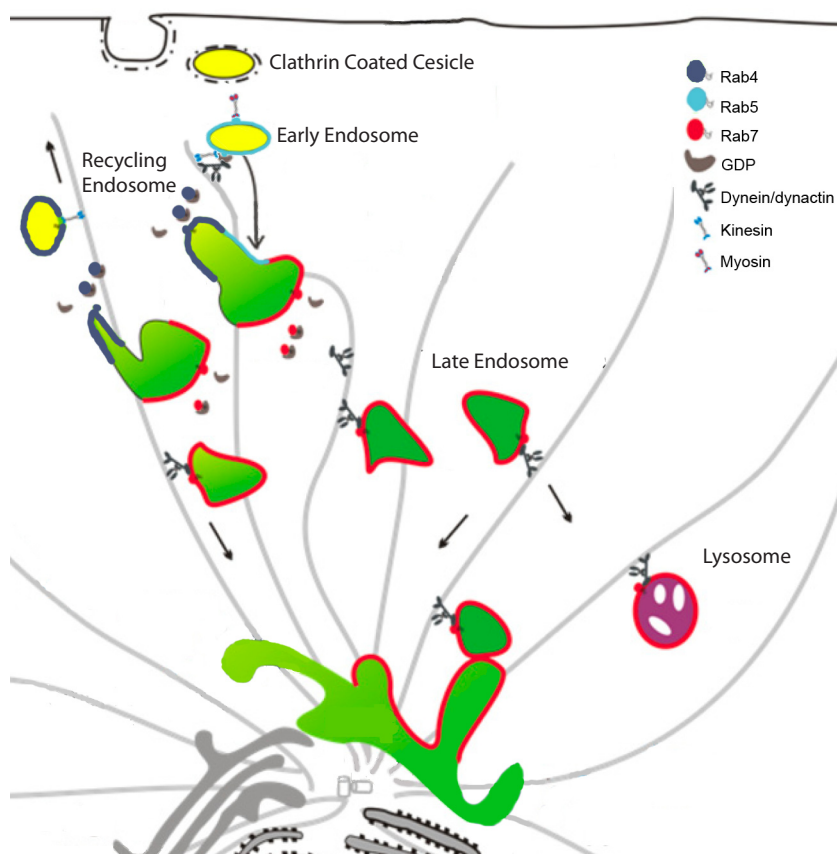
Figure 2 Transport routes of endosomes and lysosomes

Illustration of various Rabs in the endosomal/lysosomal pathways and their directionality. Rab5 (light blue) regulates membrane fusion and transport of early endosomes. Rab4 (green) recycles the content of the early endosomes back to the plasma membrane. Rab7 (red) facilitates dynein-mediated transport towards the endosomal recycling compartment and to the lysosomes, while Rab11 (dark blue) controls a second round of recycling towards the plasma membrane. Figure adopted and modified from Chen H.Y., 2008, Biophys J. 54(4), 1508-1520.

5.5 Melanosomes play hide and seek

Melanosomes are lysosome-related organelles; they share several characteristics of lysosomes including the presence of lysosomal hydrolases. The melanosomes contains a polymeric pigment called melanin. In mammals melanosomes are formed in melanocytes, which are localized mainly in the skin and the eye. The skin melanocytes are located near the basal layers of the epidermis and hair bulbs and transfer melanosomes to the nearby keratinocytes. This results in pigmentation of the skin and hairs and protects the skin against ultraviolet light damage. In the retina melanophores

are thought to absorb stray light to minimize light scatter (Schraermeyer and Heimann, 1999). Fish, reptiles and amphibians have different types of pigment cells called chromatophores. These chromatophores are responsible for the sometimes spectacular skin colours of these animals. Colour changes of skin can be achieved by dispersion or aggregation of melanosomes. This results in a darker or a lighter skin colour, respectively, and plays a role in camouflage and social behaviour (Fujii, 2000).

The distribution of melanosomes is characterized by movements along both the microtubules and the actin filaments, and is driven by Kinesin-2, cytoplasmic dynein and Myosin-V. The role of Rab GTPases in melanosome movement became clear when Rab27 was identified as a factor involved in the Griscelli syndrome (GS) (Menasche et al., 2000; Wilson et al., 2000; Menasche et al., 2003). This syndrome is characterized by pigmentary dilution of the skin and hair and accumulation of melanosomes in melanocytes. The mouse models *Dilute*, *Ashen* and *Leaden* show phenotypical similarities to GS patients and are characterized by coat colour mutations (Mercer et al., 1991; Provance et al., 1996; Wilson et al., 2000; Provance et al., 2002). Genetic and biochemical data identified myosin-Va as a gene involved in GS. Other data from the *Ashen* and *Leaden* mouse implied the involvement of melanophilin and Rab27a. Myosin-Va binds Rab27 via the effector protein melanophilin and transports melanosomes along the actin filaments. Rab7 in complex with RILP might control the minus-end directed movement of the melanosomes with the dynein/dynactin motor complex. This could have been expected based on the lysosomal origins of the melanosomes (Tuma et al., 1998; Fukuda et al., 2002; Nagashima, et al., 2002; Wu et al., 2002; Jordens et al., 2006). Recently, Rab32 was also implicated in melanosome transport as a factor with A-kinase anchoring protein (AKAP) properties. PKA is recruited by Rab32 and regulates melanosome distribution. Rab32 might be involved in the plus-end directed transport of melanosomes along the microtubules. The overexpression of Rab32 was shown to inhibit melanosome aggregation by melatonin (Park et al., 2007).

Both fish and *Xenopus* melanophores have been extensively used to investigate signaling pathways underlying the regulation of melanosome movement. Gross *et al*. (2002) and Rodionov *et al*. (2003) showed that elevated levels of intracellular cAMP under the control of melanin stimulating hormone (MSH) activate protein kinase A (PKA). This leads to dispersion of melanosomes. Melanin concentrating hormone (MCH) reverses this process and results in melanosome aggregation (Gross et al., 2002; Rodionov et al., 2003). When phosphorylated by PKA, melanophilin might inhibit dynein function on the melanosomes which leads to plus end directed transport by kinesin-2 (Sheets et al., 2007). When melanosomes reach the ends of the microtubules, melanophilin recruits and activates myosin-Va for further transport along the actin filaments (Li et al., 2005).

5.6 Mitochondrial movement is essential for the local energy supply

Mitochondria are membrane-enclosed organelles that generate the cellular energy supply in the form of adenosine triphosphate (ATP). The need for energy, changing membrane potentials and growth factors are all signals that influence the cellular distribution of mitochondria (Morris and Hollenbeck, 1995). Mitochondria displacements involve both the actin filaments and

the microtubule network, required for short and long-distance transport, respectively (Chada and Hollenbeck, 2003; Hollenbeck and Saxton, 2005).

One of the best-studied adaptors for mitochondria movement is Milton, which was initially identified in *Drosophila* photoreceptors as a factor implicated in axonal transport of mitochondria (Stowers et al., 2002). Abolishment of the function of Milton interferes with the transport of mitochondria in optical neurons of the fruit fly, resulting in blindness. Milton was shown to recruit Kinesin-1 to mitochondria in *Drosophila*. Miro, a Rho-like GTPase, connects Milton to mitochondrial membranes (Guo et al., 2005). Dynein is involved in retrograde transport of mitochondria and disruption of this motor complex results in impaired mitochondrial movement (Varadi et al., 2004). The adaptor molecules for dynein have not been identified yet, but interesting observations have been made regarding mitochondrial movement in *Drosophila* neuronal cultures. Horiuchi *et al* identified Aplip1 in a yeast two-hybrid screen using Kinesin-1 heavy chain as bait, suggesting that Aplip1 is an adaptor for kinesin-based movement. However, Aplip1 promotes dynein driven motility, indicating that it might be an important part of motor-cargo linkage complexes for both Kinesin-1 and dynein (Horiuchi et al., 2005).

Less is known about the movement of mitochondria in mammals, but similar motors are probably involved. Kinesin-1 (Kif5b) knock out in mice results in an abnormal clustering of mitochondria in the perinuclear region (Tanaka et al., 1998). Similar to flies, a complex containing the mammalian Milton and Miro participates in binding Kinesin-1 to mitochondrial membranes (Glater et al., 2006). Rab32, a GTPase that is also involved in melanosome distribution, might play a role in this process. It colocalizes with mitochondria and a Rab32 mutant deficient in GTP binding induces a collapse of mitochondria at the MTOC (Alto et al., 2002). Another factor that might be involved in mitochondrial transport is Kinesin-binding protein (KBP), which interacts with Kinesin-3 Kif1Bα (Wozniak et al., 2005). It should be mentioned that the molecular connection between KBP and mitochondria has not been identified yet.

5.7 Transport routes towards the plasma membrane: an unexplored field

The process of exocytosis is essential for the release of neurotransmitters and other signalling compounds. Exocytotic vesicles undergo a series of events, such as motor based movement towards the release sites, vesicle tethering, docking and finally membrane fusion, which results in the release of the vesicle content. Various Rab proteins are known to be involved in these processes. Rab27, which is described above, is involved in the exocytosis of melanosomes. Other exocytotic Rab GTPases include Rab3, Rab6 and Rab8. Rab3 isoforms are mainly expressed in neurons and other specialised secretory cells. Rab3-GTP binds synaptic vesicles and plays a role in the last steps of exocytosis (Holz et al., 1994; Geppert et al., 1997). Functional screens on Rab8 show that Rab8 is located at the Golgi and plays a role in vesicle transport towards the plasma membrane (van der Sluijs et al., 1992; Ang et al., 2003). One of the effector proteins of Rab8 is Optineurin (also known as FIP-2), which was shown to link Myosin-VI to Rab8 and might function in Golgi ribbon formation (Sahlender et al., 2005). Interestingly, Optineurin might in addition regulate

dynein and kinesin mediated transport via Huntingtin (Engelender et al., 1997; Faber et al., 1998). The role of various motor and effector proteins in the Rab3 and Rab8 transport routes is still very unclear. More is known about mammalian Rab6. This GTPase was originally thought to facilitate transport from Golgi to ER (Martinez et al., 1994; Girod et al., 1999). Recently we demonstrated the exocytotic nature of Rab6 positive vesicles (Grigoriev et al., 2007). Also the *Drosophila* homologue of Rab6, Drab6, regulates secretion during fly development: it participates in exocytosis of the *Gurken* protein (Januschke et al., 2007). Bicaudal-D is one of the effector proteins of Rab6 and is involved in minus end directed transport by binding the dynein/dynactin complex. However, exocytotic vesicle movement is predominantly microtubule plus end directed and therefore kinesin-dependent. Importantly, mammalian Bicaudal-D (BicD) homologue BICD2 does not exclusively bind dynein/dynactin, but is also capable of associating with Kinesin-1 (Grigoriev et al., 2007).

5.8 Bicaudal-D: switching cargo and direction

Bicaudal-D is a rod-shaped protein, which functions as an adaptor between motor proteins and cargos and is highly conserved between animal species. Functional characterization of Bicaudal-D originally started in *Drosophila*. *Drosophila* Bicaudal-D (BicD) is crucial for the development of the *Drosophila* oocyte and embryo and plays an essential role in the establishment and maintenance of the microtubule network in the *Drosophila* egg (Oh and Steward, 2001). Furthermore BicD facilitates dynein-mediated transport of specific components to the oocyte during early phases of oogenesis (Suter et al., 1989; Wharton and Struhl, 1989; Suter and Steward, 1991). In later stages of *Drosophila* oogenesis the microtubule network in the oocyte is rearranged and BicD in complex with Egalitarian (Egl) is responsible for the localization of patterning factors such as *Osk* and *Grk* mRNA (Ephrussi et al., 1991; Swan and Suter, 1996; Mach and Lehmann, 1997). In addition, Bicaudal-D together with the dynein cofactor Dlis-1 also facilitates nuclear positioning within the oocyte (Swan and Suter, 1996; Mach and Lehmann, 1997; Swan et al., 1999). Interestingly BicD and Dlis-1, possibly under control of the kinase Misshapen (Msn), also play a role in the nuclear migration of the developing *Drosophila* photoreceptor cells (Houalla et al., 2005).

In mammals two homologues of Bicaudal-D are present, namely BICD1 and BICD2. Our studies were mainly focussed on one of the two protein orthologues, BICD2. The N-terminal part of BICD2 forms a triple complex with the minus end directed motor dynein and its accessory factor dynactin (Hoogenraad et al., 2001; Hoogenraad et al., 2003). The middle part of BICD2 weakly interacts with the plus end directed motor Kinesin-1 (Grigoriev et al., 2007). The carboxy terminus of BICD2 is the cargo binding part of the protein, which binds the small GTPase Rab6 (Matanis et al., 2002; Januschke et al., 2007). This interaction is conserved in flies: the *Drosophila* Rab6 homologue Drab6 and BicD facilitate the exocytosis of *Gurken* protein during oogenesis (Januschke et al., 2007).

In this thesis, we have identified RanBP2, a component of the Nuclear Pore Complex (NPC), as a new binding partner for the cargo-binding domain of BICD2 (Chapter 3). The cellular localization of mammalian BICD2 changes dramatically during the cell cycle. During G1 and S-phase, BICD2

binds to the Golgi complex and Rab6-positive vesicles. In G2 phase, BICD2 is recruited to the nuclear envelope via an interaction with RanBP2. Through this interaction, BICD2 targets dynein to the nuclear envelope and helps to position the nucleus in close proximity of the centrosomes before mitosis. The behaviour of annulate lamellae, the NPCs in the ER, and Rab6-positive vesicles verifies that BICD indeed binds cargos that are set in motion by two oppositely directed motors, cytoplasmic dynein and Kinesin-1.

BICD protein consists of 5 coiled coil domains, which are linked by flexible regions. BICD might form dimers or oligomers to assemble a functional complex (Stuurman et al., 1999; Oh et al., 2000). Due to the flexibility of BICD it is thought that it can fold back, resulting in an autoinhibited state (Hoogenraad et al., 2001). This theory is strengthened by the fact that the N- and C-terminal domains of BICD, when expressed separately, exhibit dominant negative properties and interact with their partners stronger than the full length molecule (Hoogenraad et al. 2001).

Table 1. Binding partners of mammalian and *Drosophila* Bicaudal-D
Summary of the binding partners of Bicaudal-D discussed in this chapter

Protein	Species	Reference
Dynein/dynactin	Drosophila/mammals	(Pare and Suter, 2000; Hoogenraad et al., 2001)
Kinesin-1 (Kif5b)	mammals	Chapter 2 (Grigoriev et al., 2007)
Egalitarian	Drosophila	(Mach and Lehmann, 1997)
Drab6/Rab6	Drosophila/mammals	(Matanis et al., 2002; Coutelis and Ephrussi, 2007)
RanBP2	Mammals	Chapter 3
Polo	Drosophila	(Mirouse et al., 2006)

Evidence from *Drosophila* and mammals suggests that Bicaudal-D is capable of binding oppositely directed motors. Interestingly, presence of BICD on a cargo does not correlate with the preferential direction of movement: while Rab6 vesicles move predominantly to microtubule plus ends, the G2 phase nucleus is a cargo transported in the opposite direction, towards the minus ends of microtubules. How the switching is regulated and whether both motor complexes bind simultaneously to BICD is still unknown. Both motor complexes might be essential to form a processive complex, because more evidence is now available that the disruption of one motor also inhibits movement in the opposite direction (Martin et al., 1999; Gross et al., 2002; Berezuk and Schroer, 2007; Grigoriev et al., 2007).

5.9 Conclusions

Rab GTPases form a large group of proteins that regulate transport of membrane structures. A variety of regulatory factors controls membrane insertion and activation and inactivation of GTPases. Rab effector proteins promote motor binding, vesicle docking and membrane fusion.

When we compare the motor-cargo interaction models discussed here, both common and divergent properties emerge. Some Rab GTPases bind motor complexes via effector proteins like Milton, RILP, HAP1 or BICD, which are often coiled coiled proteins, some of which may have common ancestry. Other GTPases bind directly to parts of dynein, dynactin or kinesin motors. Interestingly, several complexes have been shown to bind motors of opposite polarity. We have shown that Rab6 together with BICD binds both dynein/dynactin and Kinesin-1 (Grigoriev et al., 2007). A complex containing Rab5 and Huntingtin might organise both microtubule and actin transport via HAP1 and HAP40, respectively (Engelender et al., 1997; McGuire et al., 2006; Pal et al., 2006). Other cargos bind more than one GTPase to regulate directionality. Rab7 and Rab27 work together on melanosomes to switch from the microtubule network to actin filaments, and Rab32 might facilitate their plus end directed movement. Bidirectionality does not seem to be a simple "tug of war" between motors. Opposite polarity motors might be available in one large complex and there is accumulating evidence that groups of motors with the same polarity are switched on or off.

The biggest challenge now is to unravel the extra- and intracellular signalling pathways that drive and regulate transport. It is known that mitochondria stall when they meet locally elevated Ca^{2+} concentrations, a signal for increased energy need (Werth and Thayer, 1994; Hollenbeck, 1996; Zucker, 1999). The GTPase Miro contains two calcium binding EF hands and it is likely that elevated Ca^{2+} levels disrupt the Miro-Milton interaction (Glater et al., 2006). This would inhibit the plus end directed movement and possibly also the minus end directed transport and help to accumulate mitochondria in cell areas where the energy need is high (Glater, Megeath et al. 2006). Melanosomes in fish and frog melanophores are regulated by cAMP and PKA via MSH and MCH (Sheets et al., 2007;Gross et al., 2002; Rodionov et al., 2003), shifting them from the microtubule organizing centre to the cell periphery and vice versa. Our own studies (Chapter 3) provided an example of a cell cycle regulated motor switch – G2 phase-specific recruitment of BICD2, dynein and Kinesin-1 to the NPC that is required to regulate nuclear positioning during mitotic entry. However, it is still unclear which factors control the switch. Polo like kinase, an important mitotic regulator, might be involved in this process. Another potential candidate is the kinase Misshapen. Both Polo and Misshapen are known to phosphorylate *Drosophila* BicD and could play also a role in the regulation of the cellular functions of mammalian BICD. To study bidirectionality *in vivo,* one would like to employ a system with a clear output. The ability of BICD to couple both kinesin and dynein motors to nuclear pore complexes and Annulate Lamellae (AL) could lay the basis for an *in vivo* assay with a solid read out. Via phosphorylation mapping and mutating the specific phosphorylation sites it might be possible to regulate specifically the direction of the AL. Due to these proporties BICD might be an

important factor for unraveling the molecular basis of bidirectional motility. Dissecting the various signalling pathways that control this specific switching would be a step forward in understanding vesicle and organelle transport, one of the most basic aspects of eukaryotic cell physiology.

Table 2. Organelles, their GTPases, motors and effector proteins
Summary of the GTPase/effector protein complexes and their interacting motors discussed in this chapter

Organelle	GTPase	Motor protein	Effector protein/ complex	Adaptor structure	Species	References
Early endosome	Rab5	Dynein	Huntingtin/HAP1	PolyQ HAP domain	Mammals	(Engelender et al., 1997)
	Rab5	Myosin-VI	Huntingtin/HAP40	PolyQ Coiled-coil	Mammals	(Pal et al., 2006)
	Rab5	Kinesin-3 Kif16b	Direct binding to PI(3)P	-	Mammals	(Hoepfner et al., 2005)
	Rab5	Kinesin-14 KifC1	Unknown	-	Mammals	(Nath et al., 2007)
	Rab5	Dynein	Huntingtin/HAP1	PolyQ HAP domain Coiled-coil	Mammals	(Engelender et al., 1997)
Recycling endosome	Rab4	Kinesin-2 Kif3	Direct interaction	-	Mammals	(Imamura et al., 2003)
	Rab4	Dynein	Direct interaction-	-	Mammals	(Bielli et al., 2001)
Late endosome/ lysosome	Rab7	Dynein	Rilp/ORP1L	Coiled-coil	Mammals	(Johansson et al., 2007)
Exocytotic vesicle	Rab6	Dynein	BICD or direct binding via DIC	Coiled-coil	Mammals/ Drosophila	(Hoogenraad et al., 2001)
	Rab6	Kinesin-1 (Kif5A/B)	BICD	Coiled-coil	Mammals	(Grigoriev et al., 2007)
Melanosome	Rab27	Myosin-V	Melanophilin	Coiled-coil	Mammals/ Xenopus	(Fukuda et al., 2002)
	Rab7	Dynein	RILP/ORP1L	Coiled-coil	Mammals	(Jordens et al., 2006)
	Rab32	Kinesin-2	?	?	Xenopus	(Park et al., 2007)
Mitochondrion	Miro	Kinesin-1	Milton	Coiled-coil	Drosophila	(Guo et al. ,2005)
	?	Kinesin-1	Aplip1	SH3, JIP	Drosophila	(Horiuchi et al., 2005)
	?	Kinesin-3 Kif1Bα	Kinesin Binding Protein		Mammals	(Wozniak et al., 2005)
	Rab32	Kinesin	?	?	Mammals	(Alto et al., 2002)
	?	Dynein	Aplip1 ?	SH3, JIP	Drosophila	(Horiuchi et al., 2005)

5.10 References

Alto, N. M., J. Soderling, et al. (2002). "Rab32 is an A-kinase anchoring protein and participates in mitochondrial dynamics." J Cell Biol 158(4): 659-68.

Ang, A. L., H. Folsch, et al. (2003). "The Rab8 GTPase selectively regulates AP-1B-dependent basolateral transport in polarized Madin-Darby canine kidney cells." J Cell Biol 163(2): 339-50.

Aschenbrenner, L., T. Lee, et al. (2003). "Myo6 facilitates the translocation of endocytic vesicles from cell peripheries." Mol Biol Cell 14(7): 2728-43.

Bananis, E., J. W. Murray, et al. (2003). "Regulation of early endocytic vesicle motility and fission in a reconstituted system." J Cell Sci 116(Pt 13): 2749-61.

Bananis, E., S. Nath, et al. (2004). "Microtubule-dependent movement of late endocytic vesicles in vitro: requirements for Dynein and Kinesin." Mol Biol Cell 15(8): 3688-97.

Bartz, R., C. Benzing, et al. (2003). "Reconstitution of vesicular transport to Rab11-positive recycling endosomes in vitro." Biochem Biophys Res Commun 312(3): 663-9.

Berezuk, M. A. and T. A. Schroer (2007). "Dynactin enhances the processivity of kinesin-2." Traffic 8(2): 124-9.

Bielli, A., P. O. Thornqvist, et al. (2001). "The small GTPase Rab4A interacts with the central region of cytoplasmic dynein light intermediate chain-1." Biochem Biophys Res Commun 281(5): 1141-53.

Bucci, C., P. Thomsen, et al. (2000). "Rab7: a key to lysosome biogenesis." Mol Biol Cell 11(2): 467-80.

Cantalupo, G., P. Alifano, et al. (2001). "Rab-interacting lysosomal protein (RILP): the Rab7 effector required for transport to lysosomes." Embo J 20(4): 683-93.

Chada, S. R. and P. J. Hollenbeck (2003). "Mitochondrial movement and positioning in axons: the role of growth factor signaling." J Exp Biol 206(Pt 12): 1985-92.

Chavrier, P. and B. Goud (1999). "The role of ARF and Rab GTPases in membrane transport." Curr Opin Cell Biol 11(4): 466-75.

Christoforidis, S., H. M. McBride, et al. (1999). "The Rab5 effector EEA1 is a core component of endosome docking." Nature 397(6720): 621-5.

Christoforidis, S., M. Miaczynska, et al. (1999). "Phosphatidylinositol-3-OH kinases are Rab5 effectors." Nat Cell Biol 1(4): 249-52.

Coutelis, J. B. and A. Ephrussi (2007). "Rab6 mediates membrane organization and determinant localization during Drosophila oogenesis." Development 134(7): 1419-30.

Deacon, S. W., A. S. Serpinskaya, et al. (2003). "Dynactin is required for bidirectional organelle transport." J Cell Biol 160(3): 297-301.

Dollar, G., E. Struckhoff, et al. (2002). "Rab11 polarization of the Drosophila oocyte: a novel link between membrane trafficking, microtubule organization, and oskar mRNA localization and translation." Development 129(2): 517-26.

Engelender, S., A. H. Sharp, et al. (1997). "Huntingtin-associated protein 1 (HAP1) interacts with the p150Glued subunit of dynactin." Hum Mol Genet 6(13): 2205-12.

Ephrussi, A., L. K. Dickinson, et al. (1991). "Oskar organizes the germ plasm and directs localization of the posterior determinant nanos." Cell 66(1): 37-50.

Faber, P. W., G. T. Barnes, et al. (1998). "Huntingtin interacts with a family of WW domain proteins." Hum Mol Genet 7(9): 1463-74.

Fujii, R. (2000). "The regulation of motile activity in fish chromatophores." Pigment Cell Res 13(5): 300-19.

Fukuda, M., T. S. Kuroda, et al. (2002). "Slac2-a/melanophilin, the missing link between Rab27 and myosin Va: implications of a tripartite protein complex for melanosome transport." J Biol Chem 277(14): 12432-6.

Geppert, M., Y. Goda, et al. (1997). "The small GTP-binding protein Rab3A regulates a late step in synaptic vesicle fusion." Nature 387(6635): 810-4.

Girod, A., B. Storrie, et al. (1999). "Evidence for a COP-I-independent transport route from the Golgi complex to the endoplasmic reticulum." Nat Cell Biol 1(7): 423-30.

Glater, E. E., L. J. Megeath, et al. (2006). "Axonal transport of mitochondria requires milton to recruit kinesin heavy chain and is light chain independent." J Cell Biol 173(4): 545-57.

Goltz, J. S., A. W. Wolkoff, et al. (1992). "A role for microtubules in sorting endocytic vesicles in rat hepatocytes." Proc Natl Acad Sci U S A 89(15): 7026-30.

Grigoriev, I., D. Splinter, et al. (2007). "Rab6 regulates transport and targeting of exocytotic carriers." Dev Cell 13(2): 305-14.

Gross, S. P., M. C. Tuma, et al. (2002). "Interactions and regulation of molecular motors in Xenopus melanophores." J Cell Biol 156(5): 855-65.

Gross, S. P., M. A. Welte, et al. (2002). "Coordination of opposite-polarity microtubule motors." J Cell Biol 156(4): 715-24.

Grosshans, B. L., D. Ortiz, et al. (2006). "Rabs and their effectors: achieving specificity in membrane traffic." Proc Natl Acad Sci U S A 103(32): 11821-7.

Guo, X., G. T. Macleod, et al. (2005). "The GTPase dMiro is required for axonal transport of mitochondria to Drosophila synapses." Neuron 47(3): 379-93.

Hales, C. M., J. P. Vaerman, et al. (2002). "Rab11 family interacting protein 2 associates with Myosin Vb and regulates plasma membrane recycling." J Biol Chem 277(52): 50415-21.

Harrison, R. E., C. Bucci, et al. (2003). "Phagosomes fuse with late endosomes and/or lysosomes by extension of membrane protrusions along microtubules: role of Rab7 and RILP." Mol Cell Biol 23(18): 6494-506.

Hoepfner, S., F. Severin, et al. (2005). "Modulation of receptor recycling and degradation by the endosomal kinesin KIF16B." Cell 121(3): 437-50.

Hollenbeck, P. J. (1993). "Products of endocytosis and autophagy are retrieved from axons by regulated retrograde organelle transport." J Cell Biol 121(2): 305-15.

Hollenbeck, P. J. (1996). "The pattern and mechanism of mitochondrial transport in axons." Front Biosci 1: d91-102.

Hollenbeck, P. J. and W. M. Saxton (2005). "The axonal transport of mitochondria." J Cell Sci 118(Pt 23): 5411-9.

Holz, R. W., W. H. Brondyk, et al. (1994). "Evidence for the involvement of Rab3A in Ca(2+)-dependent exocytosis from adrenal chromaffin cells." J Biol Chem 269(14): 10229-34.

Hoogenraad, C. C., A. Akhmanova, et al. (2001). "Mammalian Golgi-associated Bicaudal-D2 functions in the dynein-dynactin pathway by interacting with these complexes." Embo J 20(15): 4041-54.

Hoogenraad, C. C., P. Wulf, et al. (2003). "Bicaudal D induces selective dynein-mediated microtubule minus end-directed transport." Embo J 22(22): 6004-15.

Horiuchi, D., R. V. Barkus, et al. (2005). "APLIP1, a kinesin binding JIP-1/JNK scaffold protein, influences the axonal transport of both vesicles and mitochondria in Drosophila." Curr Biol 15(23): 2137-41.

Horiuchi, H., R. Lippe, et al. (1997). "A novel Rab5 GDP/GTP exchange factor complexed to Rabaptin-5 links nucleotide exchange to effector recruitment and function." Cell 90(6): 1149-59.

Houalla, T., D. Hien Vuong, et al. (2005). "The Ste20-like kinase misshapen functions together with Bicaudal-D and dynein in driving nuclear migration in the developing drosophila eye." Mech Dev 122(1): 97-108.

Imamura, T., J. Huang, et al. (2003). "Insulin-induced GLUT4 translocation involves protein kinase C-lambda-mediated functional coupling between Rab4 and the motor protein kinesin." Mol Cell Biol 23(14): 4892-900.

Januschke, J., E. Nicolas, et al. (2007). "Rab6 and the secretory pathway affect oocyte polarity in Drosophila." Development 134(19): 3419-25.

Johansson, M., N. Rocha, et al. (2007). "Activation of endosomal dynein motors by stepwise assembly of Rab7-RILP-p150Glued, ORP1L, and the receptor betaIII spectrin." J Cell Biol 176(4): 459-71.

Jordens, I., M. Fernandez-Borja, et al. (2001). "The Rab7 effector protein RILP controls lysosomal transport by inducing the recruitment of dynein-dynactin motors." Curr Biol 11(21): 1680-5.

Jordens, I., W. Westbroek, et al. (2006). "Rab7 and Rab27a control two motor protein activities involved in melanosomal transport." Pigment Cell Res 19(5): 412-23.

Kural, C., H. Kim, et al. (2005). "Kinesin and dynein move a peroxisome in vivo: a tug-of-war or coordinated movement?" Science 308(5727): 1469-72.

Li, X. D., R. Ikebe, et al. (2005). "Activation of myosin Va function by melanophilin, a specific docking partner of myosin Va." J Biol Chem 280(18): 17815-22.

Ligon, L. A., M. Tokito, et al. (2004). "A direct interaction between cytoplasmic dynein and kinesin I may coordinate motor activity." J Biol Chem 279(18): 19201-8.

Mach, J. M. and R. Lehmann (1997). "An Egalitarian-BicaudalD complex is essential for oocyte specification and axis determination in Drosophila." Genes Dev 11(4): 423-35.

Martin, M., S. J. Iyadurai, et al. (1999). "Cytoplasmic dynein, the dynactin complex, and kinesin are interdependent and essential for fast axonal transport." Mol Biol Cell 10(11): 3717-28.

Martinez, O., A. Schmidt, et al. (1994). "The small GTP-binding protein rab6 functions in intra-Golgi transport." J Cell Biol 127(6 Pt 1): 1575-88.

Matanis, T., A. Akhmanova, et al. (2002). "Bicaudal-D regulates COPI-independent Golgi-ER transport by recruiting the dynein-dynactin motor complex." Nat Cell Biol 4(12): 986-92.

McGuire, J. R., J. Rong, et al. (2006). "Interaction of Huntingtin-associated protein-1 with kinesin light chain: implications in intracellular trafficking in neurons." J Biol Chem 281(6): 3552-9.

Menasche, G., C. H. Ho, et al. (2003). "Griscelli syndrome restricted to hypopigmentation results from a melanophilin defect (GS3) or a MYO5A F-exon deletion (GS1)." J Clin Invest 112(3): 450-6.

Menasche, G., E. Pastural, et al. (2000). "Mutations in RAB27A cause Griscelli syndrome associated with haemophagocytic syndrome." Nat Genet 25(2): 173-6.

Mercer, J. A., P. K. Seperack, et al. (1991). "Novel myosin heavy chain encoded by murine dilute coat colour locus." Nature 349(6311): 709-13.

Mirouse, V., E. Formstecher, et al. (2006). "Interaction between Polo and BicD proteins links oocyte determination and meiosis control in Drosophila." Development 133(20): 4005-13.

Morris, R. L. and P. J. Hollenbeck (1995). "Axonal transport of mitochondria along microtubules and F-actin in living vertebrate neurons." J Cell Biol 131(5): 1315-26.

Muller, M. J., S. Klumpp, et al. (2008). "Tug-of-war as a cooperative mechanism for bidirectional cargo transport by molecular motors." Proc Natl Acad Sci U S A 105(12): 4609-14.

Murray, J. W., E. Bananis, et al. (2000). "Reconstitution of ATP-dependent movement of endocytic vesicles along microtubules in vitro: an oscillatory bidirectional process." Mol Biol Cell 11(2): 419-33.

Nagashima, K., S. Torii, et al. (2002). "Melanophilin directly links Rab27a and myosin Va through its distinct coiled-coil regions." FEBS Lett 517(1-3): 233-8.

Nath, S., E. Bananis, et al. (2007). "Kif5B and Kifc1 interact and are required for motility and fission of early endocytic vesicles in mouse liver." Mol Biol Cell 18(5): 1839-49.

Nielsen, E., F. Severin, et al. (1999). "Rab5 regulates motility of early endosomes on microtubules." Nat Cell Biol 1(6): 376-82.

Oh, J., K. Baksa, et al. (2000). "Functional domains of the Drosophila bicaudal-D protein." Genetics 154(2): 713-24.

Oh, J. and R. Steward (2001). "Bicaudal-D is essential for egg chamber formation and cytoskeletal organization in drosophila oogenesis." Dev Biol 232(1): 91-104.

Pal, A., F. Severin, et al. (2006). "Huntingtin-HAP40 complex is a novel Rab5 effector that regulates early endosome motility and is up-regulated in Huntington's disease." J Cell Biol 172(4): 605-18.

Pare, C. and B. Suter (2000). "Subcellular localization of Bic-D::GFP is linked to an asymmetric oocyte nucleus." J Cell Sci 113 (Pt 12): 2119-27.

Park, M., A. S. Serpinskaya, et al. (2007). "Rab32 regulates melanosome transport in Xenopus melanophores by protein kinase a recruitment." Curr Biol 17(23): 2030-4.

Pereira-Leal, J. B. and M. C. Seabra (2000). "The mammalian Rab family of small GTPases: definition of family and subfamily sequence motifs suggests a mechanism for functional specificity in the Ras superfamily." J Mol Biol 301(4): 1077-87.

Pfeffer, S. R. (2001). "Rab GTPases: specifying and deciphering organelle identity and function." Trends Cell Biol 11(12): 487-91.

Pilling, A. D., D. Horiuchi, et al. (2006). "Kinesin-1 and Dynein are the primary motors for fast transport of mitochondria in Drosophila motor axons." Mol Biol Cell 17(4): 2057-68.

Popoff, M. R., E. Chaves-Olarte, et al. (1996). "Ras, Rap, and Rac small GTP-binding proteins are targets for Clostridium sordellii lethal toxin glucosylation." J Biol Chem 271(17): 10217-24.

Provance, D. W., T. L. James, et al. (2002). "Melanophilin, the product of the leaden locus, is required for targeting of myosin-Va to melanosomes." Traffic 3(2): 124-32.

Provance, D. W., Jr., M. Wei, et al. (1996). "Cultured melanocytes from dilute mutant mice exhibit dendritic morphology and altered melanosome distribution." Proc Natl Acad Sci U S A 93(25): 14554-8.

Rodionov, V., J. Yi, et al. (2003). "Switching between microtubule- and actin-based transport systems in melanophores is controlled by cAMP levels." Curr Biol 13(21): 1837-47.

Rogers, S. L., I. S. Tint, et al. (1997). "Regulated bidirectional motility of melanophore pigment granules along microtubules in vitro." Proc Natl Acad Sci U S A 94(8): 3720-5.

Sahlender, D. A., R. C. Roberts, et al. (2005). "Optineurin links myosin VI to the Golgi complex and is involved in Golgi organization and exocytosis." J Cell Biol 169(2): 285-95.

Schraermeyer, U. and K. Heimann (1999). "Current understanding on the role of retinal pigment epithelium and its pigmentation." Pigment Cell Res 12(4): 219-36.

Schultz, J., T. Doerks, et al. (2000). "More than 1,000 putative new human signalling proteins revealed by EST data mining." Nat Genet 25(2): 201-4.

Segev, N. (2001). "Ypt and Rab GTPases: insight into functions through novel interactions." Curr Opin Cell Biol 13(4): 500-11.

Sheets, L., D. G. Ransom, et al. (2007). "Zebrafish melanophilin facilitates melanosome dispersion by regulating dynein." Curr Biol 17(20): 1721-34.

Simonsen, A., J. M. Gaullier, et al. (1999). "The Rab5 effector EEA1 interacts directly with syntaxin-6." J Biol Chem 274(41): 28857-60.

Stowers, R. S., L. J. Megeath, et al. (2002). "Axonal transport of mitochondria to synapses depends on milton, a novel Drosophila protein." Neuron 36(6): 1063-77.

Stuurman, N., M. Haner, et al. (1999). "Interactions between coiled-coil proteins: Drosophila lamin Dm0 binds to the bicaudal-D protein." Eur J Cell Biol 78(4): 278-87.

Suter, B., L. M. Romberg, et al. (1989). "Bicaudal-D, a Drosophila gene involved in developmental asymmetry: localized transcript accumulation in ovaries and sequence similarity to myosin heavy chain tail domains." Genes Dev 3(12A): 1957-68.

Suter, B. and R. Steward (1991). "Requirement for phosphorylation and localization of the Bicaudal-D protein in Drosophila oocyte differentiation." Cell 67(5): 917-26.

Swan, A., T. Nguyen, et al. (1999). "Drosophila Lissencephaly-1 functions with Bic-D and dynein in oocyte determination and nuclear positioning." Nat Cell Biol 1(7): 444-9.

Swan, A. and B. Suter (1996). "Role of Bicaudal-D in patterning the Drosophila egg chamber in mid-oogenesis." Development 122(11): 3577-86.

Tanaka, Y., Y. Kanai, et al. (1998). "Targeted disruption of mouse conventional kinesin heavy chain, kif5B, results in abnormal perinuclear clustering of mitochondria." Cell 93(7): 1147-58.

Tuma, M. C., A. Zill, et al. (1998). "Heterotrimeric kinesin II is the microtubule motor protein responsible for pigment dispersion in Xenopus melanophores." J Cell Biol 143(6): 1547-58.

Ullrich, O., S. Reinsch, et al. (1996). "Rab11 regulates recycling through the pericentriolar recycling endosome." J Cell Biol 135(4): 913-24.

Valetti, C., D. M. Wetzel, et al. (1999). "Role of dynactin in endocytic traffic: effects of dynamitin overexpression and colocalization with CLIP-170." Mol Biol Cell 10(12): 4107-20.

van der Sluijs, P., M. Hull, et al. (1992). "Reversible phosphorylation--dephosphorylation determines the localization of rab4 during the cell cycle." Embo J 11(12): 4379-89.

Varadi, A., L. I. Johnson-Cadwell, et al. (2004). "Cytoplasmic dynein regulates the subcellular distribution of mitochondria by controlling the recruitment of the fission factor dynamin-related protein-1." J Cell Sci 117(Pt 19): 4389-400.

Welte, M. A. (2004). "Bidirectional transport along microtubules." Curr Biol 14(13): R525-37.

Werth, J. L. and S. A. Thayer (1994). "Mitochondria buffer physiological calcium loads in cultured rat dorsal root ganglion neurons." J Neurosci 14(1): 348-56.

Wharton, R. P. and G. Struhl (1989). "Structure of the Drosophila BicaudalD protein and its role in localizing the the posterior determinant nanos." Cell 59(5): 881-92.

Wilson, S. M., R. Yip, et al. (2000). "A mutation in Rab27a causes the vesicle transport defects observed in ashen mice." Proc Natl Acad Sci U S A 97(14): 7933-8.

Wozniak, M. J., M. Melzer, et al. (2005). "The novel protein KBP regulates mitochondria localization by interaction with a kinesin-like protein." BMC Cell Biol 6: 35.

Wu, X. S., K. Rao, et al. (2002). "Identification of an organelle receptor for myosin-Va." Nat Cell Biol 4(4): 271-8.

Zerial, M. and H. McBride (2001). "Rab proteins as membrane organizers." Nat Rev Mol Cell Biol. 2(2): 107-17.

Zucker, R. S. (1999). "Calcium- and activity-dependent synaptic plasticity." Curr Opin Neurobiol 9(3): 305-13.

Summary

Transport is a very important process in our daily life and the movement of people and cargoes is essential to keep our society organised. The same applies to the cells of our body: intracellular transport is crucial for the maintenance of cell viability and for the organisation of multicellular tissues and organs. Vesicles and multimolecular complexes are transported along microtubules and actin filaments, which form fibrous structures inside the cells. Cargos are routed towards various cellular destinations, such as the plasma membrane for secretion of signalling molecules and insertion of receptors, or to the cell interior, where membrane organelles like the Golgi, Endoplasmic Reticulum and lysosomes are located. Motor proteins, which move along the microtubules and the actin filaments, generate forces for cargo transport.

In this thesis I investigated the Bicaudal-D (BICD) protein and tried to address several transport-related scientific questions regarding bidirectional transport and the organization of the dynein/dynactin complex.

BICD is highly conserved during evolution; it functions as a linker protein between cargos and microtubule-dependent motors. The microtubule minus end-directed dynein/dynactin motor complex and the small GTPase Rab6 were already identified as binding partners of BICD. In chapter 2 we investigated the function of Rab6 and analysed the movement of Rab6 positive vesicles. We showed that these vesicles are involved in exocytosis and that they are transported by the Kinesin-1 motor towards the cell periphery, to the plus ends of microtubules. Previously, it was thought that BICD could only facilitate the transport in the opposite direction, by attaching the dynein motor to cargo. Our mass spectrometry analysis identified Kinesin-1 as a new binding partner of BICD, helping to explain the behaviour of Rab6 vesicles.

Bidirectional movement of membrane structures was investigated in more detail in chapter 3. We describe a new binding partner of BICD, RanBP2, which is a part of the Nuclear Pore Complex. In interphase cells, BICD is bound to Rab6 vesicles and participates in their kinesin-dependent movement to the cell periphery. Just before cell division, BICD switches cargo: it is targeted to the nuclear envelope by RanBP2. The predominant direction of BICD-dependent movement also changes, as the nucleus is pulled by dynein towards the cell centre where it is positioned in close proximity of the centrosome. This process likely ensures the proper formation of the mitotic spindle near the chromosomes after nuclear envelope breakdown.

The dynein/dynactin motor consists of two large complexes. Dynein is the actual motor that generates force, while dynactin is essential to keep dynein on the microtubule track. It remains unclear how the two complexes bind each other. In Chapter 4 we show that the N-terminus of BICD is able to form a triple complex with dynein and dynactin. Cross-linking experiments and mass spectrometry analysis suggest a model where BICD binds both dynein and dynactin. In vitro studies indicate that the formation of this triple complex does not result in longer run lengths or higher

velocities of the dynein motor, but increases the frequency of motility events. It appears that BICD might glue dynein and dynactin together while it is bound to a cargo, and in this way promote cargo movement along microtubules.

In chapter 5 we discuss the similarities of our BICD model with other models of intracellular transport. A surprising number of cargos associate with various motor complexes in a similar way. Small GTPases bind effector proteins that in their turn recruit motors, kinesins and dyneins, which walk to the two opposite ends of the microtubule tracks. Therefore, most cargos can move bidirectionally and frequently switch the direction of movement. The existence of adaptor molecules such as BICD, can help several different motors to associate with their cargos, may coordinate their activity, and might possibly help to explain how bidirectional motility is controlled. The next challenge is to understand how the action of BICD and other adaptor proteins is regulated.

Samenvatting

Transport is een belangrijke component in ons leven. Het vervoer van goederen en mensen is essentieel voor onze samenleving. Deze processen zijn niet alleen belangrijk voor de wereld om ons heen, maar ook voor de cellen in ons lichaam. Intracellulaire transport mechanismen zijn van groot belang voor het voortbestaan van een cel en het organisme waarvan deze cel een onderdeel uitmaakt.

Zowel het microtubule netwerk als het actine skelet vormen het wegennetwerk waarlangs membraanblaasjes en grote eiwitcomplexen vervoerd worden. Het eindstation van deze goederen kan het celmembraan zijn, hier worden receptoren geïnserteerd of signaalstoffen uitgescheiden. In de cel zelf spelen verschillende recycling en degradatie routes een rol. Hierbij zijn membraanorganellen zoals de Golgi en het Endoplasmatisch Reticulum betrokken. De intracellulaire "goederen" worden getransporteerd door motoreiwitten die letterlijk over de microtubuli en actine filamenten stappen.

In dit proefschrift onderzoek ik een aantal transport gerelateerde vraagstukken door in detail naar het eiwit BICD te kijken. Ik probeer een model te vinden voor bidirectioneel transport en ga in op de organizatie van het dynein/dynactin complex.

Het BICD eiwit is evolutionair sterk geconserveerd en is zowel in fruitvlieg als in zoogdierlijke cellen geïdentificeerd. In beide organismen functioneert BICD als een linker of adaptor eiwit dat goederen aan motoreiwitten koppelt. Een aantal bindingspartners van BICD zijn al bekend, waaronder het motoreiwit dynein en de GTPase Rab6.

In hoofdstuk 2 wordt de functie van Rab6 nader onderzocht en laten we zien dat het een factor is welke betrokken is bij een secretie route. Hoewel BICD biochemisch gezien sterk gebonden lijkt aan de dynein motor en daarmee het transport naar het midden van de cel reguleert, is de beweging van de Rab6 positieve structuren vooral gerelateerd aan kinesin-1 motoren. Deze kinesin-1 motoren transporteren goederen in de richting van het plasmamembraan. Een massaspectrometrische analyse identificeerde kinesin-1 als bindingspartner van BICD, waarmee het gedrag van Rab6 vesicles verklaard kan worden.

Het bidirectionele gedrag van BICD gebonden structuren wordt verder uitgediept in hoofdstuk 3. In dit hoofdstuk wordt een nieuwe bindingspartner beschreven: RanBP2. RanBP2 is een component van het Nuclear Pore Complex. In de G2-fase van de celcyclus, vlak voor de celdeling, wisselt BICD van bindingspartner. In plaats van gebonden te zijn aan Rab6 vesicles bindt BICD nu via RanBP2 de celkern. Tevens wisselt de transport richting, eerst was deze in hoofdzaak gericht op transport richting het plasmamembraan. Echter in de G2 fase wordt vooral gebruik gemaakt van de dynein motor. De celkern wordt vervolgens door BICD en de dynein motoren vlakbij het centrosoom in het

midden van de cel gepositioneerd. Mogelijk kunnen de centriolen zich hierdoor makkelijker om de kern heen verplaatsen wat mogelijk van belang is voor de positionering van de mitotische spindle.

Hoofdstuk 4 beschrijft de binding van BICD aan het dynein/dynactin motorcomplex. Dit complex bestaat uit twee grote subcomplexen. Het dynein complex en het dynactin complex. Dynein vormt het kracht genererende deel van de motor en het dynactin complex is *in vivo* belangrijk om dynein op de microtubule te houden. Transport gerelateerde GTPases kunnen direct of via verschillende adaptor eiwitten, zoals BICD, binden aan dit motorcomplex. Het N-terminale deel van BICD bindt zeer sterk aan dynein/dynactin en vormt een drievoudig complex. Met behulp van cross-linking technieken en massaspectrometrie hebben we aanwijzingen gekregen dat BICD zich waarschijnlijk bevindt op het raakvlak tussen dynein en dynactin en als een soort lijm beide complexen bij elkaar houdt. Motility assays laten zien dat dynein motoren met BICD N-terminus echter niet langere afstanden afleggen over de microtubules. Wat echter wel gebeurt is dat een dynein motor vaker op een microtubule start.

In de discussie in hoofdstuk 5 wordt het BICD model met andere modellen vergeleken. Verrassend veel ladingen binden op eenzelfde manier aan motoren. Een GTPase identificeert een lading, waarna een adaptor eiwit een motoreiwit recruteert en de goederen getransporteerd kunnen worden. Tevens vertonen veel goederen bidirectioneel gedrag waarbij ze heen en weer over de microtubuli bewegen. Een zeer plausibele verklaring voor dit gedrag is dat verschillende groepen motoren binden aan eenzelfde lading, waarna motoren die in dezelfde richting bewegen aan- of uitgeschakeld worden. BICD is een adaptor eiwit dat motoren van tegenovergestelde directionaliteit kan binden. De regulatie van BICD is echter nog zeer onduidelijk en vergt verder onderzoek.

Dankwoord - Acknowledgements

Na vier jaar bij de afdeling Celbiologie en een beetje bij Neurowetenschappen is er nu een einde gekomen aan mijn AIOschap. Dit is een periode geweest waarin ik heel veel heb geleerd, zowel technisch als theoretisch. Voorop stond toch het plezier in mijn werk en de mooie afdeling waar ik deel van heb uitgemaakt. Dit alles komt niet vanzelf tot stand en er zijn veel mensen bij betrokken geweest. Ik zal dan ook beginnen met iedereen te bedanken die, in welke vorm dan ook, heeft bijgedragen aan dit proefschrift. Uiteraard zijn er een aantal mensen die ik in het bijzonder wil bedanken voor hun hulp.

Allereerst wil ik Frank Grosveld bedanken voor zijn "banktijd". Helaas is het er de laatste twee jaar niet veel meer van gekomen. Gelukkig kon ik altijd binnen lopen voor een vraag of handtekening en maakte je daar altijd 5 minuten voor vrij.

Anna, mijn co-promotor, tijdens mijn eerste jaren als aio liet je op mij een indruk achter van iemand die bijna alles wist. Microtubules, Rab GTPases, eetbare paddestoelen, kalashnikovs en biologische wapens je kon het zo gek niet bedenken. Uitspraken als: "je hebt 3,6% kans dat dit gaat werken" waren voor mij later een trigger om het tegendeel te bewijzen. Helaas je hebt toch vaak gelijk gehad. Je wetenschappelijk inzicht en pracktische manier van werken resulteerden in doordachte en degelijke experimenten. Eigenschappen die je nodig hebt om te werken naar een publicatie. Je hebt me echter wel de vrijheid gegeven om wat aan te rommelen, dit is echter niet altijd even nuttig geweest. Laat ik vooral twee weken dubbele pieken zoeken en andere briljante X-link experimenten niet oprakelen. Je hebt me heel veel geleerd, van het gebruik van negatieve controles tot de essentie van een hoogtepunt aan het eind van een tekst. Zeker dit laatste jaar heb je me er doorheen gesleept. Dat heb ik nodig gehad. Bedankt voor alles!

Niels, in jou lab ben ik eigenlijk begonnen. Bedankt voor je hulp in de afgelopen jaren. Het is erg fijn dat je secretaris wilt zijn van mijn promotiecommissie. Hierbij wil ik ook Gert bedanken voor het lezen van mijn proefschrift en het geven van commentaar en Rob Willemsen voor het plaats nemen in mijn promotiecommissie.

Veel data uit dit proefschrift is tot stand gekomen met de hulp van anderen. Mijn bijzondere dank gaat uit naar Rene Medema en Marvin Tanenbaum. Marvin ik denk dat je nu een nieuwe hobby hebt: cellen tellen en oligo's testen. Verder wil ik Frauke Melchior, Annette Flotho, Dieuwke Engelsma en Maarten Fornerod bedanken. Special thanks to all the members of the lab of Stephen King. Especially Dave and Steve, thanks for teaching me a set of new "tricks". I had a great time in Kansas City. Your barbecue still amazes me!

Vervolgens wil ik alle mensen uit lab 10.30 bedanken. Frank je hebt me altijd verbaasd met je ritme, 's ochtends in de "ignore mode" en na 14:00 gaat de knop om. Suzanne, het M&M meisje je heerlijke naïviteit heeft me altijd tot het uiterste gedreven platjes, pinda's aan bomen het kon niet gek genoeg. Gelukkig neem je steeds minder van me aan. Surfdude Michael, als jij begon te juichen kon het niet anders of het ging stormen, waaien en regenen. Ana, good luck in Porto and most likely we will meet there or here with or without pancakes who knows.

Miss Casanova, thanks for the cell culture fun and stop waving to your naked HeLa cells, they don't wave back you know. See you in Madrid I would say.

Marco wanneer gaan we weer eens wagentjes kijken? Wie weet in Braunschweig. Bedankt dat ik veel van je gastvrijheid gebruik heb mogen maken, je hebt me veel geholpen ondermeer met het verschaffen van onderdak. Marja bedankt voor je advies, ik heb al een beetje naar je geluisterd.

Dies Clooney, zo kan ik je nu wel noemen nu je echte koffie bent gaan drinken. Bedankt voor de schrijf- en computer ruimte die je me beschikbaar hebt gesteld. Noori en Gina thanks for keeping me company in the office and showing me all the ingredients of these delicious Spanish and Indian dishes. By the way watch out for each others eyes when you start throwing pencils again.

Martijn, harstikke bedankt dat je me zo hebt geholpen met de wide field. Je programmeer kunsten hebben me goed op weg geholpen.

Jeroen je massspec is de basis geweest voor veel van mijn experimenten, tot de volgende vastenavond in de Mortier? Toch geweldig dat we elkaar hier weer tegen het lijf liepen.

Uiteraard zonder de ondersteuning van Melle, Marieke en Jasperina, de computer guys en de dames in de spoelkeuken hadden een hele hoop zaken in het honderd gelopen. Bedankt voor jullie support.

Tevens wil ik mijn ouders, familie, schoon familie en vrienden bedanken voor hun getoonde interesse in mijn onderzoek. Ik begrijp dat het geen gemakkelijk kost was. Eiwitten en cellen zijn geen toegankelijke onderwerpen. Misschien dat dit boekje jullie een indruk kan geven van wat ik de afgelopen jaren nu echt heb uitgespookt.

Tenslotte natuurlijk Boren, je hebt veel geduld moeten opbrengen de afgelopen jaren. Dat is je gelukt en daar ben ik erg trots op. Bedankt voor je steun en onze mooie dochter Amber.

Curriculum Vitae

Name   Gustav Daniël Splinter

Birth date   4th of May 1977

Birth place   Alphen a/d Rijn, The Netherlands

2008 - 2009
Post doctoral fellow
Department of Neurosciences, ErasmusMC, Rotterdam
Isolation and characterisation of native receptor complex components

2004 - 2008
PhD student
Department of Cell Biology and Genetics, ErasmusMC, Rotterdam
Bicaudal-D: switching motors, cargo and direction
Prof.dr. F. Grosveld (promoter) & Dr. A. Akhmanova (co-promotor)

2007
Short term visit, Department of Biological Sciences, University of Missouri, Kansas City
Purification of dynein and dynactin from bovine brain

2001 – 2004
Msc, Molecular Biology, Leiden University
Traineeship, Institute for Molecular Plant sciences, University of Leiden
Stress responses in rice

1996 – 2000
Bsc, Biochemistry, Hogeschool Brabant, Etten-Leur
Traineeship, Department of Haematology, Erasmus University Rotterdam
Functional characterization of TRIAD1

1994 – 1996
HAVO, Mollerlyceum, Bergen op Zoom

1989 – 1994
MAVO, Mollerlyceum, Bergen op Zoom

Publications

Daniël Splinter and Anna Akhmanova
Moving back and forth along the microtubule; who is in control of the gearbox.
Article in preparation

Daniël Splinter, David S. Razafsky, Jeroen Demmers, Nanda Keijzer, Casper C. Hoogenraad, Stephen J. King and Anna Akhmanova
Bicaudal D2 regulates the interaction between dynein and dynactin complexes.
Article in preparation.

Daniël Splinter, Marvin E. Tanenbaum, Annette Flotho, Ilya Grigoriev, Dieuwke Engelsma, Nanda Keijzer, Jeroen Demmers, Ka Lou Yu, Maarten Fornerod, Frauke Melchior, Casper Hoogenraad, René H. Medema and Anna Akhmanova
Bicaudal-D2, dynein and kinesin-1 associate with nuclear pore complexes and regulate centrosome positioning during mitotic entry.
submitted to Developmental Cell

Grigorev I., Gouveia SM., van der Vaart B., Demmers J., Smyth JT., Honnappa S., **Splinter D**., Steinmetz MO., Putney JW. Jr, Hoogenraad CC., Akhmanova A.,
STIM1 is a MT-plus-end-tracking protein involved in remodeling of the ER.
Curr Biol. 2008 Feb 12;18(3):177-82

Wanschers BF, van de Vorstenbosch R, Schlager MA, **Splinter D**, Akhmanova A, Hoogenraad CC, Wieringa B, Fransen JA.
A role for Rab6B Bicaudal-D1 interaction in retrograde transport in neuronal cells.
Exp Cell Res. 2007 Oct 1;313(16):3408-20

Grigoriev I., **Splinter D**., Keijzer N., Wulf P., Demmers J., Ohtsuka T., Modesti M., Maly I., Grosveld F., Hoogenraad C., Akhmanova A.
Rab6a regulates transport and targeting of exocytotic carriers.
Dev Cell. 2007 Aug;13(2):305-14.

Presentations at conferences

D. Splinter, M. Tanenbaum, I. Grigorev, J. Demmers, D. Engelsma, M. Fornerod, C. Hoogenraad, F. Grosveld, R. Medema and Anna Akhmanova
Switching Alliances Before Mitosis.
47th Annual ASCB meeting, Washington, USA (poster)

D. Splinter
Bicaudal-D: A cell cycle regulated linker between cargo and microtubule motors
The 17th MGC-Symposium, Rotterdam, The Netherlands (oral presentation)

Splinter D., Schmitt E., Hoogenraad C., Grosveld F., King S., Akhmanova A.
The role of mammalian Bicaudal-D2 in recruitment of cytoplasmic dynein to vesicle cargo.
EMBO Workshop, 7th Annaberg Conference 2007, Goldegg, Austria (poster)